NTNU
Norwegian University of
Science and Technology

Concept Development of an Aluminum Pedestrian Bridge

Christian Arne Raknes Brekke

Mechanical Engineering
Submission date: June 2017
Supervisor: Christer Elverum, MTP

Norwegian University of Science and Technology
Department of Mechanical and Industrial Engineering

Preface

This is my master's thesis in mechanical engineering at the Norwegian University of Science and Technology (NTNU). It is a part of my 2-year study program of Product Development and Materials with specialization in Advanced Product Simulation. The thesis was carried out during the spring semester of 2017.

Cooperation with Marine Aluminum AS (MA) was established through the NTNU Aluminum Innovation Center (NAPIC). The background for the project and cooperation is a combination of the growing market for lightweight land-based pedestrian bridges and MA's experience with off-shore gangways.

During the spring, I was at a two and a half week long stay at MA's construction department at Karmøy. Working in an environment with highly skilled and friendly employees, helped me learn a lot about aluminum as a construction material. My orienteering skills also had an exponential increase during the stay, after attending to several orienteering races with the MA employees.

I would like to thank Harald Vestøl for giving me the opportunity to cooperate with MA through NAPIC. Steinar Lundberg and all the employees at MA for the hospitality and help. Last, I want to thank my supervisor at NTNU, Christer Elverum for help and guidance.

Trondheim, 2017-06-30

Christian Arne Raknes Brekke

[This page is intentionally left blank]

Abstract

As part of new initiatives from Norwegian Public Road Administration (NPRA) and Nye Veier AS towards reduced cost of road construction and maintenance, alternative materials for bridges are being considered. For the construction phase, quick installation and utilization of prefabricated units are being requested. For the operational phase, solutions not requiring periodical maintenance are favorized. In total, these new requirements are well suited for the use of aluminum. Especially for pedestrian bridges crossing roads with heavy traffic. The primary objective of this thesis is to evaluate the potential of aluminum solutions within pedestrian bridges. This seen in competition with common steel and concrete solutions as well as new materials such as fiber reinforced polymer (FRP). The thesis contains a literature study on aluminum as construction materials and a concept development of an aluminum pedestrian bridge. This concept bridge is compared to one of two baseline solutions from NPRA.

Many existing and successful aluminum pedestrian bridges demonstrates aluminum's potential in this sector. As a construction material, aluminum contains several advantages. High specific strength, high corrosion resistance, no need of periodic maintenance, low residual stresses caused by constrained thermal deformation and it is field proven bridge material. A pedestrian bridge can be designed with unique solutions by utilizing the possibilities of friction stir welding and extrusion of profiles. There is a general lack of knowledge and a historical lack of standards and guidelines for aluminum. The building sector's reliance on acquisition cost and warranty condition for their investments and not life-cycle cost analysis (LCCA) have put a limitation for aluminum pedestrian bridge projects. The initial evaluation of the bridge concept provides a 23-ton bridge structure with a fabrication cost of 6.65 MNOK. Compared to the baseline solution from NPRA the aluminum bridge only has 45% of the weight in aluminum as FRP in the baseline solution. The estimated fabrication cost ended up almost equal for the two concepts, and only the significant deviation in weight is differentiating them.

Aluminum has a bright future if increased knowledge among builders and engineers, better standards and guidelines, and increased focus on LCCA becomes a reality. The development of the aluminum pedestrian bridge in this thesis demonstrates aluminum capabilities applicable for pedestrian bridges in Norway.

[This page is intentionally left blank]

Sammendrag på Norsk

Som en del av nye tiltak fra Statens vegvesen (NPRA) og Nye Veier AS for å reduserte kostnader for veibygging og vedlikehold, vurderes alternative materialer for broer. For byggefasen, blir rask installasjon og bruk av prefabrikkerte enheter forespurt. I driftsfasen favoriseres løsninger som ikke krever periodisk vedlikehold. Til sammen er disse nye kravene godt egnet for bruk av aluminium. Spesielt for fotgjengerbroer som krysser veier med tung trafikk. Hovedformålet med denne oppgaven er å evaluere potensialet for aluminiums løsninger innenfor fotgjengerbroer. Dette sett i konkurranse med vanlige stål- og betongløsninger, samt nye materialer som fiber forsterket polymer (FRP). Avhandlingen inneholder en litteraturstudie om aluminium som byggemateriale samt en konseptutvikling av en aluminiums gangbro. Denne konseptbroen er sammenlignet med en av to broløsninger fra NPRA.

Mange eksisterende og vellykkede gangbroer av aluminium viser materialets potensial i denne sektoren. Som byggemateriale inneholder aluminium flere fordeler. Høy spesifikk styrke, høy korrosjonsbestandighet, ikke behov for periodisk vedlikehold og lave restspenninger forårsaket av fastholdte termiske deformasjoner. Materialet er også utprøvd over tid som bromateriale. En fotgjengerbro kan designes med unike løsninger ved å benytte mulighetene friksjonssveising og ekstrudering av profiler. Begrenset bruk av aluminium som bromateriale skyldes hovedsakelig mangel på kunnskap og historisk mangel på standarder og retningslinjer. Byggesektorens tillitt til anskaffelseskostnad og garantistilling for sine investeringer og ikke livssykluskostands analyser (LCCA) har også satt en begrensning. Den første evalueringen av gangbro konseptet gir en 23-tonn brostruktur med en fabrikasjonskostnad på 6,65 MNOK. Sammenlignet med broen fra NPRA har aluminiumbroen kun 45% av vekten i aluminium som FRP i NPRA broen. Anslått produksjonskostnad ble nesten lik for de to konseptene, og den betydelige forskjellen i vekt skiller de.

Aluminium har en lys fremtid om økt kunnskap blant entreprenører og ingeniører, bedre standarder og retningslinjer, samt økt fokus på LCCA blir en realitet. Utviklingen av aluminiumgangbroen i denne oppgaven har vist aluminiumsegenskaper som er anvendbare for fotgjengerbroer i Norge.

[This page is intentionally left blank]

Table of Contents

List of figures

List of tables

Abbreviations

DfM	Design for manufacturing
DfA	Design for assembly
FE	Finite element
FRP	Fiber reinforced plastic
FSW	Friction stir welding
GFRP	Glass fiber reinforced plastic
LBD	Longitudinal bridge deck
LC	Load combination
MA	Marine Aluminum
NPRA	Norwegian Public Road Administration
NUM	New Mexican University
RH	Royal Haskoning DHV
TBD	Transverse bridge deck
TDA	Time dependent analysis
URS	United Research Services

[This page is intentionally left blank]

1 Introduction

1.1 Background and Motivation

As part of new initiatives from Norwegian Public Road Administration (NPRA) and Nye Veier AS towards reduced cost of road construction and maintenance, alternative materials for bridges are being considered. For the construction phase, quick installation and utilization of prefabricated units are being requested. For the operational phase, solutions not requiring periodical maintenance are favorized. In total, these new requirements are well suited for the use of aluminum. Especially for pedestrian bridges crossing roads with heavy traffic, it's assumed a significant business potential for aluminum solutions.

1.2 Project Scope

The study will be based on two planned bridges from NPRA. One already developed for fiber reinforced polymer (FRP) and one that is currently designed in steel with a diagonal tubular arch.

1.2.1 Objectives

The main objective of this study is to evaluate the potential of aluminum solutions within pedestrian bridges, in competition with common steel and concrete solutions as well as new materials such as FRP.

- Provide a short description of key requirements for bridge materials and how aluminum compares to other alternatives within this application
- Describe the manufacturing capability of Marine Aluminium AS (MA)
- Evaluate the feasibility of introducing aluminum solutions for the two bridges from NPRA, based on manufacturing at MA
- Select the most suitable case, and develop an aluminum concept
- Perform initial evaluation of structural capabilities, weigh and cost of the proposed concept
- Based on available information, compare performance of aluminum concept with baseline solution from NPRA

1.2.2 Research Questions

Are aluminum bridges competitive considering weight, cost and structural capabilities in the Norwegian light weight pedestrian bridge market?

1.2.3 Delimitations

The thesis only includes development of the aluminum bridge structure. Surrounding concrete foundation and bridge bearings is not included. Also fatigue calculation have been left out of the scope for this thesis.

1.2.4 Thesis Structure

This thesis consists of several chapters, including an introduction, a theory chapter, a case study, conclusion, reference list, and appendices. Throughout the concept development, the results are evaluated consecutively after each chapter.

Chapter 1: This is the introduction to the thesis and describes the background, project scope, objectives. It also presents the research questions.
Chapter 2: presents the theory about aluminum as a construction material. It first starts off with the aluminum history as a bridge material, then describes aluminum properties as construction material and the manufacturing of aluminum. Further, a bridge material comparison and existing pedestrian bridge solutions in aluminum are highlighted. The end of this chapter ends with design aspects for pedestrian bridges.
Chapter 3: in this chapter, the baseline solution from NPRA is presented and chosen for further use in the case study.
Chapter 4 -11: is these chapters the development of the aluminum pedestrian bridge concept is described. It starts with the product development methodology and briefly explains the product development process and present the user demand specification. FEA and calculation in accordions with NS EN-1999-1-1 is performed in these chapters as well.
Chapter 12: the initial evaluation of the pedestrian bridge concept is presented and evaluated with weight on structural integrity, weight and fabrication.
Chapter 13: this chapter compares the developed aluminum pedestrian bridge concept with the baseline solution from NPRA. Structural capabilities, weight and cost is the main factors in the comparison.
Chapter 14: here the thesis is summarized, discussed and concluded. Also recommended further work is written in this chapter
Chapter 15: The thesis ends with a reference list.

2 Theory

2.1 History of Aluminum in Bridges

The history of aluminum bridges goes back to 1933 when the first aluminum bridge deck was built in the United States [1]. Since then, many similar bridge decks have been installed. Aluminum bridge decks have reduced weight, is easy to install with only a short closure time of traffic, easy to transport and possible to prefabricate. In 1950, Arvida the first all-aluminum bridge was built over the Saguenay River in Canada [1] as illustrated in Figure 1. In 1996 Norway's first all-aluminum road bridge was constructed at Forsmo. The Forsmo bridge has no reported damage or maintenance issues related to the bridge [2]. The first aluminum bridge built in Europe is the Schwansbell Bridge build in 1956. Also this bridge had minimal degradation after over 50 years in service reported in 2006 [2].

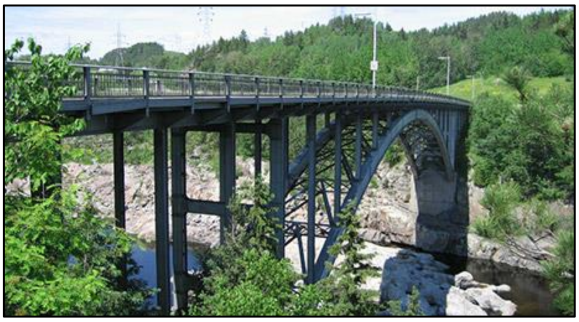

Figure 1: Arvida bridge [3].

Figure 2: Forsmo bridge [1].

Over several decades aluminum in bridge application has proven to be a sustainable material. Compared to steel the high initial costs are often held against aluminum. When considering the life-cycle cost (LCC) of aluminum, there are large benefits with the material [1, 2, 4]. Aluminum is increasingly strengthening its position as a bridge material as the LCC approach becomes more familiar and accepted. Seen in perspective of the first aluminum bridges the aluminum alloys now has gained 50% more strength [1]. One of the most dominating reasons for the limited use of aluminum in bridges is the lack of knowledge among builders and bridge engineers [2, 4]. Also, the historical lack of adequate construction standards and guidelines has restricted aluminum as a bridge construction material [2, 5]. The lack of construction guidelines can for instance be illustrated by the absence of aluminum guidelines in NPRA handbook N400. In the last decade, a significant contribution has been put into the development of harmonized design and execution standards like the Eurocodes with National Annexes [6]. The use of aluminum in pedestrian bridges seems to be increasing, and several companies now deliver a variety of prefabricated bridges in both the US and Europe.

2.2 The Properties of Aluminum as Construction Material

Aluminum consists of eight groups of aluminum alloys which are numerically classified by the American Association. The first four digits are the primary alloying element, and the three others are the secondary alloying elements. The most common alloying series for bridge construction is the 5000 series and the 6000 series. In the 5000 series, magnesium is the primary alloying element. This series is often used in welded construction without suffering too much strength loss in the heat affected zone [7]. The 6000 series, magnesium, and silicon constitute as alloying elements. The 6000 series is especially suitable for extrusion and welding [7] and 6082 T6 is the strongest alloy in the series. The suffix T6 indicates that the material is heat treated and then artificial aged to increase the strength of the alloy [8]. A good way to describe aluminum as a construction material is to compare it with the much more common construction material, steel. The main differences between the two materials are that the density and Young's modulus of aluminum is one-third of steel. Aluminum is also more corrosion resistant than steel. Whereas steel typically needs corrosion protection in most environments, a thin inert oxide film is formed on exposed surfaces of the aluminum [7]. This oxide film protects the aluminum from further corrosion. Still, construction details must be properly designed to avoid crevice, pitting and galvanic corrosion of the aluminum.

A stress-strain curve comparison between the materials shows that both materials follows linear elastic behavior with differentiated slopes, see Figure 3. After the linear elastic area, aluminum has a continuous strain-hardening while steel has a defined perfect plastic plateau. A significant difference is that aluminum's ultimate deformation is about 10% lower than for steel [7]. The parameter f/γ ratio is considered highly important [7], and a comparison between several materials is conducted in Section 2.4. f_0 is the yield strength of steel and $f_{0.2}$ the yield strength of aluminum. γ is the material density. For aluminum this ratio can vary from 8 – 17, this is superior compared to mild steel which is in the range of 3 – 4.5 [7]. It is not always possible to utilize this advantage in aluminum constructions due to the low Young's modulus. Local buckling can occur under compression load. The elastic deformations are also three times larger than for steel [9]. There are several complications related to the reduced Young's modulus of aluminum. According to the article [9] which is related to aluminum in the ship industry, an equivalent structural panel of aluminum and steel has approximately the same natural frequency of vibration. Aluminum structures will have a lower vibration frequency when exposed to a high level of nonstructural mass. This reduced frequency could lead to resonant problems [9]. Resonant problems combined with larger susceptibility of fatigue damage [9] makes it a limiting factor in aluminum design. Other differences are that aluminum has higher thermal expansion coefficient than steel. This thermal expansion coefficient makes aluminum more prone to thermal induced vibration. Residual stresses caused by constrained thermal deformation is on the other hand about 30% lower than steel [7]. High temperatures also create other problems for aluminum. Aluminum has a much lower melt temperature compared to steel. This comparingly low melt temperature reduces aluminums structural capabilities when exposed to high temperatures like a fire. Unlike the high temperature properties, aluminum have excellent properties at low temperatures. Due to aluminums face-centered-cubic crystal structures it will retain good ductility and adequate toughness at subzero temperatures [10].

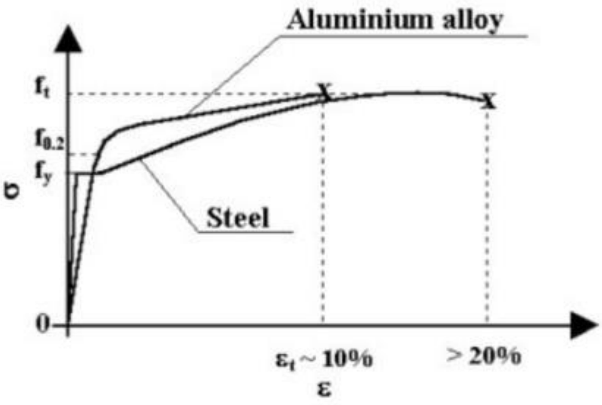

Figure 3: A general stress – strain curve comparison between aluminum alloy and steel [7].

As discussed aluminum have low density and a large cross-section with thin wall thickness must be used to utilize the property. Welded joints in aluminum trusses designed would in most cases be the limiting factor. This limitation is due to the strength reduction in the heat affected zone (HAZ). Internal ribs will therefore not be necessary for the compression members. It is usually more beneficial to increase the cross-section thickness and avoid cross-section class 4 than adding internal stiffeners. Cross-section class 4 is prone to local buckling before the attainment of proof stress in parts of the cross-section [11].

2.3 Manufacturing and Joining of Aluminum

Structural components made of aluminum alloys can be manufactured with a variety of different methods. Rolling, casting, extrusion and drawing processes are all available methods. The most important method which makes aluminum stand out from for instant steel and FRP is the extrusion process. This process is more thoroughly explained in Section 2.3.1. Beneficial bridge structural members can be produced by combining extrusion and welding techniques [12].

Concerning joining of aluminum friction stir welding (FSW), fusion welding, cohesive bonding, bolting and riveting are all well-known methods. FSW and fusion welding is further explained in Section 2.3.2 and 2.3.3.

2.3.1 Extrusion

One of the big advantages aluminum has compared to steel is ease of forming and the possibility of extruding complex profiles. This gives the possibility to design a multifunctional profile without extra cost. Bridges with free span between 50-60 m can be obtained with special extrusions presses with more than 8000 tons of force [6, 13]. There is a variety of different extrusion processes. In general, the extrusion is a process where cast billets is shaped by pressing it through a die. The metal flows continuously out of the orifice and appears as a long profile. The profile will have the approximately same shape as the orifice geometry [14]. The profile is stretched immediately after and during the extrusion. The stretching is to ensure straightness and to avoid accumulation of material right after it comes hot out of the die. An extrusions press is illustrated in Figure 4.

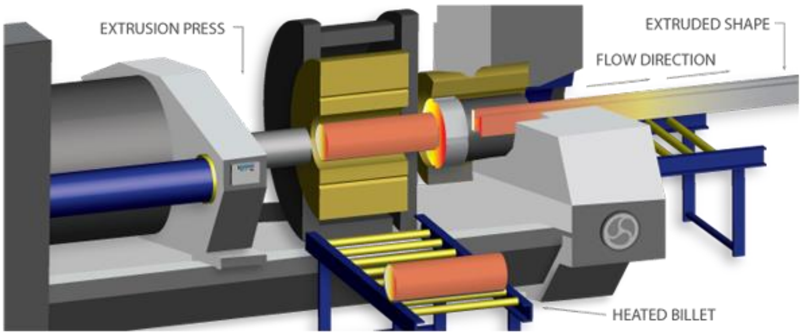

Figure 4: Extrusions press [15].

The standard cost of extruded profiles is 30 NOK/kg. Large profiles are more expensive to produce. This increased cost is not only because of the kg price but also because there are much fewer large extrusion presses in the world. Fewer extrusion presses give the production plants the opportunity to charge a higher price. SAPA construction manual [16] presents some guidelines for profile design making the extrusion process more economical and easier. Simple, round shapes with arched corners are preferable. It is impossible to extrude sharp corners, but it is sufficient with a radius between 0.5-1 mm. SAPA also recommend small variations in the wall thickness even though the different thickness is often acceptable. The recommendation is to ensure an even material flow during the extrusion process and finished profile. As an exception, for profiles designed for high bending resistance, the mass should be placed far away from the neutral axis as possible. With this design principal, the wall thickness may vary with thicker walls further away from the neutral axis.

2.3.2 Friction Stir Welding

Because of strength reduction during welding of aluminum, The Welding Institute of UK invented FSW in 1991 as a solid state joining technique. It is classified as a solid state joining technique since the temperature does not exceed the melt temperature of the workpiece. FSW consists of a non-consumable rotating tool with a shoulder and a pin as illustrated on Figure 5. The tool has two primary functions, heat and stirs the material to create a joint. Heat is a result of friction and plastic deformation of the workpiece. The tool is plunged in the material until stopped by the shoulder and translated along the weld direction when rotating. Local heat and movement of material make an FSW by local plastic deformation. Concerning the development of metal joining Mishra et al. [17] states that FSW is the most significant invention in a decade. This statement is a result of FSW energy efficiency, environment friendliness, and versatility. Other benefits with FSW are listed in Table **1**.

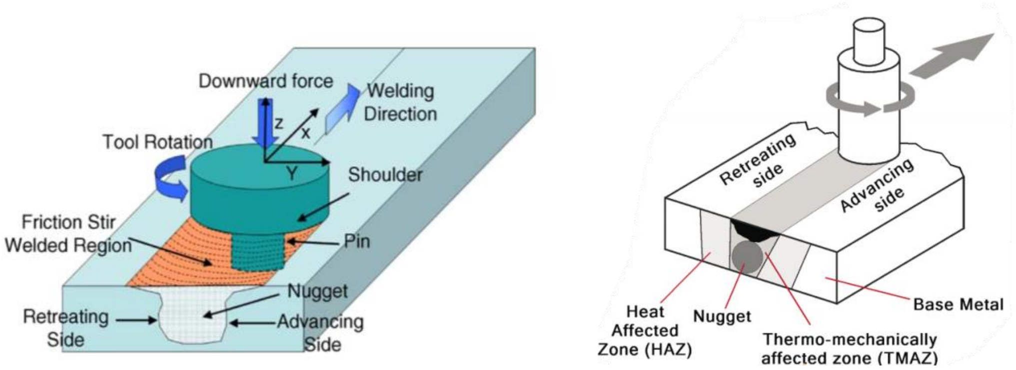

(a) (b)

Figure 5: a) Tool geometry, b) Weld affected zones.

Table 1: Key benefits of friction stir welding [17].

Key benefits of friction stir welding

Metallurgical benefits	Environmental benefits	Energy benefits
Solid phase process	No shielding gas required	Improved materials use (e.g., joining different thickness) allows reduction in weight
Low distortion of workpiece	No surface cleaning required	Only 2.5% of the energy needed for a laser weld
Good dimensional stability and repeatability	Eliminate grinding wastes	Decreased fuel consumption in light weight aircraft, automotive and ship applications
No loss of alloying elements	Eliminate solvents required for degreasing	
Excellent metallurgical properties in the joint area	Consumable materials saving, such as rugs, wire or any other gases	
Fine microstructure		
Absence of cracking		
Replace multiple parts joined by fasteners		

Concerning fatigue strength, FSW is shown to be better than both metal inert gas (MIG) welding and laser welding. This increased fatigue strength is because of the finer and more uniform microstructure for the FSW weld. The fatigue life is very much limited to surface crack initiation and significant improvement to the fatigue life can be obtained by removing a layer on both top and bottom side of the weld [17].

Aluminum is known for its excellent corrosion resistance, and in principal, FSW does not add or change the chemical composition of the base metal so the corrosion resistance should stay unchanged [18]. FSW produces different zones with differing microstructures as illustrated in Figure 5 b). These zones exhibit different corrosion susceptibility. Studies of pitting and stress corrosion cracking behavior shows that these are the most dominant in FSW welds. FSW welds showed higher pitting resistance than the base alloy [17]. Another paper by Gharavi et al. [19] concluded that FSW is susceptible for pitting corrosion and intergranular corrosion.

A limiting factor concerning FSW is the issue of clamping. Clamping is important to obtain joints with good mechanical performance. Since FSW is a solid-state process, it requires higher clamping force. A good FSW depends on several factors, and the FSW must be carefully controlled. Significant reduction in quality may be the result if the process is not monitored. Another downside with FSW is the lack of capability to weld structural joints. The amount of pressure needed to do a proper FSW makes it difficult to utilize robot arms. The largest stress is found in the joints and connection of structures. Conventional fusion welding together with bolting is the only alternative. Hopefully, new technologies like the hybrid metal extrusion & bonding developed by HyBond at NTNU can be utilized for such use in the future [20].

2.3.3 Fusion Welding

Welding is the joining of two surfaces by a coalescence of the surfaces in contact. When the two surfaces are joined by melting, it is called fusion welding. Fusion welding can roughly be placed in two main categories. Tungsten inert gas welding and MIG welding. An ideal weld would have the same properties in weld material HAZ and base material, but this is not the case for aluminum [21]. Possible defects Gene Mathers [21] lists in his book; Gas porosity; oxide inclusions and oxide filming; solidification (hot) cracking; reduced strength in the HAZ; Lack of fusion; reduced corrosion resistance; reduced electrical resistance. When designing a construction in aluminum the strength reduction in the HAZ is the most critical defect. A decrease in strength up 50% can occur as shown in Figure 6. Concerning the stiffness of the material in the HAZ, there is no to a little change in Young's modulus. The binding forces between atoms determine the modulus of elasticity and are one of the most structure-insensitive mechanical properties [22]. Heat treatment has therefore only a slight impact on the stiffness, as illustrated in Figure 6.

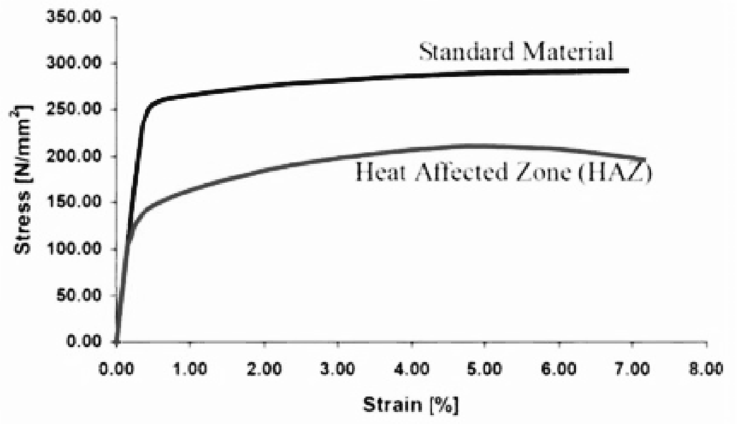

Figure 6: AA6082 T6 stress-strain curve of base material and HAZ [23].

2.4 Bridge Material Comparison

Traditionally bridges are constructed with combinations of materials to obtain the optimal solution. As an example, the lightweight London Millennium Bridge is built with a material combination of steel and aluminum. The bridges have a steel structure and a light aluminum bridge deck. As mention in Section 2.2, the strength to weight ratio is of high importance for aluminum. The comparison chart compares a variety of construction materials in Figure 7. The chart illustrates the deviation in material properties. The material offering the greatest specific stiffness-to-weight ratio lies towards the upper right corner. Concrete has a significantly lower specific strength compared to all the other construction materials. Concrete also has a lower specific stiffness. Steel and aluminum come better out of the comparison whereas GFRP comes a bit lower. Aluminum is closely related steel in this comparison but has a greater potential. Carbon fiber reinforced polymer is arguably the material with the highest specific modulus – Specific strength ratio.

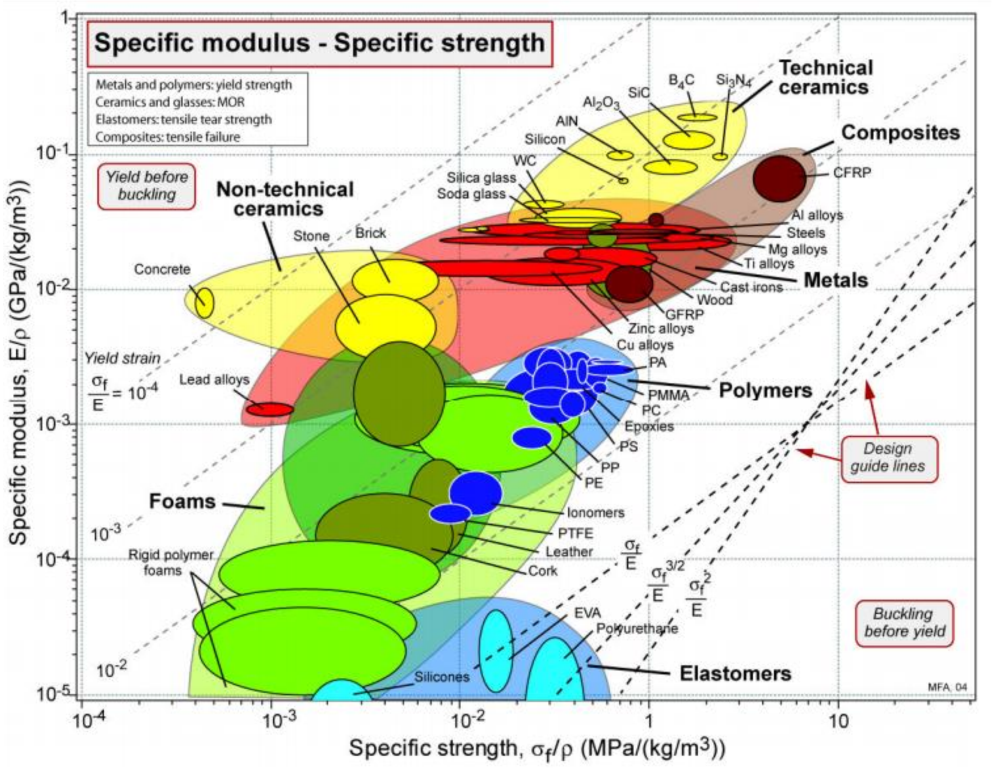

Figure 7: Specific Youngs modulus – Specific Strength comparison chart [24].

Polymers and fiber reinforced polymer material is gaining its popularity in bridge constructions due to low density, high chemical resistance, dyeability and simple forming processes. The downside polymer is lower E-module, high rheological forming, low thermal resistance and aging due to UV radiation [2]. It is also hard to predict the degradation of the materials due to temperature, environment and mechanical damage. There is still a significant need for research in this area. There is ongoing work on establishing a Eurocode for FRP bridges [2, 25]. Like aluminum, reduced weight, pre-fabrication and reduced installation time are often the arguments for composite bridges. One of the significant issues with composite as of today is the absent possibility of recyclability [2, 25]. Tension strength of GRFP can vary between 130-600 $\mathrm{N/mm^2}$ and can obtain an E modulus of 55,000 $\mathrm{N/mm^2}$ [2]. These values determined the strength in the longitudinal direction of the fibers. Load transverse of the fibers will give a much lower resistance. Good design can avoid this issue.

Another material that has gained some popularity in the bridge building sector the last years is weathering steel. This steel corrodes 6-8 times slower than regular steel under optimal conditions. Weathering steel forms an initial layer of corrosion which slows the process of further corrosion. In areas with road salting in the winter, this protective rust layer is found to have little effect [2].

2.5 Existing Pedestrian Bridge Solutions in Aluminum

Aluminum has been used as a bridge material for almost 100 years now. Since the early aluminum alloys in bridge construction, they are now 1.5 times stronger. Accounting the inflation, they have essentially the same cost [1]. Demitris Kosteas [6] states that seven pillars support the success and economically attractive application of aluminum in structures; light weight; extrusion; joint design; reliability; durability; acquisition and life-cycle cost; sustainability.

Several aluminum pedestrian bridges have now been built around the world with great success both onshore and offshore. Due to the development of knowledge and availability of aluminum the last decade, a pedestrian bridge in Germany, 2008 was estimated a price of 140.000 Euro compared to 300.000 Euro for a similar concrete solution [2]. Often bridges are built in steel or concrete. Sebastian Joux [4] write that the two main advantages of aluminum in complete LCC are longevity and low maintenance. Due to these two benefits, the to two pedestrian bridge examples studied in the article gave the best return on investment compared conventional materials. In the later years, a lot of companies have come to the market with aluminum pedestrian bridge solutions. The German based company PML and their partner in Australia, Landmark, started to deliver systems for large spans between 25 – 80 m in 2007. Bridges of 40 – 50 m in length and 2 – 3.5 m wide is delivered in the price segment of 115,000,- Euro – 200,000,- Euro [26]. That is equivalent to 1.1 – 1.9 MNOK with a currency of 9.5 NOK per 1 Euro. Also, other companies like Excel, Gator, Maadi, and Glück deliver similar solutions for aluminum pedestrian bridges. Glück claims to be the market leaders in aluminum pedestrian bridges, with over 540 structures in a variety of country’s [13].

Tomasz Siwowski concludes in his paper [1] that an effort to reduce the initial cost would increase the competitive advantage of aluminum. He also states that aluminum in bridges has a favorably LCC which further increases aluminum's potential in bridge building. A life-cycle cost analysis (LCCA) consist of four stages; development-design-material; fabrication-transport-assembly-erection; disposal-recycling; service-maintenance [6]. Studies shows that with an assumed equivalent acquisition cost it only takes 10 – 20 years before a breakeven point is reached [6]. This study is illustrated in Figure 8 from a MAADI Group study, Canada in 2011. The lifetime of a bridge is often more than 100 years, and significant money can be saved be choosing aluminum.

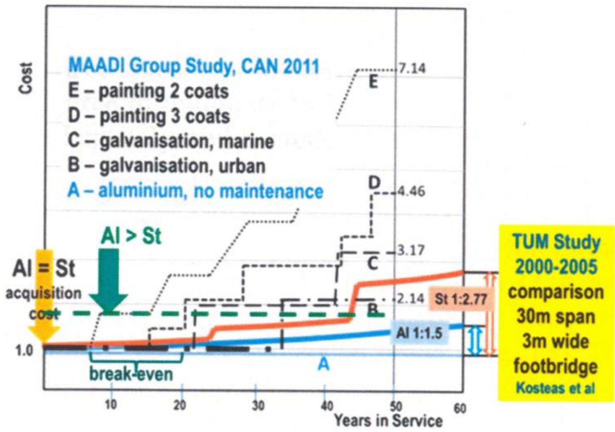

Figure 8: Life-cycle costa comparison [6]

Structural weight plays a major role concerning the acquisition cost. Earlier Norwegian studies state that if aluminum structures reach a 50% weight reduction compared to steel structures, the acquisition price is equal [6]. This estimate is now attained by pedestrian bridges as well [6]. Comparison of acquisition cost is rather rare for pedestrian bridges. This comparison is rare due to lack of access to details of bids, the material price usually just "arbitrary" set, final details and cost are adapted later in design stages [6]. The different stages in the bridge lifetime are so different that a comparison between aluminum and some bridge materials makes no sense. However, some estimates of acquisition prices are made as illustrated in Figure 9. This comparison is for a 31.7 m long and 2 m wide bridge in the UK which is based on actual bids from 2014. Due to the much lower acquisition price for the stairs and support solutions in aluminum, the total acquisition price is much lower for the untreated aluminum bridge. Even though it is hard to compare acquisition cost, the building sector still makes most of their investments based on acquisition cost and warranty condition. This fact is most likely to do with lack of knowledge and availability of data [6]. Aluminum will gain significant benefits compared to many other construction materials when LCCA gets more accepted and used.

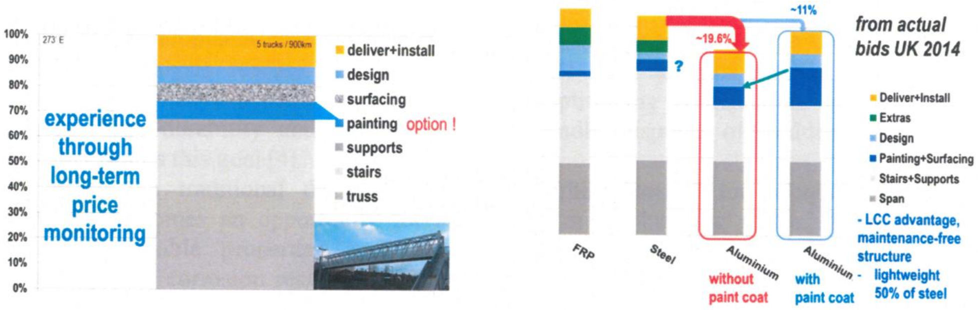

Figure 9: Cost breakdown of 31.7 m long closed frame truss bridge (left). Initial cost comparison for FRP – Steel – Aluminum (right).

2.6 Design Aspects for Pedestrian Bridges

The primary function of a pedestrian bridge is to allow people to pass obstacles safely. People directly experience the pedestrian bridge, and that's what makes them unique compared to road bridges and railway bridges. People walk over it, looks at it and touches it. That is why the bridge functionality requirements is to be so precisely analyzed and defined [27]. How a pedestrian experience to go through a closed frame truss compared to an open truss bridge are aspects to consider in the design phase. Inclined trusses or arches will result in a wider bridge construction. The pedestrian needs a finite amount of height under the arch or truss. To maintain the height above the walkway, the bridge needs to be wider. For prefabricated bridge design, this is not preferable, due to transportation and installation. In a meeting with two architects at NTNU [28], it was told that almost all bridge types could be esthetically nice if the detailing is executed properly. Detailing could be, joint design, surface finishing, railing, and lighting. These details have much to do with the closer user interference between the pedestrians and the bridge itself. Further, in this chapter, truss bridges and tied arch bridges are more explained in Section 2.6.1 and 2.6.2.

2.6.1 Truss Bridge

A truss structure consists of individual straight members which are connected at joints. It is assumed that the joints permit rotation and that the structural members only carry axial force in either tension or compression. In reality, the joints often do not allow free rotation and will introduce some bending effects to the members [29]. Truss structures are very efficient and use minimal of material and is therefore lightweight [29]. It can both be statically determined and undetermined according to the Equation 1 for a 2D truss. b: bars, j: joints.

Equation 1

$$b = 2j - 3$$

The lightest bridge structure is the simple statically determinate truss structures. For instance, the Warren truss and Pratt truss. The Pratt truss compared to the Howe truss has shorter compression elements. The Howe truss diagonal members are the compression elements which makes them a fraction longer than for the vertical compression members in the Pratt truss. The Warren truss is more economical as it requires less material on shorter spans than the Pratt truss. However, the Warren truss may be for a bridge over 40 m long, require a greater depth at the center [30]. Figure 10 illustrates the different truss configurations.

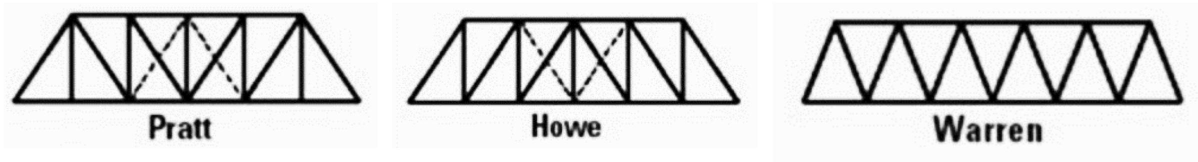

Figure 10: Truss statically determinate configuration [31].

As general rules for truss structures in steel, Kumar et.al [30] suggest that an even number of truss bays should be chosen. An even number of truss bays will avoid a central bay with crossed diagonals. Kumar et.al recommends that the angle of the trusses to be between 50º and 60 º to the horizontal. Thesis angels are recommended to have a coincident intersection point between the members to avoid bending stresses. [30, 32] Kumar et.al gives the optimum value for the span to depth ratio in the region of 10 depending on the loads applied to the bridge. Concerning the compression members, they should be designed with minimal length. The compression members should also have equal slenderness value in both directions. Tension members should be as compact as possible. For an open truss configuration, the upper chord in compression is in risk of lateral deflection. Transverse stiffeners may be added between the two upper chords. Transverse stiffeners make an efficient stabilization. On the other hand, this will change the characteristics of the bridge. The user now walks through the support structure as mention in Section 2.6.

2.6.2 Arch Bridge

As a form of support structures, the arch is one of the oldest in bridge constructions [27]. Relevant parameters when designing the arch is the starting point of the arch and the height of the arch. An unchangeable combination of an economical and efficient support structure is the ideal combination for arch design. If not, bending stresses and normal stress will occur in the arch and make material use much greater by increasing the dimensions [27]. Deflection in the arch can result in further deformations of the arch and increased stress. This phenomenon is called a geometrically non-linear effect for small deformation in the structural analysis [27].

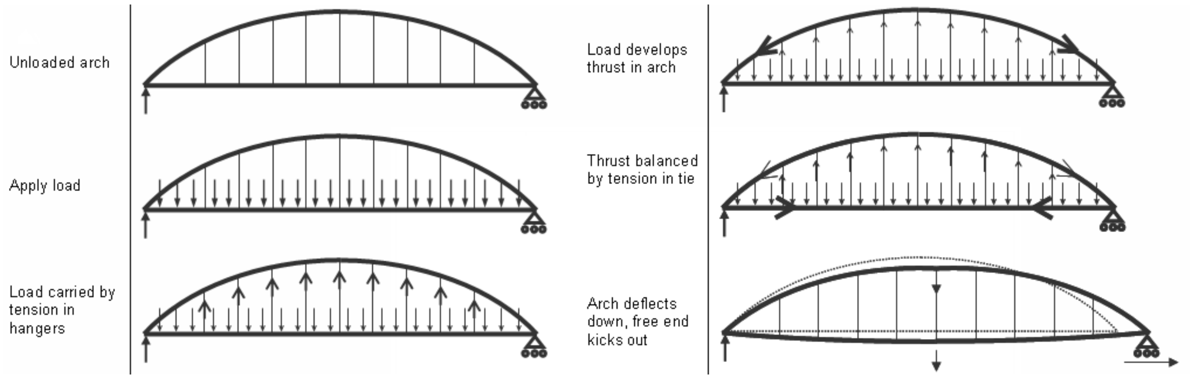

Figure 11: Tied arch bridge [33].

There are mainly two kinds of arch bridges. The standard arch bridge where the horizontal shear component is transferred to the ground below. Moreover, the tied arch bridge is where the horizontal component is transferred by a tension member in the bridge deck or through the hangers in a network arch bridge [27]. Figure 11 illustrates the load transfer in a tied arch bridge, with vertical hangers. The main advantage with the tied arch bridge is that the subsoil only takes on the vertical force from the bridge. This advantage makes it possible to prefabricate the bridge and assemble the entire structure at once.

The most common type of arch bridges has vertical hangers. This way the hangers only act as tension members. By applying crisscrossed hangers, some global shear forces will be transfers along the span as well. Full shear transfer through the triangulated web can be obtained by substituting the hangers with truss members. With this substitution, the bridge is now called a bowstring truss bridge [33]. The optimal rise of an arch bridge is approximately one tenth of its span length. Greater arch forces will be the result if a lower arch height is chosen [27].

2.6.3 Bridge Deck

There exist several types of bridge deck configurations on the market. Typical for aluminum, is bridge decks with different stiffness in longitudinal and transverse directions. These bridge decks are called orthotropic bridge decks. The bridge deck developed for Florida Department of Transportation [34] is an orthotropic bridge deck, stiffened in the transverse direction. The Alumabridge deck is engineered to withstand 44.5 kN from wheel patches of 254x508 [mm^2]. The bridge deck panels oriented perpendicular to the traffic direction and the top of the stringers act as a support. The weight without wearing surface is 85 kg/m^2 [35]. According to the report [34] on bridge decks, this was the absolute best solution for replacing the bascule steel grid decks. The results from the bascule bridge reports [34, 35] show that there are significant advantages of utilizing aluminum in bridge decks. For a pedestrian bridge application, orthotropic aluminum bridge deck would be a great benefit. The bridge deck would serve as a good point load distributor to surrounding structural members. It will also add stiffness to the superstructure. Figure 12 shows a draft of a typical orthotropic bridge deck design. This design has extruded profiles FSW together in larger configuration; this method gives fast and easy assembly [34].

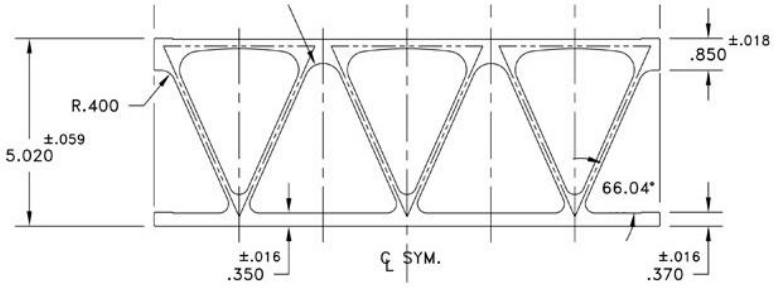

Figure 12: Alumabrige 5” Bridge deck.

2.6.4 Wearing Surface

Concerning wearing surface the report of bascule bridges [34] considered two light weight, wearing surfaces. Thin polymer overlay wearing surfaces and hot spray applied metal overlay. The main factors considered in their report when choosing a skid resistant overlay is; the unit weight; skid resistance; service life; wear resistance; bond strength; ultraviolet light resistance; chemical resistance and corrosion; tensile (flexural) strength; maintenance [34]. Lack of knowledge and experience with long-term use makes no one of the two solutions applicable. Asphalt is one of the most utilized wearing surfaces on roads and bridges. Asphalt is used to increase the durability of the bridge and protect the bridge from possible defects. For instant intrusion of salts can be harmful to the bridge structure and lead to severe corrosion attacks [36]. The biggest downside with asphalt is high density. A significant weight reduction of the bridge structure could be obtained if the development of wearing surfaces continues.

2.6.5 Transportation and Installation

There is no definitive solution to the transportation, and each transportation route needs to be studied individually. Sverre Fordal at Prøven Transport [37] claimed that there is rarely a problem with a transportation length of 30 meters. The total height should not be higher than 4.5 m. Length above 35 m needs escort cars which make the transportation more expensive. Concerning transportation of a prefabricated bridge, there will be a demand from the government that the bridge is transported to the nearest dock [37]. This requirement is to minimize transportation time onshore. Bridge modules under 3 m wide, 15 – 16 m long and 3.5 m high are referred to as a standard transportation job. For loads wider than 3 m it is required to have escort cars. For loads, over 23 m just a simple approval is needed to do the transportation job. Installation of the bridges are also an important aspect of the bridge design. As an example of the escort cost of a 30 m long and 4 m wide load can be 25k NOK during a night [37]. A street with a speed limit of 30 – 40 km/h and an annual average daily traffic (AADT) 0 -4000 and AADT heavy < 100 the road profile is 6 m wide including the clearance to the edge stone. Whereas the narrowest type of national roads with an AADT < 12 000 and a speed limit of 60 km/h is 7.5 m including road shoulders [38]. These road requirements illustrate the importance of the transport dimensions.

Loading and unloading the bridge of ships with a single crane needs to consider an engineering design requirement. Along the Norwegian coast, there are cargo ships with crane capacities between 50 – 80 tons. A normal strap angle is 45° under lifting and 60° for heavier loads. These strap angels can provide an issue concerning the total height of the crane if the lifting points are far apart. On location where the distance between each mobile crane can be miles apart. The cost of hiring one for unloading the bridge from the cargo ship can get significant. Proper transportation equipment and reduction of the crane capacity demand could give a significant cost reduction.

Where the bridge is installed over a road, the crane can be located at the center of the bridge with a minimized radius. If the bridge crosses a river or a densely trafficked road, the crane must be placed at the end of the bridge. The crane gets half of the bridge length as the radius with this solution. Figure 13 shows a complete solution from assembly to complete installation of an aluminum pedestrian bridge in Germany. This solution is based on solution 3 in Table 2 and two cranes for installation. Other installation methods can be sliding the bridge in place. This method is expensive and space demanding.

Figure 13: Aluminum pedestrian bridge assembled and installed over A5 in Germany [39].

Table 2: Transportation alternatives.

1

Pros: - Utilize most of the transportation height **Cons:** - Short transportation length 4.5 – 11m
2

Pros: - Versatile and no demands for custom equipment. **Cons:** - Both reduced transportation height 0.3 m and length 4.5 m
3
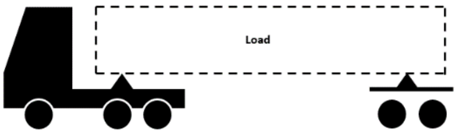
Pros: - Utilize the total transportation length of the truck **Cons:** - Give a reduced transportation height between 0.3 -0.5 m
4
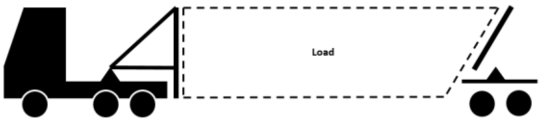
Pros: - Utilize the total height of 4.5 meters. - Can handle length up to 35 meters - Flexible - Can be designed to load the bridge without the help of a crane **Cons:** - Demands custom transportation gear

[This page is intentionally left blank]

3 Baseline solutions from the Norwegian Public Road Administration

As case studies, two bridges have been found accessible and relevant for an aluminum pedestrian bridge concept study. The bridges are further explained and evaluated for their feasibility for introducing aluminum.

3.1 Forus Bridge

The Forus bridge crosses Fv44 in Stavanger and is a part of the municipal development plan of Park-2020 “10-minutes city”. Because of this development plan the bridge is thought to be a landmark of the promising future with a monumental expression. The diagonal arch bridge design was chosen because of its landmark esthetics and affordable price. The arch was proposed in steel with the dimensions Ø610x40 [mm] with an arch height of 13 m from the bridge deck [40]. The bridge has a free span of 40 meters. The bridge deck consists of two longitudinal load bearing beams Ø508 [mm] and transverse beams with a scatter distance of 4,0 m [40]. Due to minimum free height, the transversal beams must be elongated to fit the cable anchors. Even though the bridge is proposed built in steel, new requirements have stopped the progress. With an AADT > 8000 no periodic maintenance is allowed per N400 1.1.3.3 [5]. As commonly known, steel corrodes and needs surface treatment with periodic maintenance to hinder degradation of the structure.

Figure 14: Forus Bridge.

3.2 Paradis Bridge

Paradis bridge as illustrated in Figure 15. The bridge is a proposed pedestrian bridge developed as an alternative for a stainless-steel truss bridge [41]. The Dutch company Royal HaskoningDHV (RH) in cooperation with NPRA has developed the bridge concept. No periodic maintenance, a single span of 42 m, quick installation time of less than 72 hours and easy transportation and building on the site. These requirements were the main demands of the Pardis bridge. The Paradis bridge is the first FRP bridge for NPRA. Challenges when designing an FRP bridge is to develop a bridge deck suitable for spike tires. The wet and cold climate in Bergen and Norway in general, vibration, buckling, creep, joints and cost were also challenging for RH and NPRA [41].

In the initial development of the bridge, the material of choice became GFRP with steel joints. The steel joints are both bolted and adhesively connected to the FRP structure [41]. The FRP constituted only 42 tons of the total mass of 87 tons. The remaining 45 tons consist of asphalt and steel parts. Substitution of the asphalt wearing surface with a lighter wearing surface will give a huge weight reduction.

Figure 15: Paradis Bridge.

3.3 Evaluation

The composite bridge in Paradis was chosen as the reference bridge for developing an aluminum pedestrian bridge. This choice was based on Marine Aluminum experience of building truss based pedestrian bridges for the offshore market. A meeting with Marit Reiso [42] at ÅF Engineering also highlighted the Paradis bridge as the most suitable case for introducing aluminum. GFRP and aluminum are two good material options for lightweight bridge structures. Since these two materials have many of the same properties, they are therefore interesting for a comparison study.

4 Product Development

4.1 Development Process

To illustrate the development process of the aluminum bridge, the IPM model has been utilized. Figure 16 shows the model. This model is a simplified version of the Cooper's stage-gate model [43]. For every stage, there is a milestone. At each millstone, a decision is made either to go back, terminate or proceed the development process. As this model is mainly descriptive rather than prescriptive, Design for X (DfX) is utilized as a guide and principle. The guidance and principals are follow when evaluating the different concepts during the product development process. Design for X is explained in more detail in Section 4.1.1. The book Product Design and Development [44] have been used to evaluate some parts of the concept development as well.

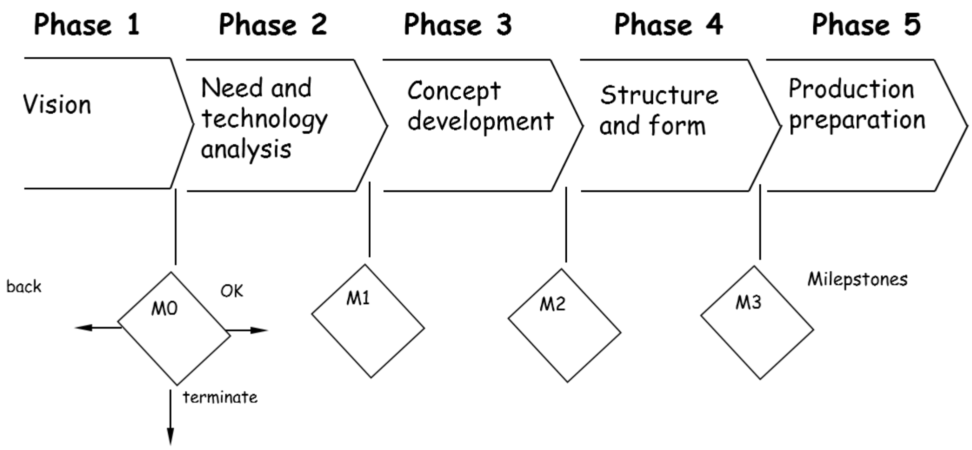

Figure 16: IPM model.

4.1.1 Design for X

Products have several abilities which are created under the development process. These abilities are often named by the common term “X” which creates the term DfX [45]. Design for manufacturing (DfM) and assembly (DfA) is two of the most important aspects to consider when designing a bridge. A lecture handout from the New Mexican University (NMU) [46] states that design decisions determine over 70% of the manufacturing costs of a product. These design decisions include the cost of material, processing, and assembly. This statement is contrary to production decisions that are claimed to just be responsible for 20%. Design for X could be seen as a strategy, method or knowledge base, but cannot be interchanged with an overall product development process [45]. A list of relevant aspects of a good DfM and DfA gathered from the Sintef report [45] is shown below. The lecture handout from NMU also stresses the importance of using standard components and avoid separate fasteners.

1. Minimize the amount of parts
2. Develop a module based construction
3. Minimize the variation between the parts
4. Design multifunctional parts
5. Design parts for easy manufacturing
6. Minimize the assembly direction where a top-down approach is desirable
7. Symmetrical parts to avoid orientation directions
8. Exaggerate unsymmetrical parts for ease of orientation
9. Avoid flexible (soft) components

4.2 User Demand Specification

<table>
<tr><td colspan="5">User Demand Specification</td></tr>
<tr><td colspan="2">Product:
Pedestrian Bridge in Aluminum</td><td>Written by:
CARB</td><td>Approved:</td><td>Page:
1 of 4</td></tr>
<tr><td colspan="3">Description</td><td>“demand”</td><td>“whishes”</td></tr>
<tr><td colspan="3">1. Function demands
1.1. Dimensions [41]

External: Single span. 42 m. Width. 7 m.
Internal: Width 6 m. minimum height 3.1 m

According to V129 [47] the slope of the bridge cannot exceed 1:20 (5%).

The minimum free width of a pedestrian bridge is 3m between the hand railing according to N100 [38]. If the width exceed 6m complementary load models has to be considered for each project [48].</td><td>√</td><td></td></tr>
<tr><td colspan="3">1.2. Weight of Paradis Bridge [41]

Superstructure < 42 tons
Total weight < 87 tons</td><td></td><td>√</td></tr>
<tr><td colspan="3">1.3. Bridge deck

Suitable for spike tires [41]</td><td>√</td><td></td></tr>
<tr><td colspan="3">1.4. Loads
1.4.1. Vibrations from pedestrian load [48]:

Vertical direction frequency ranges from 1-3 Hz
Horizontal direction frequency range from 0.5 – 1.5 Hz</td><td>√</td><td></td></tr>
<tr><td colspan="3">1.4.2. Distributed load from pedestrians [48]

Dimensioning model LM4: 5 $\mathrm{kN/m^2}$

Horizontal force Q_{flk} action along the bridge deck axis at the pavement level should be considered for footbridges only. According to section 5.4 [48].

- 10% of total uniformly distributed load.
- Or 60% of total weight of service vehicle.

The forces are considered as acting simultaneously.</td><td>√</td><td></td></tr>
</table>

User Demand Specification			
Product: Pedestrian Bridge in Aluminum	Written by: CARB	Approved:	Page: 2 of 4

Description	"demand"	"whishes"
2. Function demands 2.1.1. Service Vehicle: Yes	√	

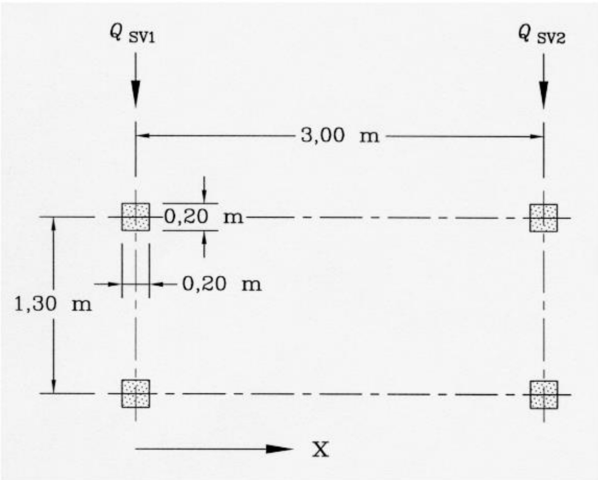

Key
x : Bridge axis direction
$Q_{sv1} = 80$ kN
$Q_{sv2} = 40$ kN

2.1.2. Snow loads [49]	√	
NA.A2.2 [6] - Snow loads shall generally not be combined with gr1, uniformly distributed load and gr2, service vehicle. Since the snow load is smaller than the distributed load, snow loads are neglected.		
2.1.3. Wind load [50, 51]:	√	
The wind loads are calculated for the specific location at Paradis in Bergen and is taken from the AIP file provided by the Public Road Administration:		
Peak pressure: $q_p(z) = \ 0.75 \text{ kN/m}^2$ Longitudinal: $W_x = 0.4 \text{ kN/m}^2$ Transversal: $W_y = 1.7 \text{ kN/m}^2$ Vertical: $W_z = 0.7 \text{ kN/m}^2$		
Per N400 5.4.3.3 there is no demands for simultaneously control of wind and traffic loads on separate pedestrian bridges.		

User Demand Specification				
Product: Pedestrian Bridge in Aluminum	Written by: CARB	Approved:	Page: 3 of 4	
Description			“demand”	“whishes”
3. Function demands 3.1.1. Thermal loads [51, 52]: The temperatures are from the area of Bergen city. Hottest temperature: $T_{e,max} = +34℃$ Coldest temperature: $T_{e,min} = -20℃$ 3.1.2. Static deflection [51]: $L/350$ [5], L is the length of the considered span. 3.2. Surface and subsurface drainage. [5] (1% longitudinal direction and 2% one sided in other) For retaining walls and abutments perforated drainage pipe shall be provided. 3.3. Capable of single crane lift under 50 or 80 tons [37] 3.4. Road transportation limitations [37] Module size must be less than 4.5 m high and 35m long			√ √ √	 √ √
4. Market demands 4.1. Cost (Steel bridge with curved trusses 25k NOK/m^2 not included installation cost) [40].				√
5. Production demands 5.1. Joining methods Bolting, welding and FSW 5.2. Max extrusion size restriction 5.3. Prefabricated elements with minimal connections on site				
6. Design demands 6.1. Timeless design 6.2. Scalable				√ √
7. User demands				

User Demand Specification			
Product: Pedestrian Bridge in Aluminum	Written by: CARB	Approved:	Page: 4 of 4

Description	"demand"	"whishes"
8. Safety demands 8.1. Handrails [51, 53] 1,4 m high, q = 1,5 kN/m. Openings for snow is max 50x50 mm	√	
9. Environmental demands 9.1. Recyclable Easy to separate components with different alloys		√
10. Additional demands		
11. Product life demands 11.1. Design working life is 100 years [48, 51] 11.2. Quick installation < 72 hrs closure of light rails [51] 11.3. N400 1.1.3.3. AADT > 8000. No periodic maintenance [5]	√ √	√

4.3 Concept Development

By utilizing a Function-/Solution Tree [54] as illustrated in Figure 17, the concept development process is orderly to follow. This way ideas for potential problems and solutions set into order. The first and most important decisions were taken when choosing the truss structure, the orientation of the bridge deck and the joint design of the trusses. There are several types of bridge designs, such as slab, truss, arch, cable-stayed, suspension, and some other kinds, like stress ribbon bridges. Because of limitations for the thesis and since the bridge is planned prefabricated and have a medium to long span, the truss bridge, arch bridge and a combination is chosen for further development. The focus has been on developing the bridge deck, truss structure, and railings with specific aluminum solutions and associated details.

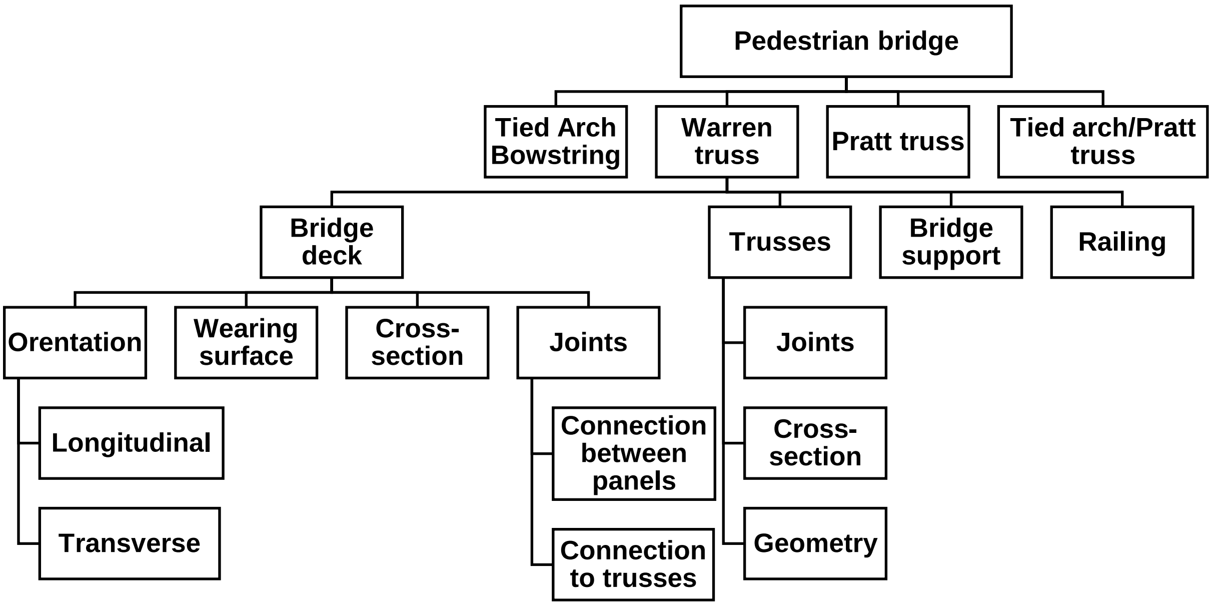

Figure 17: Function-/Solution tree.

[This page is intentionally left blank]

5 Trusses

5.1 Truss Configurations

There are requirements for the bridge to be simply supported and to be prefabricated. The most feasible alternative is tied arch bridge, and truss bridge as illustrated in Table 3. Because of the statically determinants of the Pratt and Warren truss, they are chosen for further evaluation. These truss configurations give the best weight to strength ratio. The Pratt truss is selected over the Howe truss, due to shorter compression members. Shorter compression members provide a minor reduction in buckling susceptibility. Warren truss might need a larger depth at longer spans, but it is the system with best material effectiveness for shorter spans. The tied arch bridge might be a light alternative where compression in the arch and tension in the bridge deck takes the load as explained in Section 2.6.2. The Tied arch truss bridge is a combination of the two constructions principle, where the trusses take most of the load. These alternatives are also chosen since they have their load carrying construction above the bridge deck. This design criterion gives a more versatile design where the clearance criteria to under laying roads and train tracks easier can be fulfilled. To keep the bridge design compact for transportation inwards or outwards angled trusses are not considered as feasible. Load carrying construction at the center of the bridge has the same issue where the bridge deck must be wider to keep a 6 m wide bridge deck with the clearance criteria of 3.1 m of free height.

For further evaluation, the Warren truss is chosen out of the four alternatives in Table 3. The decision is mainly based on the Warren truss material efficient construction method for shorter spans. Also, the visual aspect is found to be more appealing than the Pratt truss, which gives a more industrial expression.

Table 3: Truss alternatives.

Tied arch
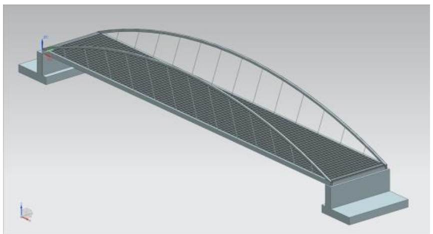
Pros: A potential light construction **Cons:** High shear forces at each end.
Pratt truss
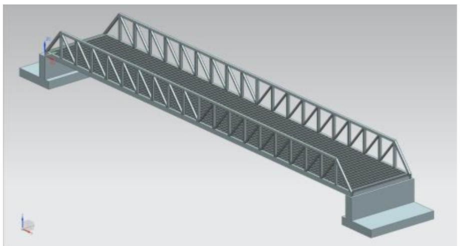
Pros: Shorter compression members than the Howie truss **Cons:** Boring design
Warren truss
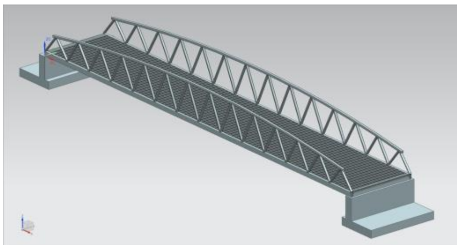
Pros: Material efficient at shorter spans **Cons:** Need a greater depth at longer spans
Tied arch truss bridge
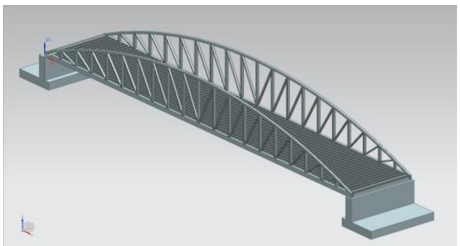
Pros: Best of both worlds? **Cons:** High shear forces at each end.

5.2 Truss Initial Analytical Calculation

As an initial estimate of the truss height, a simplified calculation is done. The bridge is considered as a simply supported beam with a distributed load q as illustrated in Figure 18. The distributed load q gives a moment, M and is provided by the 5 [kN/m^2] load. The factor of two is applied to give a better estimate and include the self-weight and combination of loads. The upper chords get compression stress, and the lower chords have tension stress. By considering the forces in the upper and lower chords as two opposing forces with a height difference. The height could be found by using the moment from q. This estimate is illustrated in Figure 18 as well. Three standard profiles from MA's assortment is used as a reference for the beam dimension size. The calculations are conducted in Excel and shown in Table 5. The reduction in strength due to HAZ in truss joints are accounted for by utilizing the force equation with the HAZ yield limit.

Table 4: Initial Truss Calculation Equations.

Equations 2:			
Moment	Force	Force from NS EN 1999-1-1, HAZ	The height, h
$M = \frac{ql^2}{8}$	$F = \frac{M_{Ed}}{h}$	$F = f_{0,HAZ} \times A / \gamma_{M1}$	$h = \frac{M_{Ed} \times \gamma_{M1}}{f_{0,HAZ} \times 2 \times A(x)}$

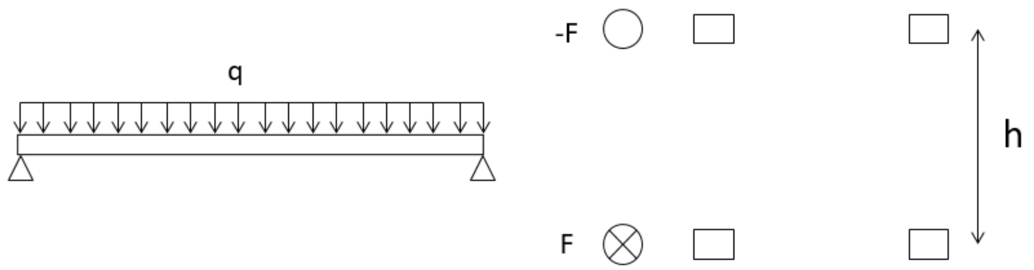

Figure 18: Assumptions for initial truss height.

Table 5: Initial truss calculations.

M [N/mm]	13230000000	
q [N/mm]	30.00	
l [mm]	42000.00	
Factor of self-weight and combination loads	2.00	
h [mm]	6288.43	h [mm]
$f_{0,HAZ}$ [N/mm^2]	125.00	
γ_{M1}	1.10	
320x320x12 [mm^2]	14440.00	4031.3
300x300x10 mm^2]	11257.00	5171.18
250x250x10 [mm^2]	9257.00	6288.43

The distance between the diagonals is chosen to give an optimal angle at each end of the truss. Optimal truss angels are explained in Section 2.6.1. The initial height of the truss is found to be 4 m for a flat truss. With the arch, an approximate average is used as illustrated in Figure 19. With an initial arch height of 2.5 m and a height of 4.5 m at the center of the bridge span. This height is exactly the maximum allowable transportation height.

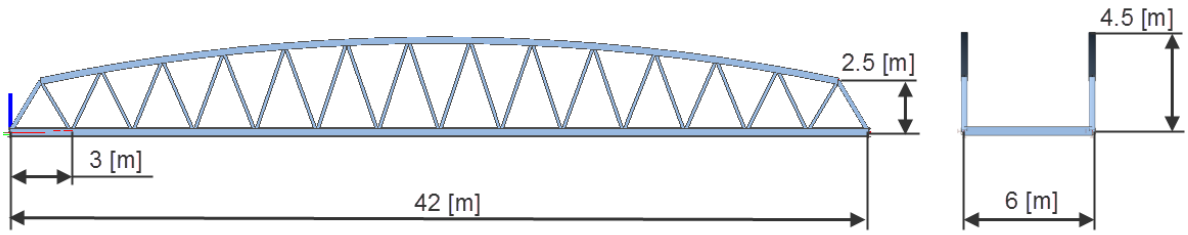

Figure 19: Initial truss design.

6 Bridge deck

During the development process, two bridge construction concepts have been found feasible. Transverse bridge deck (TBD) and longitudinal bridge deck (LBD). The Idea behind the TBD is to utilize the extrusion and FSW methods applicable for aluminum. Potentially the TBD could replace the underlying structure of the bridge. This approach could minimize the total amount of parts used in a pedestrian bridge construction. The bridge deck design is based on the helideck profiles, HMA5360 from MA.

6.1 Initial Calculation of Bridge Decks

Some simplified calculation is performed to give an indication of profile dimensions.

6.1.1 Transverse Bridge deck

Equation 3 for deflection of a beam with a point load, found in Technical Tables [55] was utilized to determine the necessary bending stiffness of the bridge deck profile. The limiting load case is the point loads from the service vehicular. Figure 20 explains the parameters in the Equation 3.

Equation 3:

$$y_{1,2} = \frac{Pc^2c_1^2}{6EIl}\left(2\frac{x}{c} + \frac{x}{c_1} - \frac{x^3}{c^2c_1}\right)$$

The deflection criteria set by de NPRA is given in Section 4.2. The super position principal is used to find the bending stiffness with two point loads. $y_1 = y_2 \rightarrow 2y = \frac{l}{350} \rightarrow y_1 = \frac{l}{700}$. Even though physical test [56] shows a load distribution of 0.2, a conservative estimate of 0.25 is used as a load distribution factor. $F = 40$ kN. $P = 0.25F$. Second moment of area about the principal x-axis:

$$I_x = \frac{0.25Fc^2c_1^2}{6EIl}\left(2\frac{x}{c} + \frac{x}{c_1} - \frac{x^3}{c^2c_1}\right)\frac{700}{l} = 7.0\times10^7 \text{ mm}^4$$

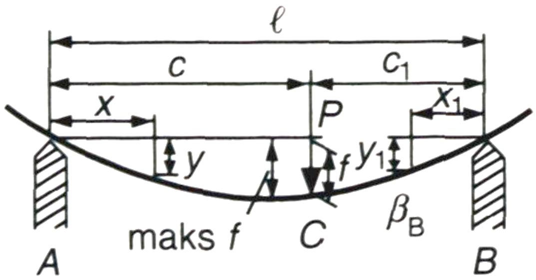

Figure 20: Beam with point load off center.

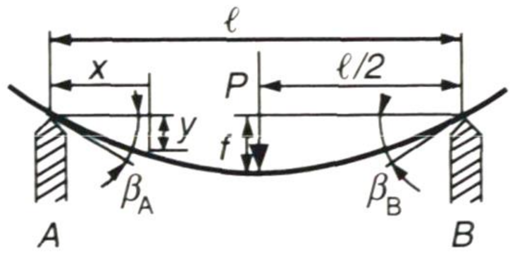

Figure 21: Point load at center.

6.1.2 Longitudinal Bridge Deck

Longitudinal Bridge Deck I-beams

With LBD I-beams, they are the weight distributing members of the bridge. The calculation is based on the same formula as the calculation conducted for the TBD solution in Section 6.1.1. The only difference is that there is assumed no load distribution. $P = F$. Which gives the second moment of area about the principal x-axis:

$$I_x = 2.8\times10^8 \text{ mm}^4$$

Longitudinal Bridge Deck Profiles

The truss joint is 3m apart. The LBD profiles need a sufficient stiffness for a 3m span. Equation 4 for the deflection of a beam with a point load, in Technical Tables [55], was utilized to find the necessary bending stiffness of the bridge deck profile. Figure 21 illustrates the parameters in the equation. The same deflection criteria are used, $f = \frac{l}{350}$. The load distribution is assumed to be the same as in Section 6.1.1, $P = 0.25F$ with $F = 40$ kN.

Equation 4:

$$f = \frac{P}{EI}\frac{l^3}{48}$$

Gives a second moment of area about the principal x-axis:

$$I_x = \frac{0.25F}{E}\frac{350}{l}\frac{l^3}{48} = 9.4\times10^6 \text{ mm}^4$$

6.2 Transverse Bridge Deck Modeling - Local Behavior

As an attempt to utilize the advantage of extrusion of complex cross-sections. The helideck profiles developed at MA transfer the point loads through torsion stiff cross-sections. MA has conducted a test on their helideck profiles of type HMA5360. This test shows a point load distribution of 80% to the surrounding profiles [56]. To evaluate the different methods of modeling the local loads from the service vehicle on the bridge deck. Figure 22 and Figure 23 illustrates the test setup with sketches. Two finite elements (FE) modeling approaches were tested in SCIA.

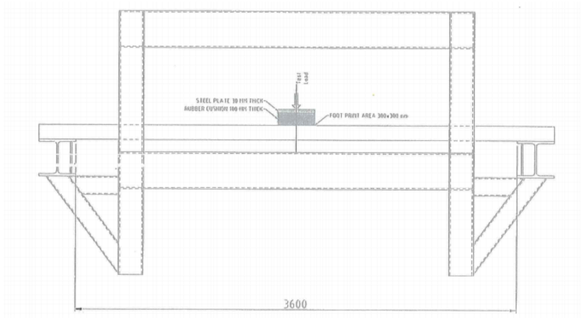

Figure 22: Longitudinal load position.

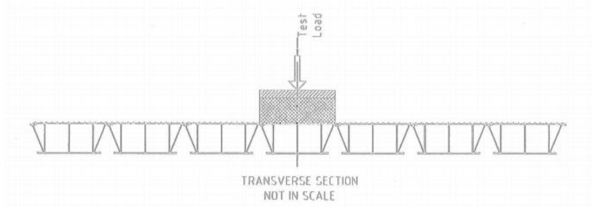

Figure 23: Transverse load position.

Appendix 1 explains method number one. The second approach is found appropriate to be applied by utilizing beam elements. An equivalent cross-section of the HMA5360 helideck profile is applied in the longitudinal direction. Point load distribution is obtained by applying beam elements with a square cross-section in the transverse direction. The height and width were adjusted to give the same vertical displacement as the physical test. The beam elements are joined with hinged cross-links. Figure 24 illustrates the cross-link. This link gives moment free couplings between the beams and the point load is placed at the center of the longitudinal center beam.

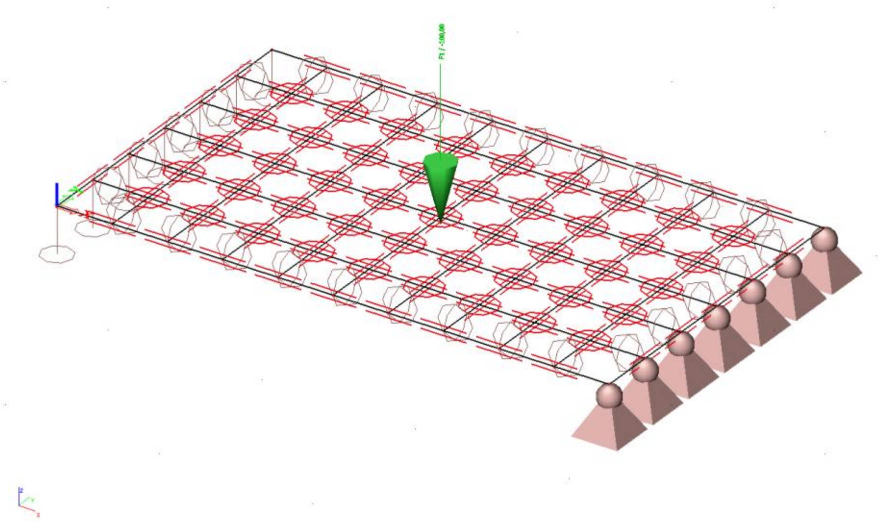

Figure 24: FSW bridge deck model.

The method showed good results for distributing the point load. The physical test conducted at MA showed a displacement of 24.15 mm at the center of the helideck test-deck. This displacement is equal to the analysis in SCIA as illustrated in Figure 25. No measurements of the deflection in the transverse direction on the physical test were conducted. Pictures from the test report show an equivalent distribution as Figure 25 shows from the analysis. The deflection is magnified on the plot. This FE modeling method is further used for the evaluation of the local bridge deck behavior.

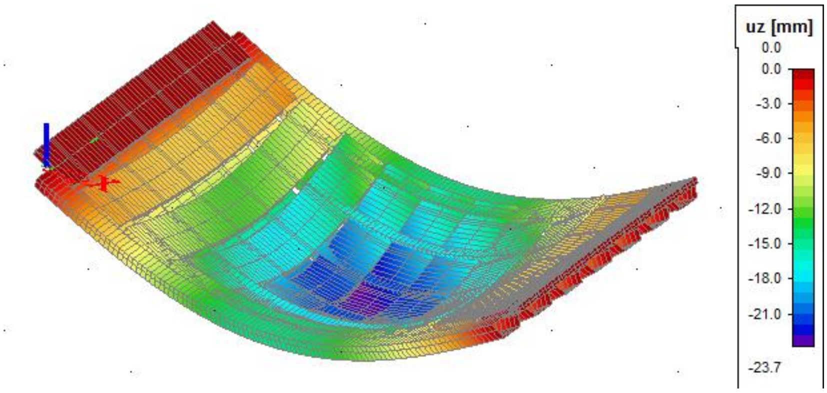

Figure 25: Vertical deflection of FSW bridge deck.

6.2 Bridge Deck Modeling – Global Behavior

If the orientation of the bridge deck is in the transverse direction, it must withstand the global shear forces. In practice, solved by utilizing FSW panels. For the local finite element analysis (FEA) with point load distribution, the bending stiffness of the transverse planks has little influence on the load distribution. The planks have therefore and arbitrary width. On the global model, this width has a large impact on the shear resistance. Therefore, the function Ribbed Slab is used to simulate the effect of an FSW-panel in SCIA.

6.3 Bridge Deck Profile

The wanted torsion stiffness is obtained with a bridge deck profile design with several closed sections. The height to width ratio also has some influence. To maintain the serenity of the load distribution from the physical test, the width was decided to be kept equal as the helideck profiles from MA. The height of the profile is the most influencing dimension concerning the moment of inertia about the x-axis. This influence can be illustrated by the second moment of area of a square or Steiner's theorem.

Equation 5: Second moment of area

$$W_x = \frac{1}{6}bh^2$$

Equation 6: Steiner's theorem

$$I_x = I_1 + b^2A$$

In Equation 6, b is the distance from the neutral axis to the neutral axis of the area A. With higher profiles, this contribution will exponentially increase since b is squared. Increasing b will have a larger impact than increasing the area A. The same can be argued based on the second moment of area of a square cross-section illustrated in Equation 5. Here the height, h is squared. Increasing the height has a larger influence than increasing the width. Figure 27 illustrates the TBD profile.

MA does not have a double sided FSW machine. Turning an FSW panel upside down to weld it on both sides are time demanding and expensive. SAPA has a double sided FSW machine in Finspong, so the technology exists. Also, the design solution as illustrated in

Figure 26 could be utilized. 100 NOK/m weld is an average estimate of FSW cost. This solution will give three times as many FSW and will increase the cost. Due to these reasons, only single sided FSW panels are considered in the evaluation. Anyhow a double sided FSW panel will give an even bigger stiffness contribution to the bridge. Almost all the FSW bridge decks out on the market are double sided [1, 34] except form the bolted solutions.

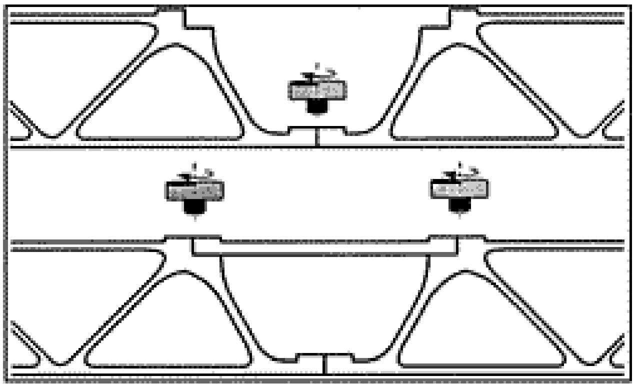

Figure 26: Hitachi design for double sided FSW panels [57].

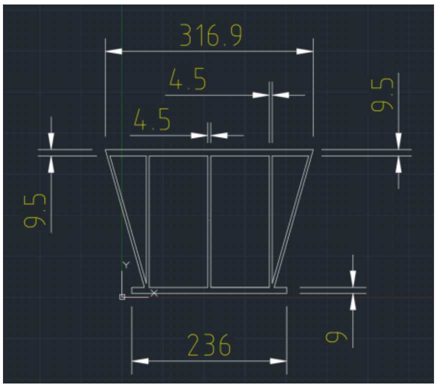

Figure 27: New bridge deck profile.

[This page is intentionally left blank]

7 SCIA Modelling

7.1 Loads

In this section, all the loads are explained in detail. Section 7.2 gives a summary of loads and load combinations.

Asphalt

The bridge is designed with an asphalt layer of 6 cm to ensure an equal basis for comparison with the Paradis bridge. This asphalt layer is equivalent to a distributed load of 150 kg/m^2. Normally a layer of 4 cm is sufficient, but snow plowing demands with 6 cm. In Trondheim municipality, all new pedestrian bridges have a 6 cm layer [58]. The load is applied as line loads on the transverse I-beams. 4.45 kN/m and 2.25 kN/m for the two end I-beams. Figure 28 illustrates the loads.

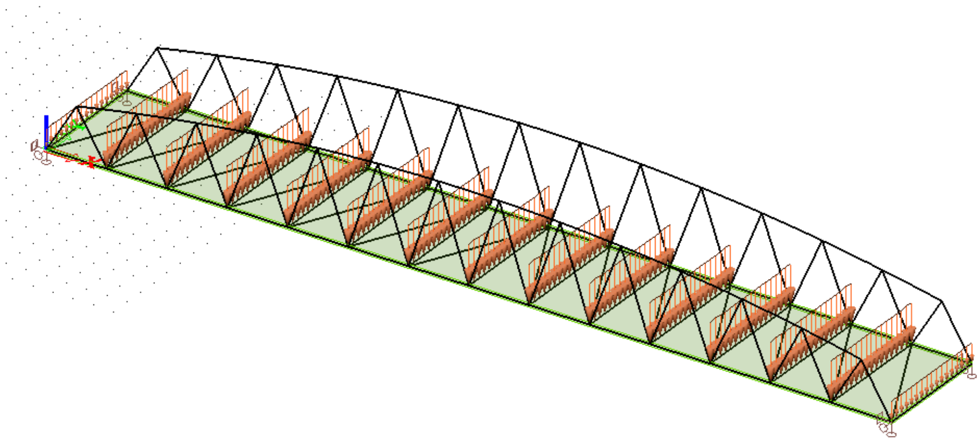

Figure 28: Distributed load spread out on the transverse I-beams as line loads**.**

Pedestrians

Load model LM4 (5 kN/m^2) from the NS EN-1991-1-2 is used [48]. The load is distributed through a load panel in SCIA and gives line loads on the transverse I-beams equal to 14.92 kN/m and 7.42 kN/m for the two end beams. Figure 28 shows the load distribution.

Self-weight of Panels for Longitudinal Bridge Deck Concept

When calculating the initial self-weight of the LBD, MA's HMA5360 helideck profiles are used as the base. This base choice is made by the calculation in Section 8. Table 6 shows the total weight estimates. The load distribution is equal to the distribution in Figure 28. Line load is -1.07 kN/m and 0.54 kN/m for the two end beams.

Table 6: Bridge deck weigh calculation.

Bridge deck weight calculation	
$q = 8 \frac{\text{kg}}{\text{m}}$	$$m = ql \frac{w_{bridge}}{w_{profile}} = 6720 \text{ kg}$$
$w_{profile} = 300 \text{ mm}$	
$l = 42 \text{ m}$	
$w_{bridge} = 6000 \text{ mm}$	To ensure a conservative weight of the bridge deck 9000 kg is used.

Self-weight of Bridge Structure

The self-weight of the structure is automatically calculated in SCIA. The self-weight of the bridge structure comes from the resultant of reaction forces in the SCIA model. The weight is calculated to be 15913 kg. The density of the aluminum is 2700 kg/m^3.

10% Horizontal Force Along the Bridge Deck

To ensure the horizontally and longitudinal stability a horizontal force is added in combination with the pedestrian load. According to EN 1991-2:2003 this force is normally adequate to ensure the stability [48]. In Equation 7 the area, A is the total area of the bridge deck, Q is the pedestrian load, and L is the total length of the bridge.

Equation 7

$$Q_{10\%} = \frac{AQ0.1}{L} = 3 \text{ kN/m}$$

The load is applied on the lower chord as a line load. The SCIA model is illustrated in Figure 29.

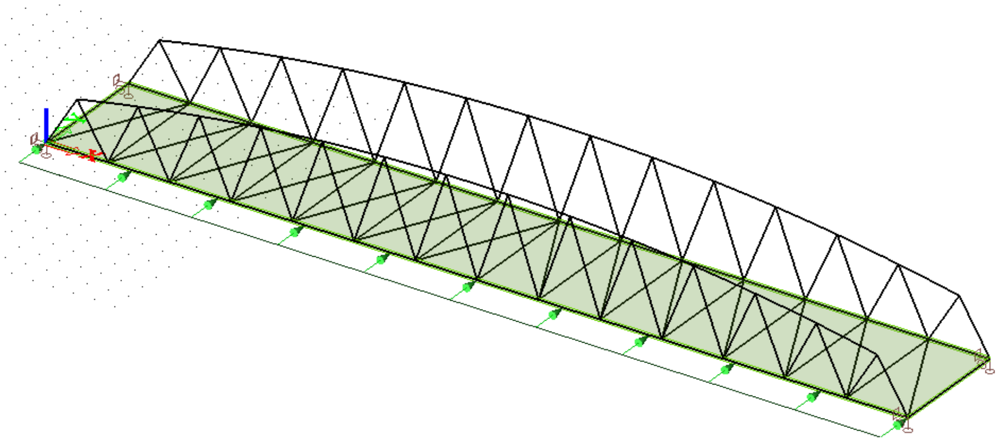

Figure 29: Vertical force along the lower chord.

Service Vehicular

The first axel has a total load of 80 kN which gives two point loads of 40 kN. The rear axle has a total load of 40 kN which gives two point loads of 20 kN. The distance between the four, wheel patches is illustrated in Section 4.2. The loads are placed at the center of the bridge. Figure 30 shows the applied load. For the splice calculation of the top and bottom chords in Section 10.4, the service vehicular is applied to the nearest I-beams closest to the splice.

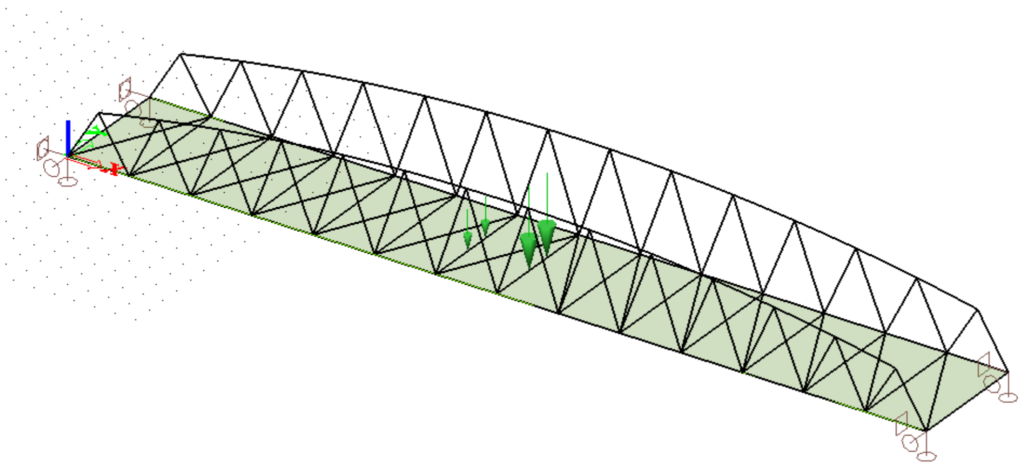

Figure 30: Point loads from service vehicular.

Wind Load

The transverse wind load is found in the user demand specification in Section 4.2. The wind load is calculated per NS EN-1991-1-4 Section 7.1.1 Lattice Structures and Scaffolding [50]. The load is illustrated in Figure 31. The solidity ratio, φ is defined by expression 7.26 in NS EN-1991-1-4 [50]:

Equation 8

$$\varphi = \frac{A}{A_c}$$

A: Sum of the projected area.

A_c: Area enclosed by the boundary of the face projected from the truss

A and A_c is found from NX computer-aided design model. $\varphi = \frac{41873091\ mm^2}{166919144\ mm^2} = 0{,}25$.

From Figure 7.33 in NS EN-1991-1-4 [50] the force coefficient c_{f0} for plane lattice structure with angle members. The force coefficient was found to be, $c_{f0e} = 1{,}6$. From Figure 7.34 in NS EN-1991-1-4 [50] the force coefficient c_{f0i} for a spatial lattice structure with angled members. The line for a box truss was utilized as the closest equivalent shape to the U-shaped truss on the concept bridge. The force coefficient is found to be, $c_{f0} = 2{,}6$. To find the c_{f0} for the second truss the differential between c_{f0e} from Figure 7.33 and 7.34 in NS EN-1991-1-4 [50]. $c_{f0i} = 2{,}6 - 1{,}6 = 1$. The line loads are calculated in Excel as shown in Table 7.

Table 7: Wind load calculation.

NS EN-1991-1-4 Wind loads: Section 7.1.1			
Wind load; W_y [kN/m^2]	1.7		
Force coefficient external: c_{f0}	1.6		
Force coefficient internal: c_{f0i}	1		
Line load: q_i	q_i=W_y*b_i*$c_{f0(i)}$		
Cross-section type	Width [m]	Line load external [kN/m]	Line load internal [kN/m]
320x320	0.32	0.8704	0.544
270x200	0.2	0.544	0.34
250x150	0.15	0.408	0.255

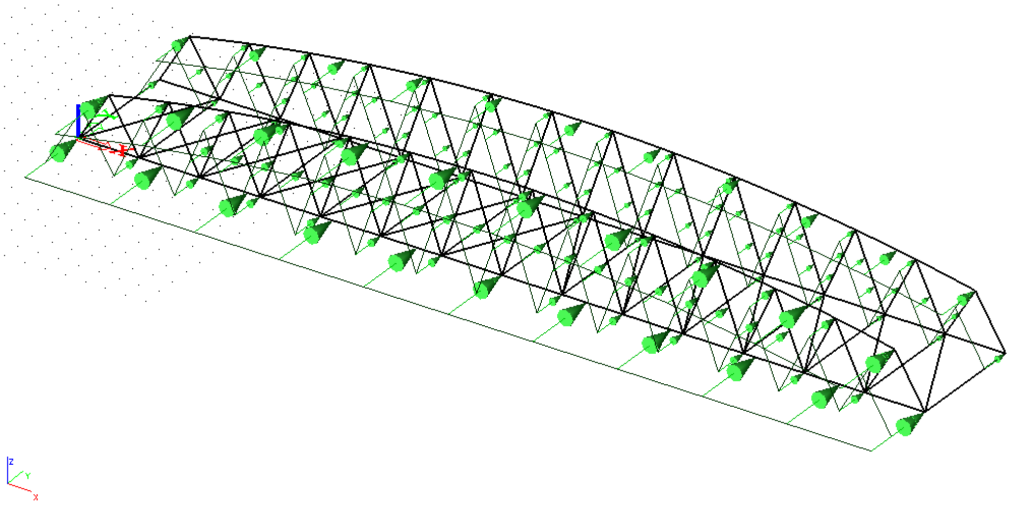

Figure 31: Wind load indicated by green arrows on SCIA model.

7.2 Summary of Loads

The loads found summarized in Table 8 with applied loads in X, Y and Z direction. Table 9 shows the load combinations (LC) used in Section 9.

Table 8: Load summary

	Description	X - direction	Y - direction	Z - direction
Self-weight		[kN]	[kN]	[kN]
1	Asphalt	0	0	371
2	Bridge deck	0	0	88.3
3	Bridge structure	0	0	157
Variable loads				
4	Pedestrian	0	0	1260
5	Horizontal Line load	0	126	0
6	Service vehicular		0	120
7	Wind	0	168	0

Table 9: Load combinations

Loads / LC*	1	2	3	4	5	6	7
1	x	x	x	x	x		
2	x	x	x			x	
3	x	x	x				x
4	x	x	x				
5							
*LC: Load combination							

7.3 Finite Element Modeling of Bridge Deck Solutions

The bridge FE model consists of beam elements connected by coincident nodes. This FE technique means that there is a stiff connection between the beam elements. The rigid connection is chosen since the truss joint is welded. The TBD beams are designed with bolted connections. With proper joint design, a rigid connection in the global model is a valid assumption. The bridge is simply supported and has supports on each end of the two lower chords. Both sides have a free rotation, whereas one side has free translation along the bridge length and the other fixed. The FE model is illustrated in Figure 33. All the profiles used in the FE model is tabulated in Table 10 and Figure 32 describes the location of the profiles. Figure 27 shows the bridge deck profile for TBD with dimensions. Table 11 summarizes the material data. The TBD profile is designed with the 6005A T6 alloy, rest of the bridge is in 6082 T6.

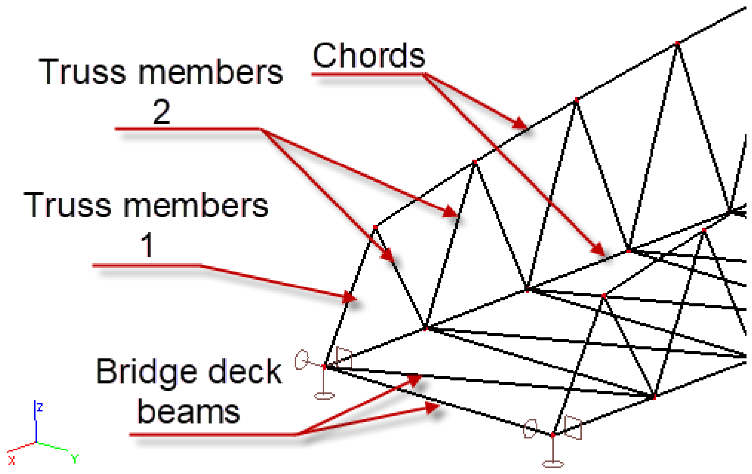

Figure 32: Bridge structure members.

Table 10: Profile dimensions.

	Transverse truss profiles	Longitudinal truss profiles
Chords	RHS 320;320;14	RHS 320;320;14
Truss members, 1	RHS 270;200;10	RHS 270;200;10
Truss members, 2	RHS 270;200;14	RHS 250;150;10
Bridge deck beams		I 420;180;15;10;21

Table 11: Material data.

	Units	EN-AW 6005A T6 (5-10)*	EN-AW 6082 T6 (5-15)
Product form		EP	EP
Unit mas	$[\mathrm{kg/m^3}]$	2700	2700
E modulus	$[\mathrm{N/mm^2}]$	70000	70000
f_0		200	260
f_u		250	310
$f_{0,haz}$		115	125
$f_{u,haz}$		165	185
Buckling class		A	A
*Alloy applied on transverse bridge deck profiles.			

For static analysis, the mesh data has no impact on the accuracy of the results. To perform an NS EN 1999-1-1 code check in SCIA, HAZ reduction is added to the ends of the truss diagonals. This HAZ reduction is indicated by the small orange arrows shown in Figure 33. In the NS EN 1999-1-1, the HAZ strength reduction is accounted for by reducing the cross-section wall thickness. The welding data applied is MIG welding and filler material in the 5xxx alloy class with a temperature of 333.15℃. The buckling length factor, k, is set to 1.5 for all the truss members is both directions. This buckling length factor is equal to a; Rotation: clamped – restrained; displacement: fixed – free, compression member per NS EN 1999-1-1 [11].

Two load cases have been applied to evaluate the two bridge deck solutions. The service vehicular load and the distributed load with the 10% horizontal load. For the LBD solution, an additional distributed force is added to simulate the weight of the bridge deck panels. This force is a conservative approach when considering the LBD alternative up against the TBD. The conservativisms are because the bridge deck panels additional stiffness is not included. Figure 28 shows the distributed load on the LBD alternative. or the global TBD analysis, the load is distributed evenly on the 2D plane with ribs. Both the 10% horizontal load and the service vehicular load is applied similarly to both bridge deck models as illustrated in Figure 29 and Figure 30. The different FEA models for the two concepts are illustrated in Figure 33 - Figure 37.

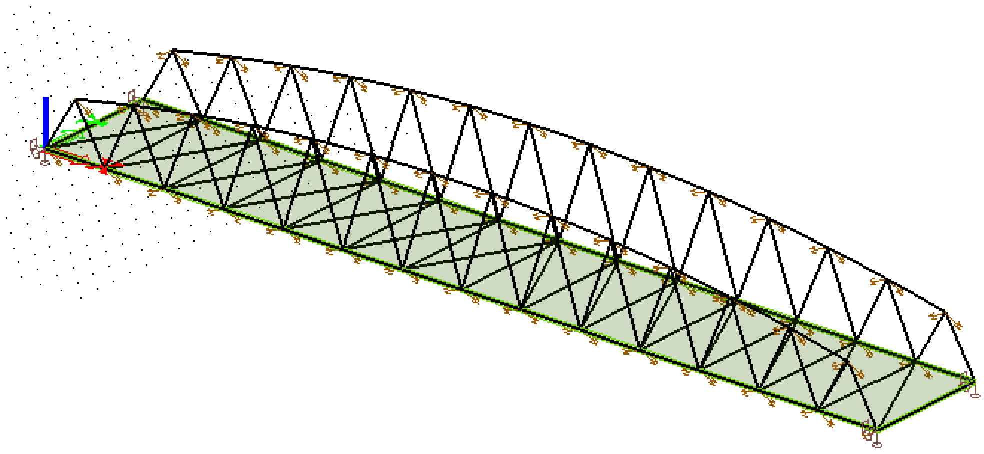

Figure 33: Longitudinal bridge deck analysis model in SCIA.

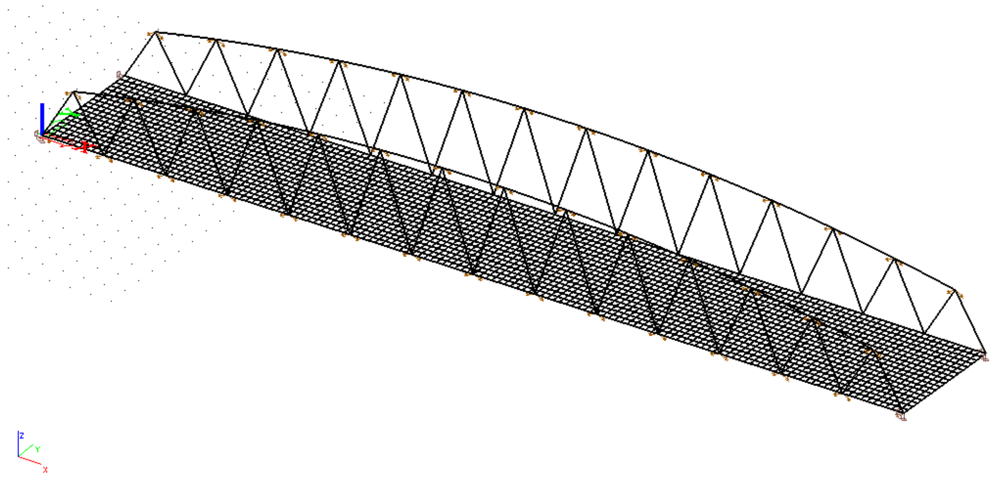

Figure 34: Transverse bridge deck model in SCIA (local loads)**.**

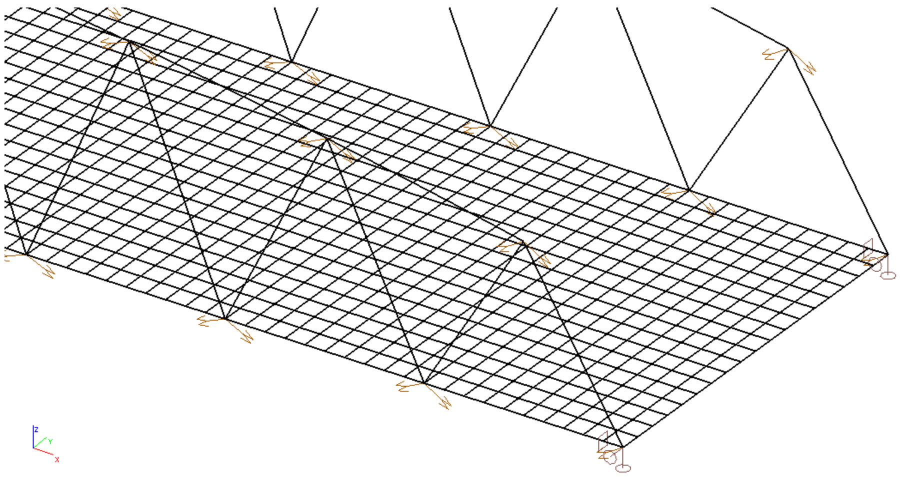

Figure 35: Transverse bridge deck model for local loads in SCIA (Close up).

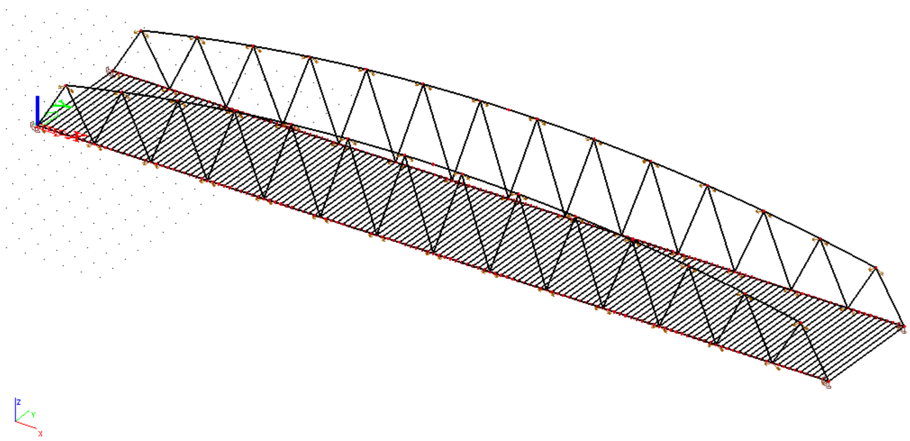

Figure 36: Transverse bridge deck model in SCIA (global).

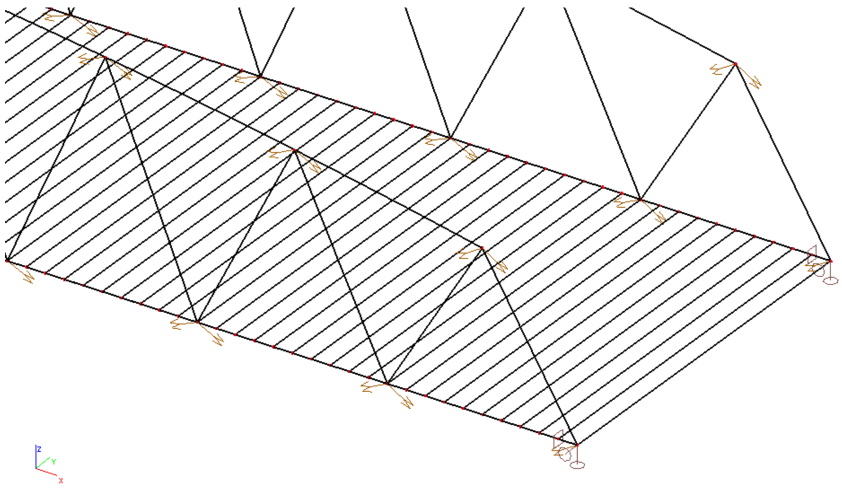

Figure 37: Transverse bridge deck model for global loads in SCIA (Close up). 2D panel with ribs. Only ribs are illustrated on the figure.

7.4 Finite Element Model of Chosen Concept

The FEA model of the chosen concept is identical to the LBD concept model except from some changes. Figure 38 illustrates the full model and the changes are listed below.

1. 6082 T6 is the new material for the bridge deck. The shape of the profiles is simple enough to be extruded in a harder material.
2. For the Eurocode check, HAZ are added where the bridge is spliced and at joined members. These HAZ are shown in Figure 39, indicated by yellow arrows.
3. FSW bridge deck is added as longitudinal beams with a cross-section of B300 x H72 [mm]. The FSW bridge deck is divided into three zones indicated by the pink color in Figure 40. Connected with moment free connections between FSW beams and bridge deck I-beams. This joint gives free rotation in the connection.

4. The diagonal bridge deck I-beams is modeled with joints with free rotation in both ends. Figure 41 illustrates the joint. This assumption is made, so the detailed design of the joint is coincident with the assumptions made in the global model.

For nonlinear analysis and the linear stability analysis, the mesh data has a large influence on the end results [59]. Both the stability and eigenfrequency analysis is dependent on an adequate mesh refinement to find critical modes. Both wrong mode shapes and eigenfrequencies can be missed out from the calculation with course mesh. To ensure adequate mesh refinement, SCIAs recommended mesh setup for time-dependent analysis is used [60]. The recommended parameters are listed below.

- Minimal distance between two points ł 0.001 m
- The average number of tiles of a 1D element must be ł 2.
- Generation of nodes under concentrated loads on beam elements = on.
- For reasons of numerical stability of TDA solver it is recommended to adjust: Minimal length of beam element = 0.05 m.

These settings give a total of 520 nodes and 601 1D elements in the FE model.

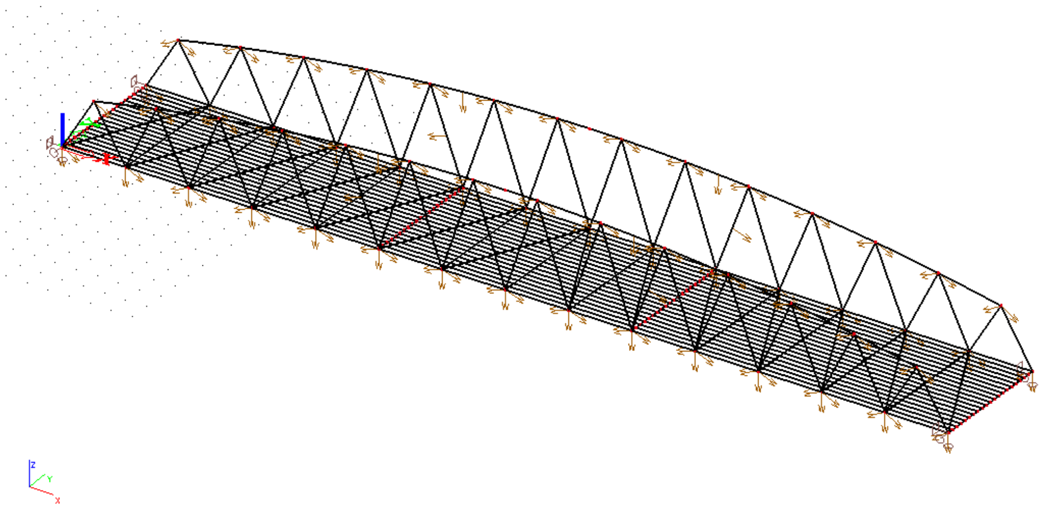

Figure 38: Chosen concept model.

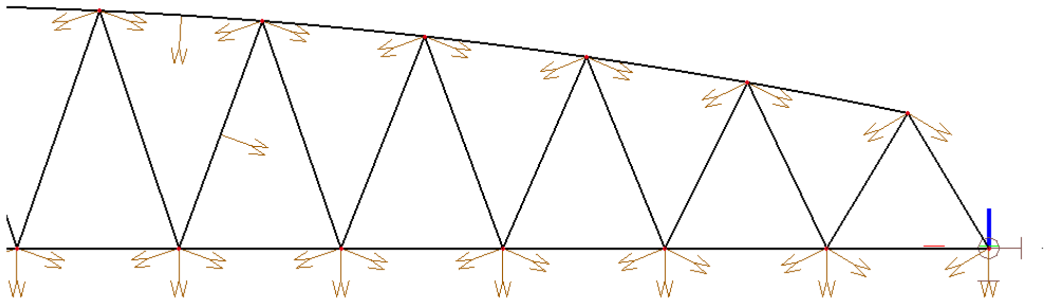

Figure 39: HAZ indicated by arrows.

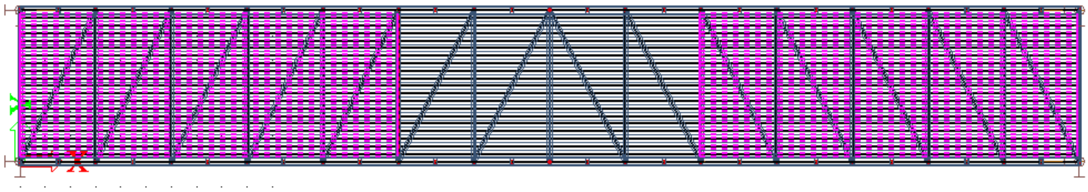

Figure 40: FSW panels model as beams in three lengths in the longitudinal direction. Marked by pink-gray-pink zones.

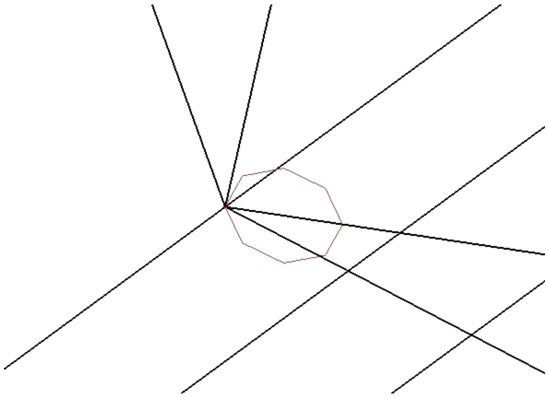

Figure 41: Free support as joint boundary conditions for diagonal I-beam.

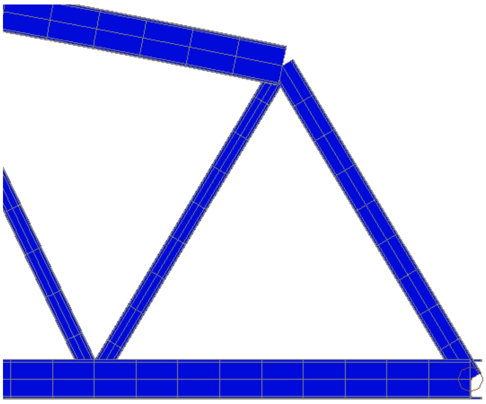

Figure 42: Illustration of the mesh.

[This page is intentionally left blank]

8 SCIA Results of Bridge Deck Solutions

8.1 Transverse Bridge Deck

The service vehicular is the limiting load when analyzing the bridge deck locally. The deflection criteria is given by:

Equation 9

$$d = L_t/350 = 17.1 \text{ mm}$$

As shown in Figure 44, the relative deflection of the transverse bridge span is no more than 7 mm. This deformation is according to the the deflection criteria from NPRA, approved. Also, the von Mises stress was held below the yield limit of the extruded 6005 alloy with only 24.2 N/mm^2 as shown in Figure 43. From the load distribution plots, the method of modeling the distribution of point loads seems to be satisfying on larger models. The method also gives a good interpretation of the load distribution. The low stress and displacement gives room to improve the TBD design for this load case and reduction in weight could be obtained.

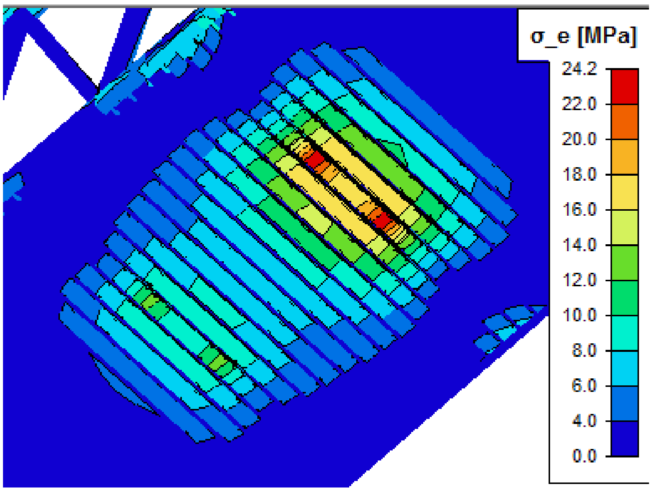

Figure 43: Stress plot from underneath the bridge.

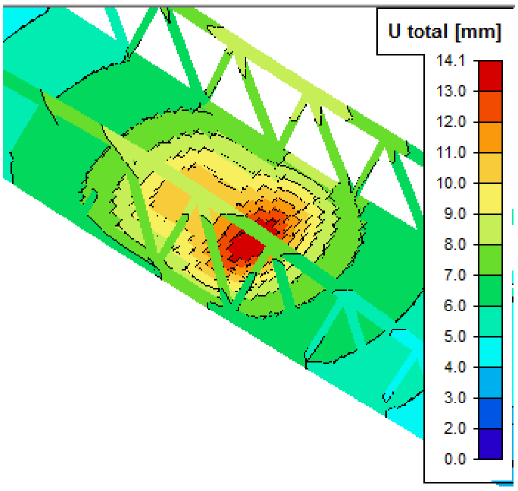

Figure 44: Distribution of point load in total displacement.

The two models are geometrically identical, but the TBD model has larger profile dimesion in the diagonals. The cross-sections are tabulated in Table 10, and the geometry of the bridge is illustrated in Figure 33. The deflection criteria for the longitudinal deflection is given by:

Equation 10

$$d = L_l/350 = 120 \text{ mm}$$

Figure 45 shows a U total of 132.9 mm. This displacement exceeds the deflection criteria, and the truss height or chord dimension must be increased to meet the demand. The von Mises stress is well below the yield limit for the HAZ as illustrated in Figure 46. There is also stress concentration around the truss joints. This concentration is an indication of practical analysis results since it naturally there will be higher stress levels around joints. Aluminum is a relatively soft material with a low young's modulus as appointed in Section 2.2. The deflection of aluminum is therefore often the limiting criteria. In this case, the von Mises stress is much lower than the displacements relative to the rules.

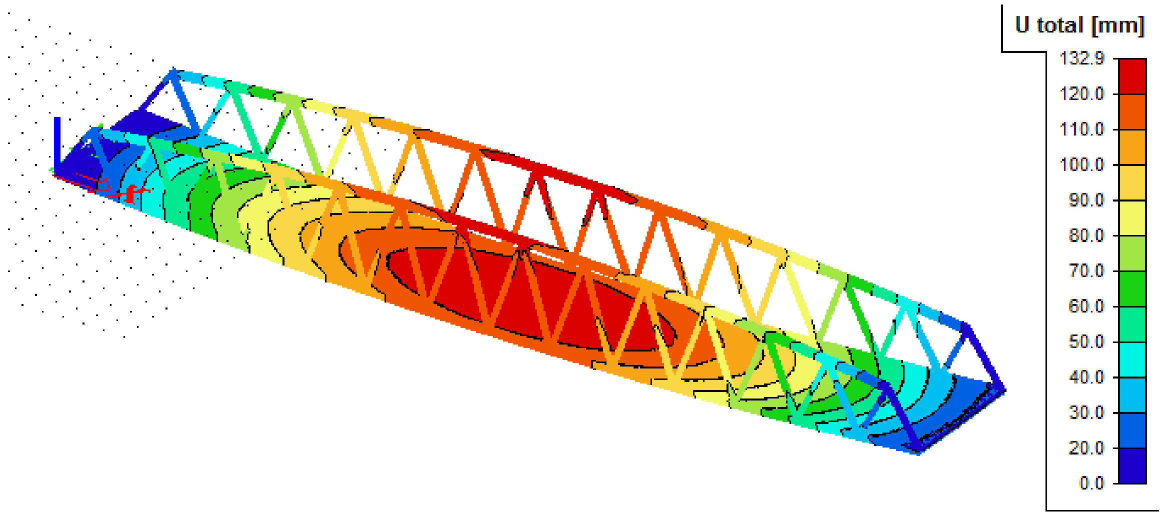

Figure 45: Total displacement from the distributed load combination.

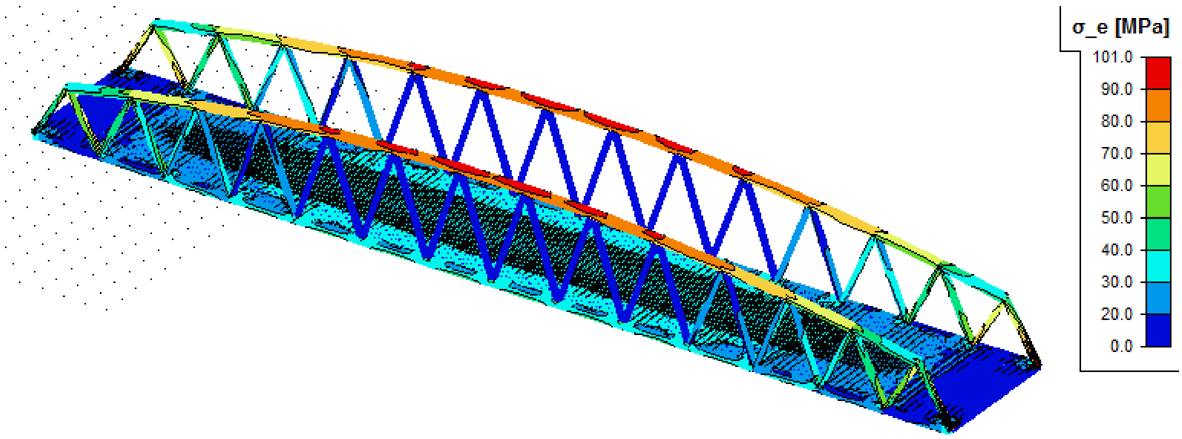

Figure 46: Stress plot from the distributed stress plot.

The bridge was checked up against the NS EN-1999-1-1 in SCIA. Beam B2 and B3 are the two first diagonals in the trusses. They are the two truss members that are subjected to the largest magnitude of the shear force. These forces are equal to the two members on the opposite side of the bridge. Even though the cross-section is increased compared to the LBD concept, it did not fulfill the criteria for the stability check. Concerning the top chord, B4, and B32 as shown in Table 12, the stability check failed since it has a buckling length of 1.5×39 m. This buckling length is unrealistic because a global buckling of the whole truss must happen. Sideways buckling of the top chord is therefore not considered in the bridge deck comparison. This phenomenon will be equally critical for both concepts.

Table 12: Excerpt of the NS EN 1999-1-1 code check.

Beam Case	Css Material	dx [m]	Unity check [-]	Stability Check [-]	Section check [-]
B2 CO1/2	CS11 - RHS EN-AW 6082 (EP/O,EP/H,ET) T6 (5-15)	0,000	**1,07**	1,07	0,60
B3 CO1/2	CS11 - RHS EN-AW 6082 (EP/O,EP/H,ET) T6 (5-15)	0,000	**1,07**	1,07	0,60
B4 CO1/2	CS9 - RHS EN-AW 6082 (EP/O,EP/H,ET) T6 (5-15)	19,636	**16,42**	16,42	0,42

8.2 Longitudinal Orientation SCIA Analysis

The deflection criteria in the transverse direction are 17.1 mm as found in Section 8. The relative vertical deflection is found to be approximately 10 mm as seen in the color plot in Figure 48 below. The maximum von Mises stress is 44.4 N/mm^2 at to top and bottom flange of the beam supporting the front axle of the service vehicular. Figure 47 illustrates the stress plot. Both the stress and deflection of the transverse beam is well within the criteria. There may also be potential for weight savings by optimizing the beam dimensions.

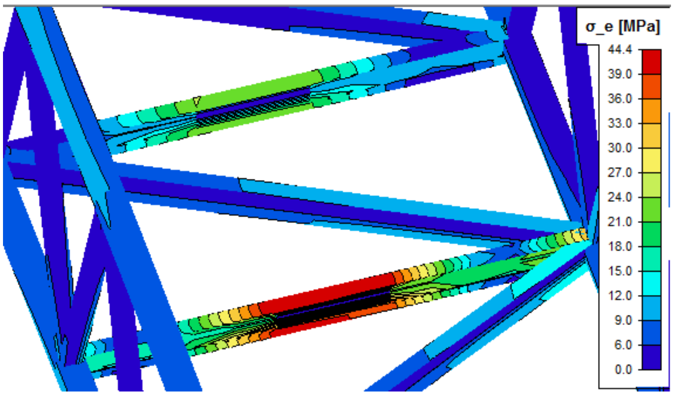

Figure 47: Stress plot from service vehicular load.

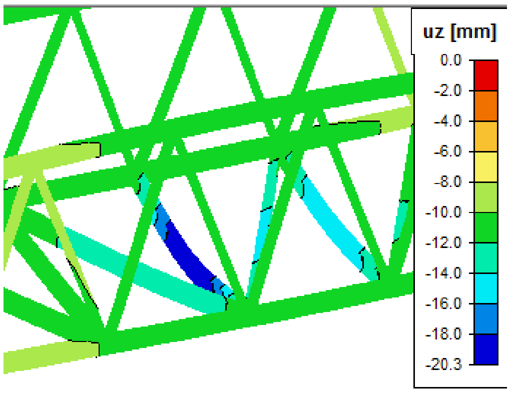

Figure 48: Vertical displacement from service vehicular.

In Section 8.1 the longitudinal deflection criteria were found to be 120 mm. The color plot at Figure 49 shows a total deflection in the negative z direction is 92.7 mm. This deformation is below the deflection criteria. Concerning the von Mises stresses the highest stresses is at the first diagonal truss members on each truss side. The stress is decreasing closer to the truss center as the shear force decreases. There are also stress concentrations around the truss joints as shown in Figure 50 with near 52 N/mm^2. Concerning the NS EN 1999-1-1 code check, the LBD concept had a value below one on the unity checks for all the members, except B4 and

B32. B4 and B32 are as mention in Section 8.1 a case of global buckling. Because of this, the sideways buckling of this member is ignored at this stage.

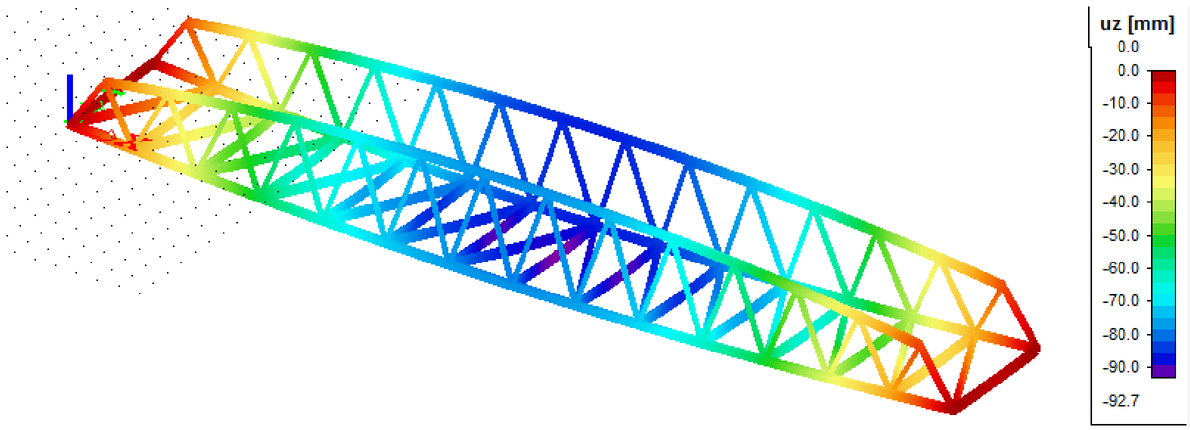

Figure 49: Vertical displacement from distributed load case.

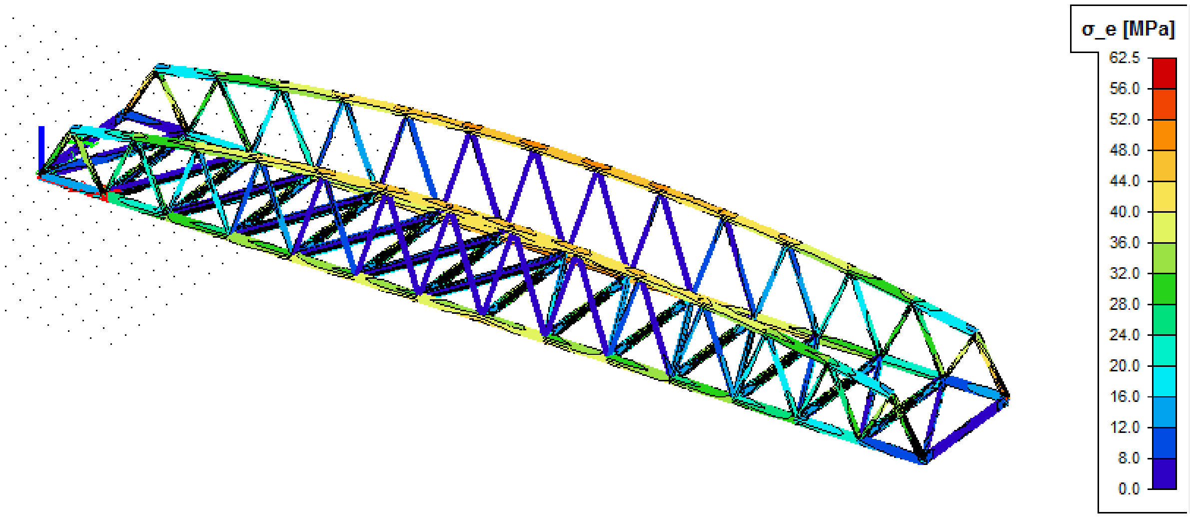

Figure 50: Stress plot from distributed load case.

8.3 Bridge Deck Evaluation

From the book, Product Design and Development [44] a concept-scoring matrix is used to validate the two different concepts. The TBD is chosen as the reference concept, and the LBD concepts are rated by using simple codes. + for “better than,” 0 for “same as” and – for “worse than.”

The summarized analysis data for the comparison is found in Table 13. The LBD concept is almost superior the TBD concept in all the analysis result. The TBD had a lower relative deflection in the transverse direction, but both concepts were well within the deflection criteria. The LBD had a significant less deflection over the longitudinal bridge span compared to the TBD concept. The LBD beams have diagonal members between the transverse. These were added to obtain stiffness in the transverse horizontal direction. Analysis result shows however that they also contribute to the vertical deflection over the longitudinal bridge span. For the TBD analysis, it is only a 10 mm plate that contributes to vertical stiffness over the longitudinal bridge span. This estimate is considered as a good, due to the bridge deck profiles design with only a top side FSW. However, no physical test has been conducted to verify it, and the TBD may contribute more than the analysis shows. Due to these results, the LBD concept is rated better than the TBD concerning the structural integrity. LBD concept is also rated much better on self-weight with an 8.2 tons’ lighter construction. The self-weight is an important criterion due to installation, transportation and crane lifting capacity. Both options have room for structural optimization and improvement.

Table 13: Analysis comparison chart.

	Longitudinal bridge deck	Transverse bridge deck
Displacement U total [mm] longitudinal	92.7	132.9
Displacement U total [mm] transverse	10	7
Von Mises stress [N/mm^2]	62.5	101.0
Self-weight (ton)	25.6	33.8
NS EN-1999 code check	√	-

For rest of the selection criteria, the two concepts are found to be equally good. Table 14 gives the selection matrix. Considering the ease of manufacturing both concepts have their pros and cons. As the list for DfM in Section 4.1.1 implies, reduction of parts, ease the manufacturing process. For the LBD concept, there is an increase of different parts compared to the LBD which is a con. By laying the bridge deck in the longitudinal direction, the FSW panels could be produced much larger. Due to max transportation dimension, a maximum of six bridge decks modules for LBD compared to a minimum of fourteen for the TBD. This difference makes both the manufacturing and installation easier for LBD. Since the manufacturing and installation are considered equal in this phase of the product development, the cost is also found to be similar for the two concepts. The only deviation is if the material cost plays a significant role, then the LBD concept has an advantage. Concerning the aesthetics, they are rated "similar as." The LBD may have a thicker bridge deck construction, but slimmer truss construction and the opposite for TBD.

Table 14: Selection matrix.

	Concepts	
Selection Criteria	A Longitudinal bridge deck	B (Reference) Transverse bridge deck
Ease of manufacturing	0	0
Ease of installation/assembly	0	0
Transportation	0	0
Weight/material usage	+	0
Cost	0	0
Esthetics	0	0
Structural integrity	+	0
Sum +'s	1	0
Sum 0's	5	7
Sum –'s	1	0
Net Score	2	0
Rank	1	2
Continue?	YES	NO

9 SCIA Result for Chosen Concept

In this section, all the analysis is divided into different LC and presented in chronological order from 1 - 5. All the combined loads in the different LC is tabulated in Table 9 in Section 7.2. At the end of the section, the results are summarized in Table 17 and discussed.

9.1 Load Combination 1

LC 1 is the most critical LC concerning the global integrity of the bridge construction. As appointed in Section 8.1, the deflection criteria for the longitudinal bridge span is 120 mm. As illustrated with a color plot in Figure 51 the total displacement of 89.3 mm is well within that criteria. The largest deflection is found at the center of the bridge, marked with dark red. In Figure 52 shows how the moment stiff joints between chords and truss diagonals make the trusses deflect inwards. A cross-bracing at the top of the bridge will hinder this motion. The peak stress of 188.7 N/mm^2 which is indicated by the color bar in Figure 53, is seen at the support at each end of the bridge. It is below the material yield limit and located in a very concentrated area. On the rest of the structure, one can observe that there is stress concentration around the truss diagonals and at the top chords. The fixed joint condition takes bending moment in the coupling and creates stress concentrations.

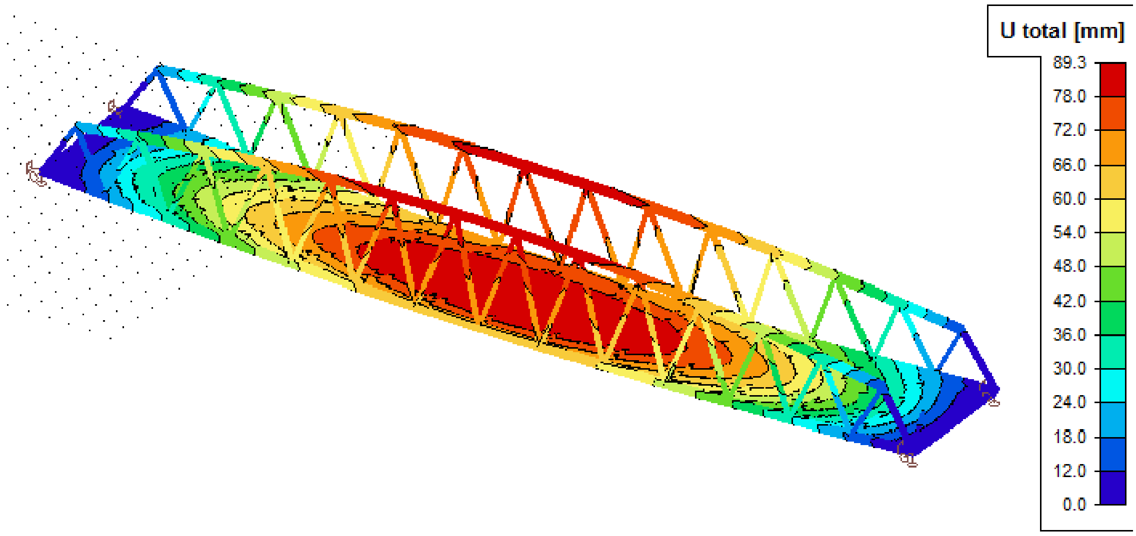

Figure 51: Total displacement plot for load condition 1.

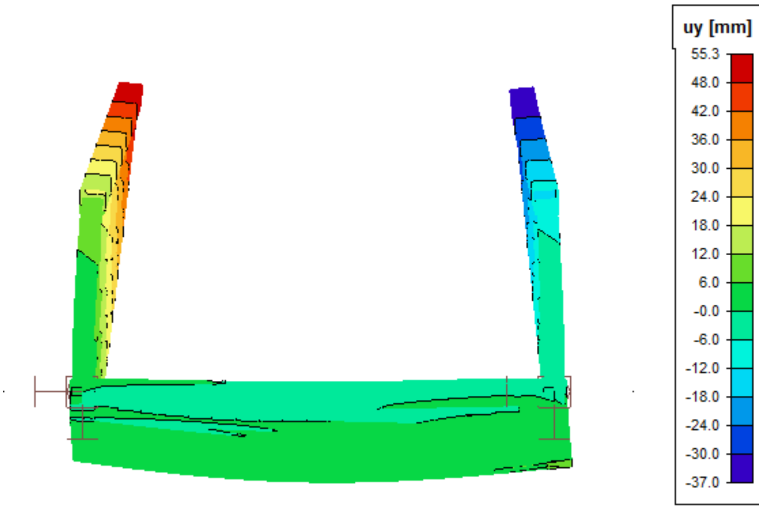

Figure 52: Displacement y- direction.

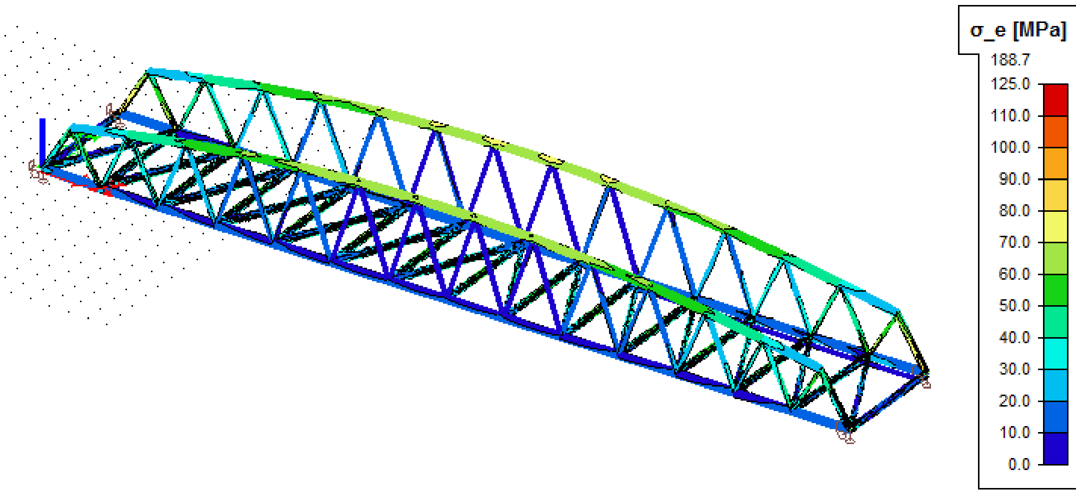

Figure 53: von Mises plot for load condition 1. Bridge deck planks are not displayed but included in the analysis.

Due to the issue of buckling length factors addressed in Section 8.1. In this section, the top chords failed the SCIAs NS EN 1999-1-1 check, because of unreasonable long local buckling length. LC1 also fails the Eurocode check for the same reason. The check for each member is found in Appendix 3 for LC1. Linear stability analysis of the bridge is performed with LC1 to ensure adequate resistant against global buckling. The analysis helps to find the critical global buckling modes and buckling loads of the bridge structure. It is usually the first mode with the lowest critical load coefficient that makes a collapse possible [61]. In the analysis, it is assumed physical linearity; members are taken ideally straight and have no imperfection; the load is guided to the mesh nodes; the load is static; between the nodes, the forces are taken as constant [61]. Mesh refinement is necessary as addressed in Section 7.4. to ensure a satisfactory result. The structure becomes unstable when the loading reaches an applied load equal the current applied load, multiplied by the critical load factor. The first buckling mode is illustrated in

Figure 54 a). The buckling mode seems realistic since the highest compression forces are found at the center of the top chord. The shear forces are taken by the diagonal trusses at the bridge ends. A buckling load factor of 3.42 is found from the first mode. A buckling load factor of this size can to some extent ensure that a global buckling of the bridge will not happen with normal load condition. Findings from nine aluminum pedestrian bridges in China state however that linear elastic theory’s applied on aluminum half-open bridges is not considered safe [62]. This unsafety is due to out-of-plane buckling of upper chords in the first buckling modal. The nonlinear inelastic analysis should be adopted in the further development of the bridge. The two next, higher order buckling modes are illustrated in Figure 54 b) and c).

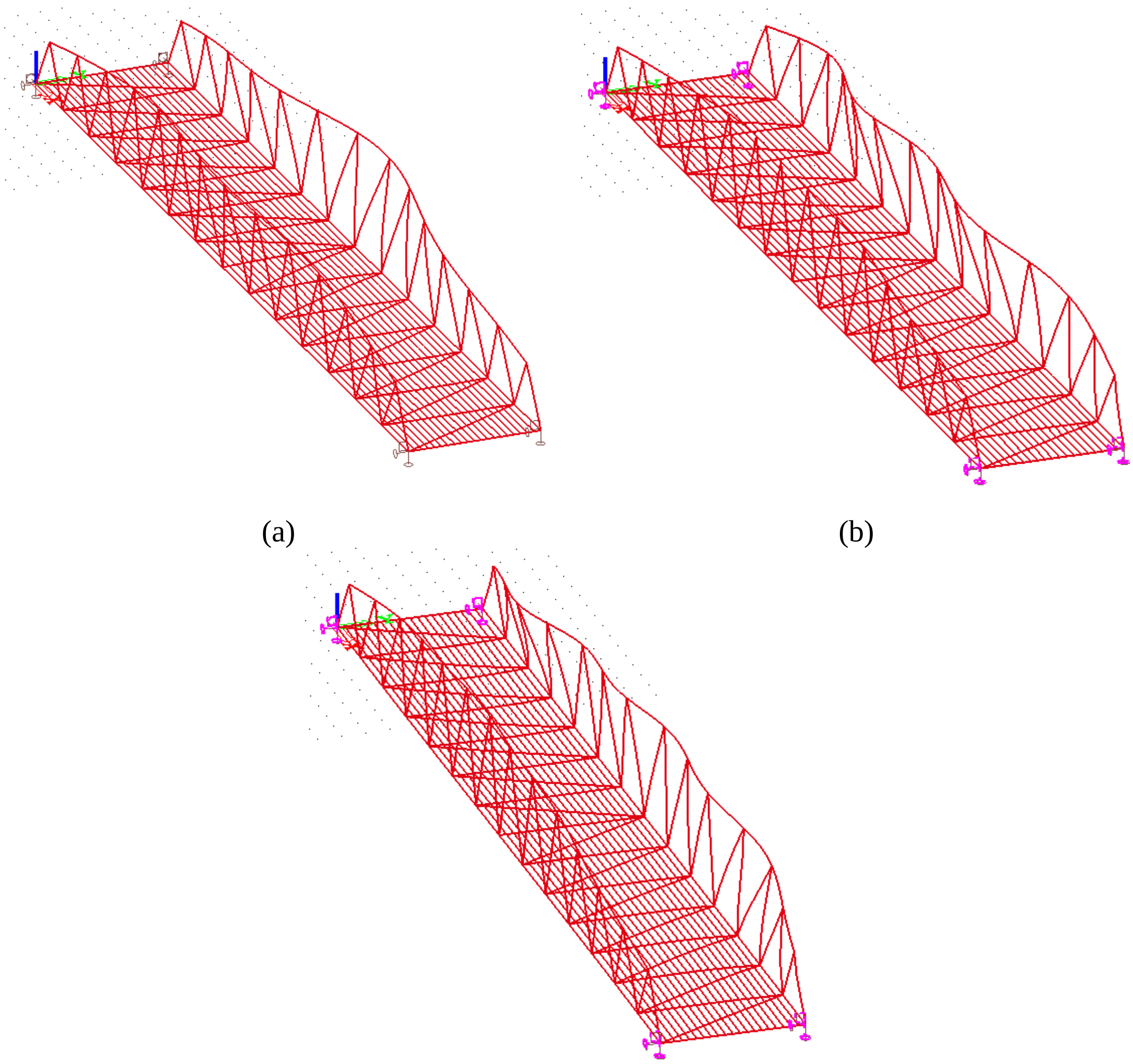

(a) (b)

(c)

Figure 54: Linear stability analysis: a) Mode 1 – 3.42, b) Mode 2 5.22, c) Mode 3 7.69**.**

9.2 Load Combination 2

This LC consists of the service vehicular load and inflict relatively high peak stresses on the structure. This LC is the most critical concerning the vertical deflection over the bridge width. The von Mises stress level is 76.5 N/mm^2 and is well below both yield limits of the base material and HAZ. The largest total displacement is found at the center of the bridge where the load is applied. This deflection is illustrated in Figure 55, marked with red. The relative deformation is calculated by utilizing the displacement found in the longitudinal center node of the lower chord. This deflection is 30 mm. This deviation gives a relative vertical deflection over the width of the bridge to be 17.2 mm. This deformation exceeds the criteria marginally with 0.1 mm, and some adjustments or refined analysis are needed to fulfill the criteria.

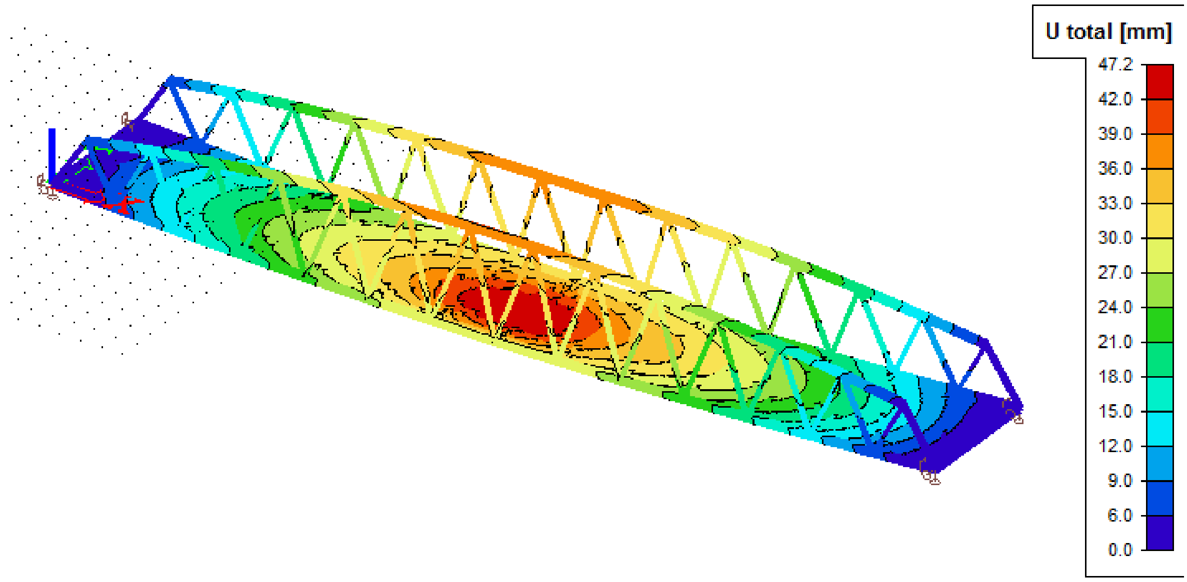

Figure 55: Displacement

9.3 Load Combination 3

For separate pedestrian bridges, there is no demand of combining wind loads and service load as appointed in the user demand specification in Section 4.2. There are no direct criteria concerning the deflection in the horizontal direction if the vertical deflection over the longitudinal span is assumed to be the criteria. The deflection is on an acceptable level below 120 mm as illustrated in Figure 56. The joint between the truss and bridge deck is rigid; this is an assumption that needs to be followed by appropriately designing detailed joints as discussed later in Chapter 10. Under the discussion of the horizontal deflection under LC1, a cross bracing at the top of the bridge was mention. This cross bracing could be the next step to improve the horizontal deflection, but will also change the user experience of the bridge. In the NPRA handbook for bridges N400 [5], this bridge is a wind class 1 bridge. With a maximum natural conciliation period of < 2 s. In this wind class, the dynamic loads are found neglectable. For aluminum, the dynamic wind load could be of interest since the material is more prone to vibration compared other materials like steel. The highest von Mises stress in the LC is 77 N/mm^2. This stress level is well below the material capacity.

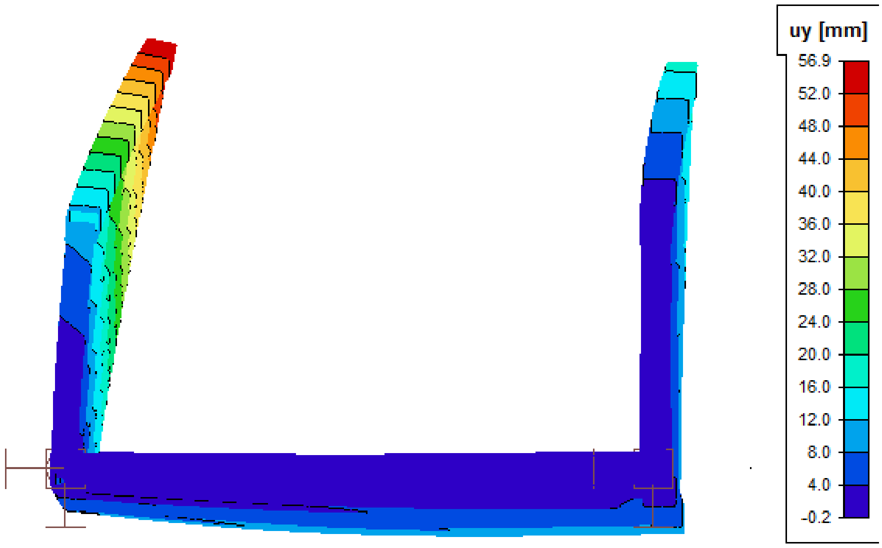

Figure 56: Displacement in y-direction.

9.4 Load Combination 4

In this LC a modal analysis is performed, and the following masses in Table X are added as self-weight to the structure. The analysis has been carried out with and without LBD planks. These FEA with no large deviation in results. In SCIA the self-weight is automatically added in the modal analysis. This self-weight only consists of the structural members and not the bridge deck and asphalt. The self-weight is therefore multiplied by a factor of 4 as calculated in Table 15. Bolts, welds, and railings in not considered. The analysis has been performed with and without LBD planks. These FEA with no substantial deviation in results.

Table 15: Self-weight load factor

Weight	$Self - weigh\ load\ factor; f$
Asphalt: 37800 kg Bridge deck: 9000 kg Bridge structure: 15913 kg Total = 62713 kg	$f = \frac{total\ mass}{bridge\ structure\ mass} = 3.94$

Dynamic frequency equation:

Equation 11

$$\omega_n = \sqrt{\frac{k}{m}}$$

Simple harmonic motion frequency formula:

Equation 12

$$f = \frac{1}{2\pi}\omega_n$$

Eigenfrequency means fluctuations a system can perform without external forces acting [63]. Equation 11 and Equation 12 illustrates that increased mass of the bridge reduces the eigenfrequency of the structure. Masses which is neglected in the analysis will, therefore, give a reduced frequency. SCIA solves the eigenfrequency problem by solving Equation 13 with the use of subspace iteration method [63]. This equation assumes the damping to be equal to 0.

Equation 13

$$\boldsymbol{M\ddot{r}} + \boldsymbol{Kr} = \boldsymbol{0}$$

M is the mass matrix, **K** is the stiffness matrix and **r** is the vector of translation and rotations in nodes where $\boldsymbol{\ddot{r}}$ is an equivalent vector for accelerations. The calculation is applied on the FE model used in the static calculation. Discretization is the difference between the models which give a finite number of degrees of freedom in the analysis [61].

As found in section 4.2 there are some critical eigenfrequency-areas for the bridge. In the vertical direction, the area is 1-3 Hz, and for the horizontal directions, the area is 0.5 – 1.5 Hz. Figure 57 illustrates four different eigenmodes. All the eigenmodes are out of reach of the critical zone. The first mode is lowest with 3,89 Hz. In this mode, the truss structure moves from side to side in a horizontal movement. The first vertical mode shape is number 5, and the first global horizontal mode is mode number 9 as illustrated in the figure below. Eigenmode number 5 and 9 is what the pedestrian is most sensitive for. These frequencies are out of the critical area.

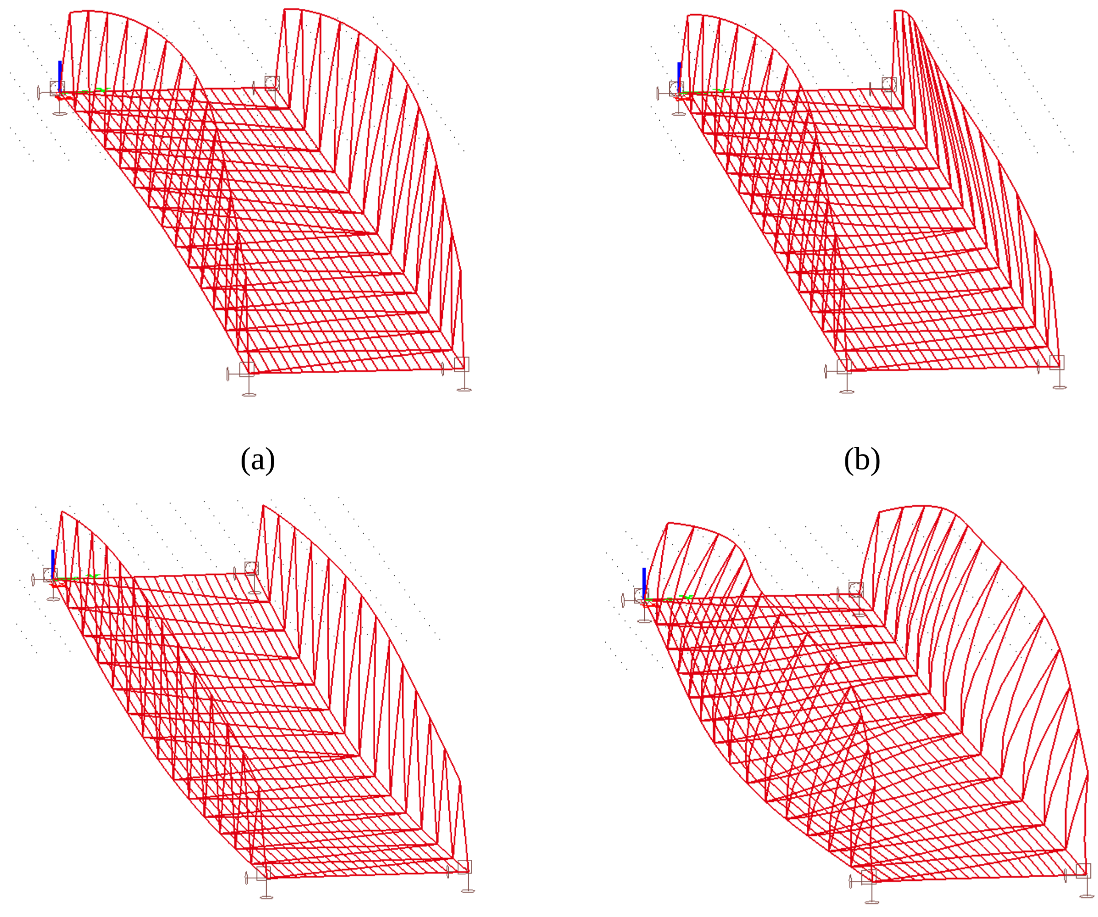

(a) (b) (c) (d)

Figure 57: Eigenmodes: a) Mode 1 – 3,89 Hz b) Mode 2 – 3,89 Hz c) Mode 5 – 7.09 Hz d) Mode 9 – 10,47 Hz.

9.5 Load Combination 5

Thermal loads are not included in the concept development due to time, effort and relevance. As mention in Section 2.2, the thermally induced stresses in aluminum is relative low, even though the expansion of aluminum is greater compared to steel. The bridge is also simply supported with fugue at one end and fixation at the other. This support makes the thermal loads less important, but must be accounted for further development of the bridge concept.

9.6 Result Summary and Evaluation

The results of the analysis show promising result concerning the structural integrity of the bridge. All the results are tabulated in Table 17. The total weight of the bridge is calculated to be 23 tons excluding the asphalt. Table 16 shows all applied loads and corresponding reaction forces in the SCIA FE model. This way one can ensure that all applied loads are included in the analysis model.

Unbiased sources for error could be optimistic joint boundary condition in the FE model. The bolted connection might be less stiff than the assumption of a rigid connection. The analysis is linearly elastic and may miss out some more complex phenomenon. The deflection calculation has not considered the HAZ, but as discussed in Section 2.3.3 the HAZ will only influence the material yield strength and not Young’s modulus.

The NS EN 1999-1-1 check for LC1 can be found in Appendix A3. The two first truss diagonal members at each end are pushed to its limit concerning buckling resistance. For LC2 the deflection criteria are not met. The relative and vertical transverse deflection exceed the standards with 0.1 mm. A more refined analysis must be conducted, to make sure the bridge is fulfilling the criteria. One method to reduce the bridge deflection is to compensate for the deformation resulted by the bridge self-weight. A small initial arc in the lower chord. The bridge will go straight when the bridge is installed. Concerning the global buckling and modal analysis, both show signs of excellent structural integrity.

Table 16: Reaction forces.

		Units	X - direction	Y - direction	Z - direction
LC1	Applied loads	[kN]	0	126	1876.3
	Reaction forces		0	126	1887.5
LC2	Applied loads		0	0	736.3
	Reaction forces		0	0	747.9
LC3	Applied loads		0	168	616.3
	Reaction forces		0	168.8	627.85

Table 17: Result summary.

Result summary					
Load combination	Displacement* [mm]	von Mises [N/mm^2]	Linear stability factor	Eigen frequency Mode 1: [Hz]	NS EN-1991-1-1
1	89.3	188.7	3.42	-	√
2	17.2	76.5	7.74	-	√
3	56.9**	77	8.65	-	√
4	-	-	-	3.89	
5	-	-	-	-	

*the displacement is relative to the considered span length
**Displacement in transverse direction and not relative

[This page is intentionally left blank]

10 Bridge Detailing

When designing structural details like joints, it is important that the assumption made in the global FEA is consistent with the joint properties. In the global analysis of the chosen concept, the transverse I-beam connection is assumed rigid. To ensure fulfillment of the assumption, a full bending moment stiff connection is required. The only two LC considered when designing the connection is LC1 and LC2. Both LC are tabulated in Table 18. The internal forces mark with green is used as applied load on the bolts and welds in the joints. The challenge by splicing and connecting beams with closed cross-section is the lack of access to tightening the bolts from the inside. One solution could be to utilize blind bolts. These bolts can be tightened only with the excess from the outside of the square beam. In slip resistance connections they are not recommended in the research program notes from the bascule bridge deck project [35]. Blind bolts are not covered in the NS EN-1999-1-1 and are therefore not investigated further in this thesis. Slip resistant bolts should be utilized in all connections to ensure high fatigue resistance [11]. All the bridge details designed in this chapter is illustrated in Figure 58.

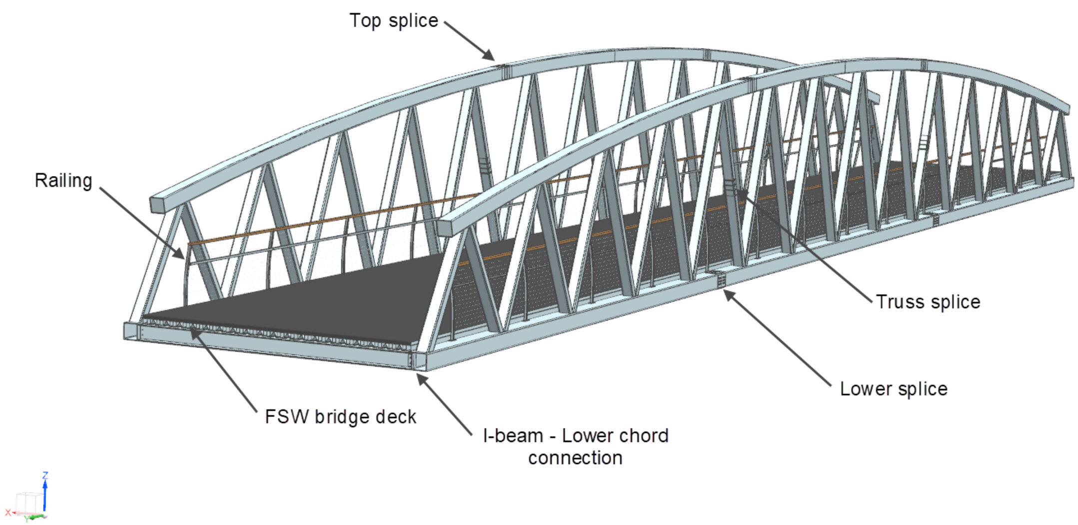

Figure 58: Bridge deck details.

10.1 Bridge Deck Profiles

The bridge deck profiles are much alike the LBD profiles designed in Section 6.1 and 6.3 and is illustrated in Figure 59. The lower flange of the profiles is designed with more area, to move the neutral axis to the center of the profile. With this configuration, a maximum utilization of the profiles bending stiffness is obtained. The end profile is design with an extra edge, to keep the asphalt in place. Otherwise, the design guidelines described in Section 2.3.1 is followed to ensure a more economical and easier production. Each corner has a small radius, and the wall thickness is fairly consistent. Detailed drawing of the profile is in Appendix A2. Further optimization of the profiles self-weight can be done by decreasing the profile wall thickness without going into cross-section class 4 and maintaining the bending stiffness.

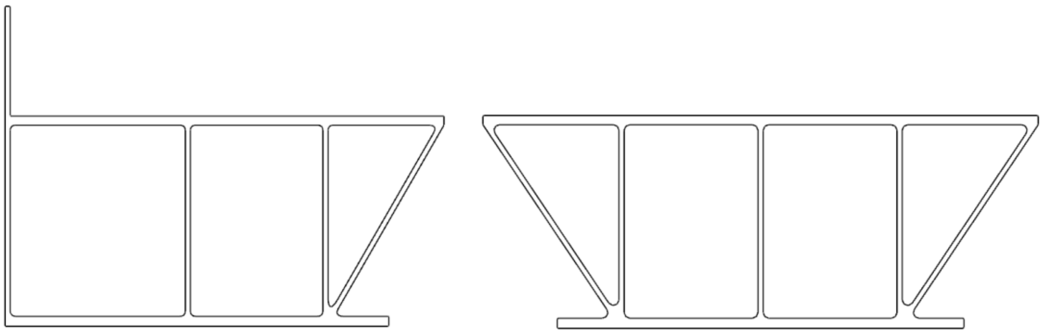

Figure 59: Bridge deck profiles. End profile (left).

10.2 Truss

The truss design is so that the neutral axis of all connecting beams meets at a coincident point. This point is coincident both in the transverse and longitudinal direction of the lower chord. The execution is illustrated in Figure 60 by a K-joint with a gap, the joints in this bridge concept have overlapping diagonals which are an equivalent solution [32]. The truss joints are welded and assumed rigid in the global analysis. No further work has been conducted concerning failure modes and weld dimension of the truss joints. The failure modes that can occur in the joints are illustrated in the graph in Figure 60; (1) The load reaches the elastic limit; (2) deformation limit reached; (3) remaining deformation limit reached; (4) crack initiation; (5) ultimate load reached [64]. Optimal truss angels are found discussed in Section 2.6.1. The truss diagonals at each end of the trusses take most of the shear forces. These truss diagonals have an angle within the optimal angle dimension. The truss diagonals at the center have a much larger angle but are inflicted less load. Bolted trusses have not been evaluated. The idea of prefabricating as large modules as possible in the workshop, makes it more feasible to use welded trusses. If the truss joint is bolted, the bridge should be delivered in single member components to the installation site as illustrated in Figure 13 in Section 2.6.5.

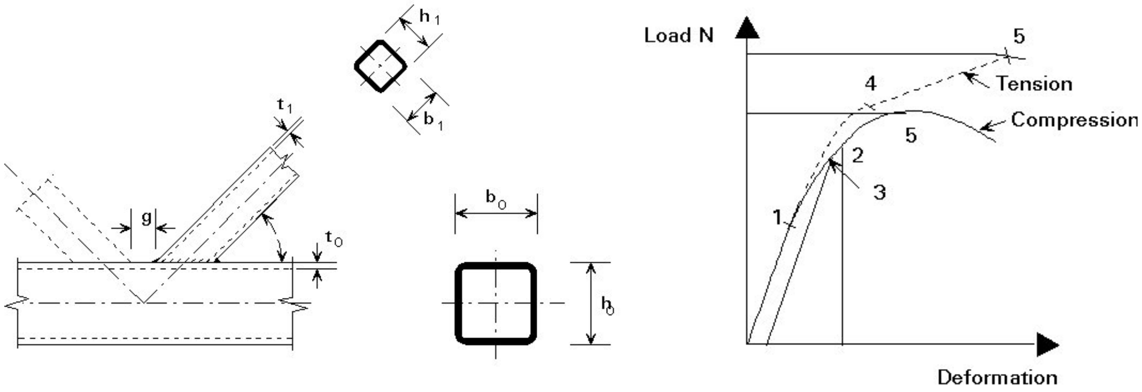

Figure 60: K-joint [64].

10.3 I-beam – Lower Chord Connection

From Table 19 solution 3 was found appropriate by an evaluation of the different pros and cons of the solutions. The main thought behind solution three is easy assembly. The truss section can be lifted on to the end of the bridge deck I-beams. Consider only LC1 and LC2 this connection transfers the tension forces directly to the top flange of the lower chord. And the compression forces at the bottom flange of the lower chord. The shear forces are taken as shear in the flange connection and tension in the top bolts. The bolt and weld capacity is calculated in accordance with NS EN-1999-1-1 Section 8.5.5 and 8.6.3. The loads are tabulated in Table 18. Beam B357 is the transverse bridge deck I beam at the center of the bridge.

Table 18: Internal forces in B357 for two different load cases.

Beam	dx [m]	Load combination	$V_{z,Ed}$ [kN]	$M_{y,Ed}$ [kNm]
B357	0	LC1	47.16	-4,18
B357	6	LC1	-29.47	1.54
B357	0	LC2	38.02	-19.42
B357	6	LC2	-41.20	-18.71

Table 19: Bridge deck beam - lower chord joint.

Name and figure	Pros	Cons
1 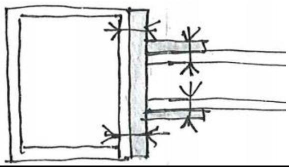	Flexible design and no heat affected zone from welding.	Needs blind bolts.
2 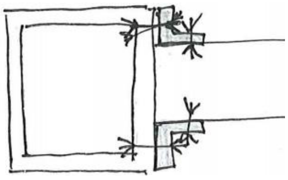	Flexible solution.	Extra parts. Needs blind bolts.
3 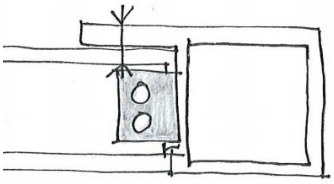	Potential easy assembly and good force transfer between I-beam and lower chord at LC1 and LC2.	Cross-section of lower chords getting even larger.
4 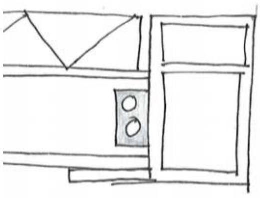	May ease the assembly by the extruded I-beam support. Improved force transfer from I-beam to HHS-beam by having internal stiffener.	HHS-beam gaining weight/meter with internal stiffener.
5 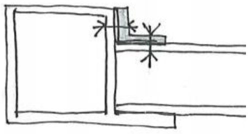	Easy assembly with the extruded I-beam support	Cross-section of lower chords getting even larger. For LC1 and LC2 not a god solution. Needs blind bolts.
6 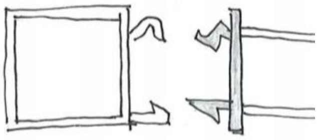	No extra parts needed under assembly.	Most likely a too weak connection. The endplate must be welded or bolted to the I-beam
7 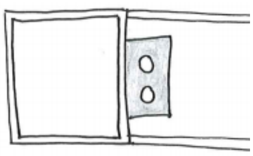	Simple shear connection.	Considered as a free joint connection.

10.3.1 Design Resistance of Bolts and Welds

Figure 61 shows the bracket designed for the I-beam lower chord connection.

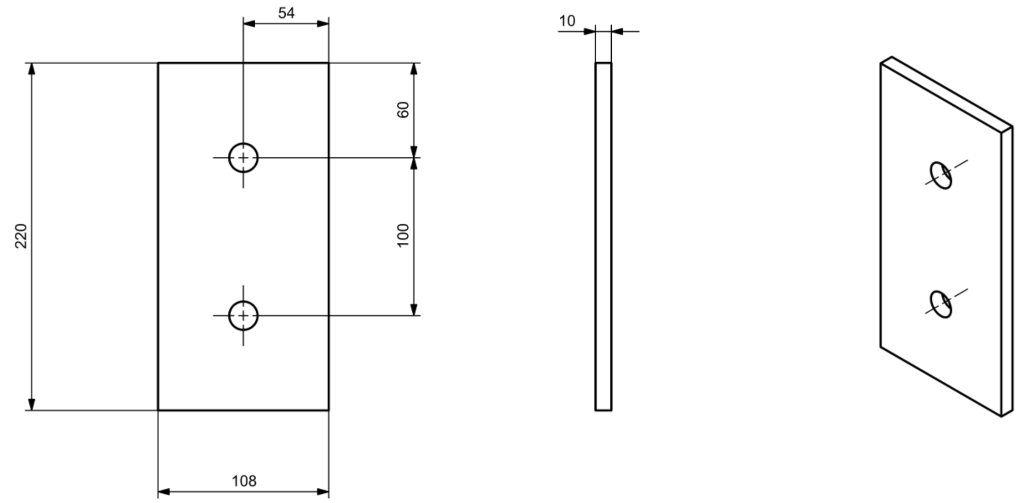

Figure 61: Bracket.

Stainless steel bolts are chosen to prevent galvanic and crevice corrosion in the bolt connection. In a dry unpolluted and rural area, stainless steel bolts on aluminum need no treatment according to Table D.2 in NS EN-1999-1-1 [11]. The bolt data is gathered from Table 3.4 in NS EN-1999-1-1 [11] and shown in Table 20.

Table 20: Stainless Steel bolt data [11].

Material	Type of fastener	Alloy Numerical designation: EN AW-.	Alloy Chemical designation: EN AW-.	Temper or grade	Diameter	f_0 $\mathrm{N/mm^2}$	f_u $\mathrm{N/mm^2}$
Stainless Steel	Bolts	A2, A4		80	≤ 39	600	800

10.3.2 Resistance of Bolts and Welds on Bracket

Shear Resistance: Bolts on Bracket

Table 8.5 from [11] is as design resistance of bolts. First, the shear resistance per shear plane is checked by Equation 14.

Equation 14:

$$F_{v,Rd} = \frac{\alpha_v f_{ub} A}{\gamma_{M2}}$$

With an elastic load distribution, the design load is calculated for two bolts by Equation 15 below. p is the distance between the two bolts.

Equation 15:

$$F_{v,Ed} = \sqrt{\left(\frac{M_{Ed}}{3p}\right)^2 + \left(\frac{V_{Ed}}{3}\right)^2}$$

Table 21: Shear resistance per shear plane [11]

Description	Values
Safety factor, γ_{M2}	1.25
Ultimate strength of bolt, f_{ub} [N/mm^2]	800
Factor, α_v	0.5
Design load, $F_{v,Rd}$ [kN]	68.6

The shear force is assumed distributed between the two bolts on the bracket and tension in the top bolts in the lower chord. When Equation 14 is solved for the shear area:

$$A = 214.3 \text{ mm}^2$$

Two M16 bolts with the stress area as tabulated in Table 22, gives sufficient shear resistance.

Table 22: Metric Hexagon Bolt data [32]

Bolt size	Stress area: A_s [mm^2]	Hole diameter: Normal
M20	245	22
M16	157	18
M12	84.3	13

Bearing Resistance

The bearing resistance is checked with the Equation 8.11 from NS EN-1999-1-1 [11] and is labeled Equation 16 in this document. The Fasteners spacing symbols are illustrated in Figure 62.

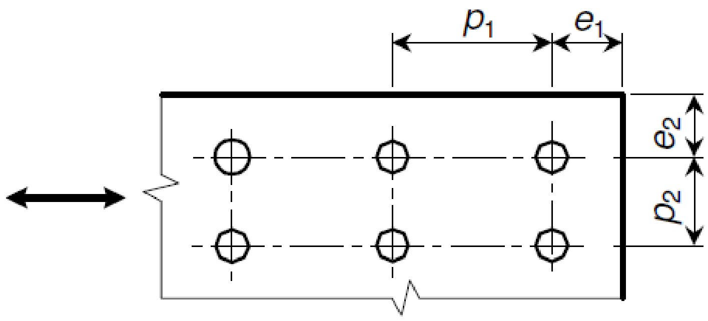

Figure 62: Fastener spacing symbols [11].

Equation 16

$$F_{b,Rd} = \frac{k_1 \alpha_b f_u d t}{\gamma_{M2}}$$

In the direction of the load transfer:

Equation 17

$$Edge\ bolts: \alpha_b = min\left\{\frac{e_1}{3d_0}; \frac{f_{ub}}{f_u}; 1\right\}$$

Equation 18

$$Inner\ bolts: \alpha_b = min\left\{\frac{p_1}{3d_0} - \frac{1}{4}; \frac{f_{ub}}{f_u}; 1\right\}$$

Perpendicular direction of the load:

Equation 19

$$Edge\ bolts: k_1 = min\left\{2.8\frac{e_2}{d_0} - 1.7\,; 2.5\right\}$$

Equation 20

$$Inner\ bolts: k_1 = min\left\{1.4\frac{p_2}{d_0} - 1.7\,; 2.5\right\}$$

By maximizing the bearing resistance, $\alpha_b = 1$. In accordance with Section 8.5.12 in the NS EN 1999-1-1 [11] the factor $k_1 = 1.5$ for single lap joints are used. These factors give us a capacity, F_{Rd} higher than the design load, F_{Ed}.

$$F_{b,Rd} = 153.6\ \text{kN}$$

The spacing of fasters becomes:

$$e_1 \geq 54 \text{ mm} \quad p_1 \geq 67.5 \text{ mm} \quad e_2 \geq 27 \text{ mm} \quad p_2 \geq 54 \text{ mm}$$

Design for Block Tearing Resistance

The block tearing resistance for the bracket is checked for a bolt group subjected to eccentric loading. The block tearing resistance is given by Equation 21. As Table 23 summarizes, the block tearing resistance is sufficient to withstand the design load found in Table 18.

Equation 21

$$V_{eff,2,Rd} = 0.5 f_u \frac{A_{nt}}{\gamma_{M2}} + \frac{1}{\sqrt{3}} f_0 \frac{A_{nv}}{\gamma_{M2}}$$

Table 23: Design for Block Tearing Resistance.

Description	Value	Validation
Area subjected to tension A_{nt} $[mm^2]$	450	
Area subjected to shear A_{nv} $[mm^2]$	1330	
6082 T6 (EP) f_0 $[N/mm^2]$ [11]	260	
6082 T6 (EP) f_u $[N/mm^2]$ [11]	310	
γ_{M2} [11]	1.10	
γ_{M2} [11]	1.25	
$V_{eff,2,Rd}$ $[kN]$	216	√
Tension and shear area are switched: $V_{eff,2,Rd}$ $[kN]$	219	√

Design Resistance of Weld Connections

The bracket illustrated in Figure 61 is welded to the lower chord with fillet welds. For double fillet weld joints, loaded perpendicular to the weld axis, the throat thickness, a, is calculated by Equation 22 and Equation 23 [11]. The throat thickness is illustrated in Figure 63. $M_{Ed,y}$ induce F_{Ed} in Equation 23. The top bolts capacity is not included in this calculation which makes it conservative. The effective weld length is taken as the total length of the weld. The perpendicular load is the most critical and a weld of 3.6 mm is required to for the connection to hold as tabulated in Table 24.

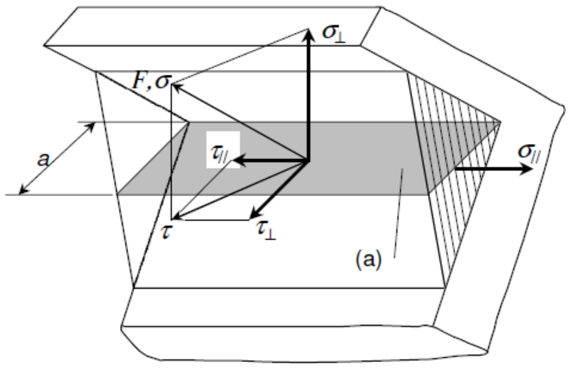

Figure 63: Throat distance a [11].

Equation 22

$$a \geq \frac{1}{\sqrt{2}} \frac{\sigma_{Ed} t}{f_w / \gamma_{Mw}}$$

Equation 23

$$\sigma_{Ed} = \frac{F_{Ed}}{tb}$$

Double fillet welded joint loaded parallel to the weld axis [11]:

Equation 24

$$a \geq \sqrt{\left(\frac{2}{3}\right)} \frac{\tau_{Ed} t}{f_w / \gamma_{Mw}}$$

Equation 25

$$\tau_{Ed} = \frac{F_{Ed}}{th}$$

Table 24: Design resistance of Welds.

Description	Value
σ_{Ed} $[N/mm^2]$	84.8
τ_{Ed} $[N/mm^2]$	21.43
t $[mm]$	10
Weld material 5xxx: f_w $[N/mm^2]$ [11]	210
γ_{Mw} [11]	1.25
a $[mm]$ (Perpendicular)	3.6
a $[mm]$ (Parallel)	1.04

Design Resistance in HAZ

By Section 8.6.3.4 in NS EN-1999-1-1 [11] the design resistance in HAZ is checked with Equation 26.

Equation 26

$$\sqrt{\sigma_{haz,Ed}^2 + 3\tau_{haz,Ed}^2} \leq \frac{f_{u,haz}}{\gamma_{Mw}}$$

$f_{u,haz} = 185\ \mathrm{N/mm^2}$. This stress level gives the satisfactory result: $92.6 \leq 148$

10.3.3 Top Bolts Resistance

As mention in Section 2.3.1, the price of an extrusion can rise significantly for profiles with a large cross-section. To minimize the dimensions of the lower chord the top bolt resistance is checked. The minimum fastener spacing is found with an acceptable bearing resistance. After minimizing the fasteners edge distance, the tearing resistance was still high enough to withstand the applied design load. Table 25 summarizes the calculation results. The same equations are used and explained in more detail earlier in Section 10.3.2.

Table 25: Top Bolts Resistance Calculations

Top Bolts Resistance			Validation
Shear force on top bolts *	N_{M_y} $[N]$	70.7	
Shear resistance for two shear planes. M16 bolts.	$F_{V,Rd}$ $[kN]$	100.5	√
Calculated minimal edge distance factor	α_b	0.526	
Minimal edge distance factor	$e_1 = \alpha_d 3 d_0$ [mm]	28.4	
Minimal edge distance factor **	$e_2 = 1.2 d_0$ [mm]	21.6	
Block tearing resistance	$V_{eff,1,Rd}$ [kN]***	804	√
Area subjected to tension	A_{nt} [mm^2]	3200	
Area subjected to shear	A_{nv} [mm^2]	840	

* 10 kN added from axial forces in the I-beam
** Minimal edge distance factor perpendicular on load direction
*** For a symmetric bolt group subjected to concentric loading.

$V_{eff,1,Rd} = f_u \frac{A_{nt}}{\gamma_{M2}} + \frac{1}{\sqrt{3}} f_0 \frac{A_{nv}}{\gamma_{M2}}$

10.3.4 Evaluation of Joint Solution 3

Since only LC1 and LC2 is utilized as design loads for the joint, the impact of LC3 was overlooked. LC3 will give a b moment in the opposite direction of LC1 and LC2. This bending moment will induce compression forces at the top of the lower chord and tension forces at the bottom. Since solution 3 only relay on the I-beam pushing itself onto the lower chord in compression, solution 3 will have a significantly reduced stiffness under LC3. This problem can be solved by adding connection bolts to the bottom flange of the connecting I-beam and add a bottom flange to the lower chord. LC3 induces much smaller forces, so the connection will still be valid if similar bolts are added as for the rest of the joint. The disadvantage of this new solution is that the lower chord profile gets larger and more expensive. The assembly will become much harder since the I-beams must be placed in between the two flanges on the lower chord. Further Investigation of this solution is needed, and a bolted flange solution, like solution 5 can be found adequate.

10.4 Splicing of Trusses and Chords

Figure 64 shows the three different places the bridge is planned sectionalized. As mention in Section 2.6 detailing of the bridge is of high importance when it comes to the aesthetics and the pedestrian's experience of the bridge. Therefore, the esthetic outcome of each solution illustrated in Table 27 is highly emphasized. Table 26 tabulates the internal forces, and different splice solutions are illustrated in Table 27. For the top chord and truss diagonal equal splice design has been chosen. No calculation on the bolts has been executed since the top chord is under compression forces. For further development of the bridge concept, the top chord splice must be further check.

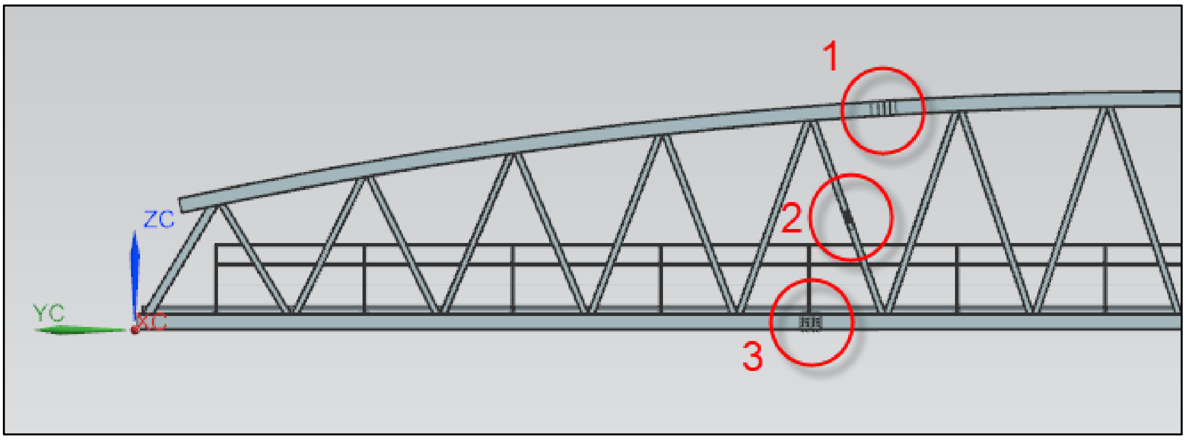

Figure 64: Splices; 1) Top chord splice (compression), 2) Truss diagonal splice (tension/compression) 3) Lower chord splice (tension).

Table 26: Internal forces in top (green), bottom chord (yellow) and truss diagonal (red).

Beam	dx [m]	Load case	N_{Ed} [kN]	$M_{y,Ed}$ [kN]	$M_{z,Ed}$ [kN]	T_{Ed} [kNm]
B4	13.6	LC1	-1029.09	1.18	-2.38	-
	13.6	LC3	-277,37	0.36	-3.08	-
	13.6	LC5	-465.46	1.38	-5.29	0.49
B34	13.6	LC1	-1072.02	1.20	1.03	-
	13.6	LC3	-424.77	0.66	-1.6	-
B348	13.3	LC1	190.99	5.77	-0.89	-
	13.3	LC3	24.53	1.59	-0.98	-
	13.3	LC5	101.56	3.70	0.45	4.21
B349	13.3	LC1	240.70	6.01	-1.53	-
	13.3	LC3	109.92	2.53	-1,23	-
B13	2.2	LC1	102.7	1,12	0,22	-

Table 27: Splice design solutions.

Name and figure	Pros	Cons
1 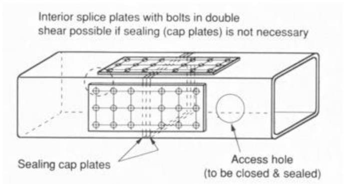 From the Steel Tube Institute [65]	Esthetically anonyms by not exceeding the beam dimension to much.	Reduced effective cross-section by introducing access hole in the beam.
2 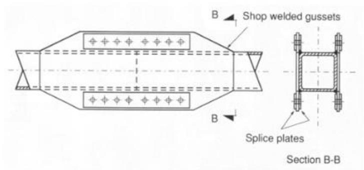 From the Steel Tube Institute [65]	Structural efficient. Takes the tension forces in shear of the bolts.	Not esthetically nice.
3 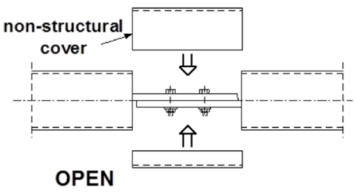 From the Steel Tube Institute [65]	Simple and esthetically pleasing.	Loose the squared tubes torsional stiffness.
4 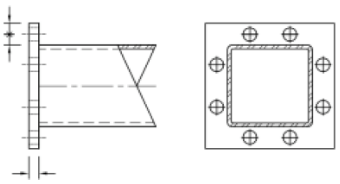 From the Steel Tube Institute [65]	Very compact and efficient splice. Maintain the torsional stiffness.	Not esthetically pleasing by exceeding the beams dimensions. In tension connection, a prying force Q must be added.
5 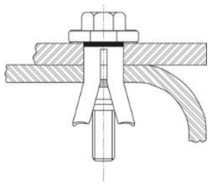 From Atlas Tube [66]	Need only access from one side of the bolt to make a connection.	Blind bolts or expansion bolts are not treated in NS-EN 1999-1-1 or -1-4. Some solutions need larger holes for the bolt.
6 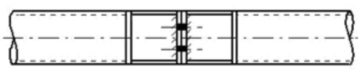 From steelconstruction.info [67]	Compact joint and esthetically pleasing if non-structural cover is used.	Demands a lot of welding. In tension, deflection of the end plates can cause problems. Extra stiffeners might be necessary to be added.

10.4.1 Truss Splice

The truss diagonal's internal forces decrease towards the center of the bridge. Therefore, a single splice at the mid of the length of the diagonal is found appropriate. This solution is structural qualified, gives an easier assembly and less loose parts. Table 28 summarizes the splice calculations. The splice is checked for tension in bolts, punching shear resistance, the butt weld between the splice and the truss diagonal and design resistance in HAZ. The same bolts and welding material are used as in Section 10.3.1. Tension resistance Equation from Table 8.5 in NS EN-1999-1-1 [11] is numbered as Equation 27 in this document. Butt weld subjected to normal stresses is shown in Figure 65.

Equation 27

$$F_{t,Rd} = \frac{k_2 f_{ub} A_s}{\gamma_{M2}}$$

Punching shear resistance is given by:

Equation 28

$$B_{p,Rd} = \frac{0.6\pi d_m t_p f_u}{\gamma_{M2}}$$

The design of butt welds by Section 8.6.3.2 in NS EN-1999-1-1 [11]. The equation is numbered as Equation 29.

Equation 29

$$\sigma_{\perp Ed} = \frac{F_{Ed}}{\sum w_i t_i}$$

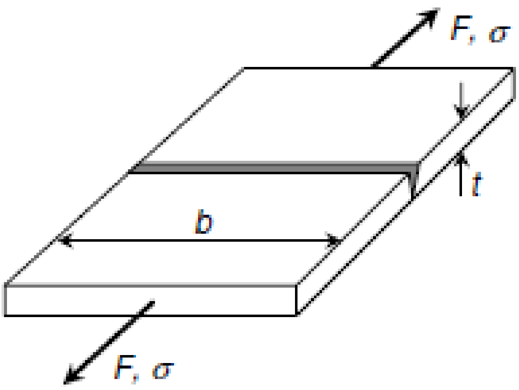

Figure 65: Butt weld subjected to normal stresses [11]

Table 28: Truss diagonal splice calculation

Truss diagonal splice calculation			Validation
Tension resistance per bolt (M16) [kN] $k_2 = 0.5\ (aluminum\ bolts)$	$F_{t,Rd}$	50.3	
Tension resistance 4 bolts (M16) [kN]	$F_{t,Rd}$	201	√
Punching shear resistance per bolt (M16) [kN] d_m = 24 mm* t_p = 10mm ** $f_{u,haz}$ = 185 N/mm^2 ***	$B_{p,Rd}$	67	
Punching shear resistance 4 bolts (M16) [kN]	$B_{p,Rd}$	268	√
Full penetration butt weld for primary load-bearing members [N/mm^2] ****	$\sigma_{\perp Ed}$	34.3	
Normal stress, tension or compression perpendicular to weld axis [N/mm^2]	$\sigma_{\perp Ed} \leq \frac{f_w}{\gamma_{Mw}}$	$34.3 \leq 168$	√
Design resistance HAZ [N/mm^2] $A = 8068\ mm^2$	σ_{Ed}	12.8	
HAZ butt welds	$\sigma_{Ed} \leq \sigma_{haz,Ed}$	$12.8 \leq 148$	√
* d_m: is the mean of the across points and across flats dimensions of the bolt head or the nut or if washer. Whichever is smaller. ** Thickness of plate *** Conservative approach with HAZ yield limit of base material *** Only the two top welds in the connection are used in the check			

10.4.2 Lower Chord Splice

As mention as a con in Table 27, solution 6 is prone to endplate deflection, which makes the coupling less stiff. Solution 1 is found best to avoid this endplate deflection problem. Solution 1 avoids the end plate deflection problem by taking the tension load in shear at the bolts. This solution also gives the splice a neutral aesthetic expression. The calculation is summarized in Table 29 where the tension load of 240.7 kN is used as design criteria. From the calculation, the splice is found to be sufficiently strong. The calculations are similar to the shear connection between the lower chord and I-beams, these calculations are explained in more detail in Section 10.3.2. The bolt quality is equivalent to the bolt listed in Table 20.

Table 29: Splicing of lower chord calculation summary.

Splicing of lower chord			Validation
Shear resistance 24 shear planes [kN]: (M20)	$F_{v,Rd}$	1881.6	√
Bearing resistance [kN] $k_1 = 1, \alpha_2 = 2.5$	$F_{b,Rd}$	5734.4	√
Block tearing resistance [kN]: $A_{nt} = 1232\ \mathrm{mm}^2$ $A_{nv} = 2688\ \mathrm{mm}^2$	$V_{eff,1,Rd}$	628	√
Cross-section hand hole reduction, design stress [$\mathrm{N/mm}^2$]:	σ_{Ed}	14.6	√

10.4.3 Evaluation of Splice Solution

To summarize the evolution of the splice designs further work should be accomplished to ensure structural adequateness. Slip resistance connections has not been calculated but should be investigated in the further work of the bridge. These connections will improve fatigue resistance. From the calculation utilized in this section shows promising results based on the internal forces from the SCIA analysis. The solution gives the bridge an appealing look, by basing the splice design on a relatively aesthetic solution.

11 Concept Evaluation

In the initial evaluation, the aluminum pedestrian bridge concept, the structural capabilities, weight, functionalities, and cost of the proposed concept is discussed. The bridge concept is illustrated in Figure 66. Detailed drawing of the bridge components and assemblies can be found in Appendix 2. The bridge weight in aluminum is 23 tons. A fabrication cost estimate from MA gives an approximate cost of 6 650 000 NOK for the bridge. Chapter 12 takes this discussion further.

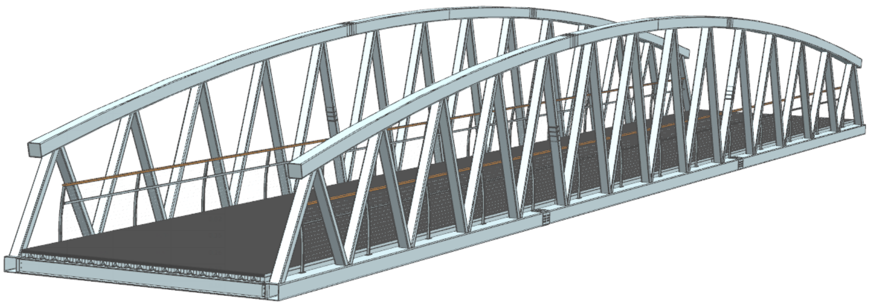

Figure 66: Bridge concept.

11.1 Transportation

The thought behind the bridge assembly is to divide the trusses into three sections as illustrated in Figure 67. The I-beams and trusses are transported separately and assembled close to the installation site. By dividing the bridge into three parts, the splice is moved away from the area at the center with the highest internal forces. If the bridge modules were kept under 3 m wide, 15 – 16 m long and 3.5 m high, it is a referred to as a standard transportation job. The mid truss sections are 4.5 m high, but still within the requirements of the maximum transportation height as found in Section 2.6.5. The transportation solution which utilizes the total transportation height should be used. This design will ensure efficient transportation and short assembly time with few parts to assemble.

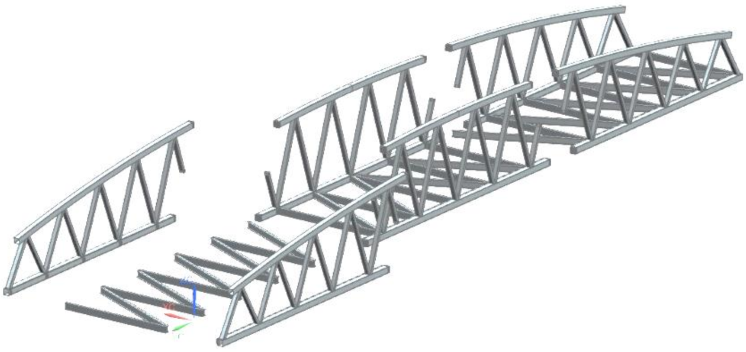

Figure 67: Bridge assembly for transportation.

11.2 Connections and Splices

Most of the connections and splices are all illustrated in Figure 68 from a) – d). The lower chord splice is shown in Figure 69. The same design is used on the upper chord splice as the truss diagonals and is therefore not illustrated explicitly. Principals from DfX found in Section 4.1.1 were utilized in the development. Multifunctional parts, minimized the amount of parts and design for easy manufacturing are all principals used. One of the DfX principles suggests that the assembly directions should be minimized, where a top-down approach is most desirable. These principles are only partly fulfilled since most assembly directions are used. The structural integrity of the joint should be adequate according to the calculation done in Section 10.4. Further work has to be done to ensure that all the joints have sufficient stiffness, especially the lower chord – I-beam connection and the upper chord splice.

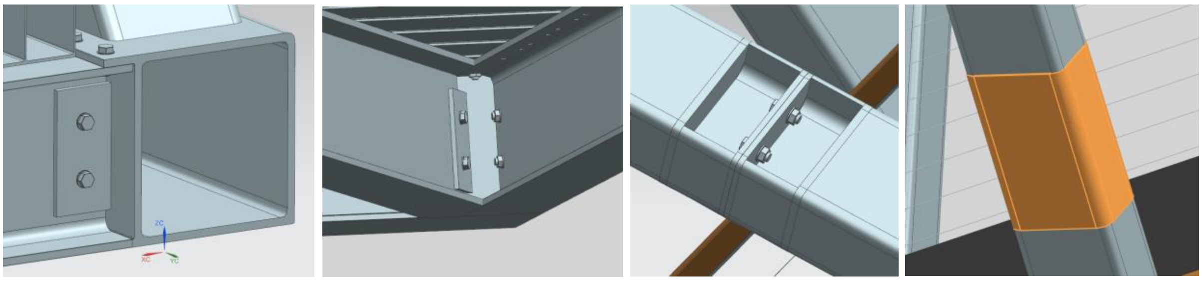

(a) (b) (c) (d)

Figure 68: Connections and splices: a) Lower chord – I-beam b) Lower chord – I-beam diagonal c) Truss diagonal splice without non-structural cover. d) Non-structural cover (marked with orange).

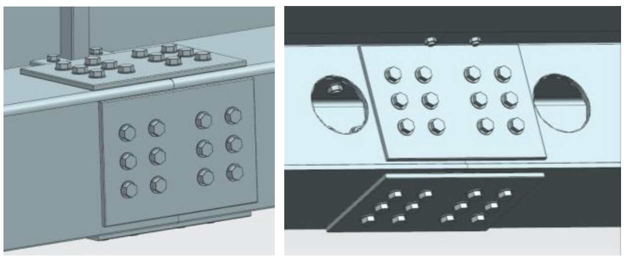

(a) (b)

Figure 69: Lower chord splice: a) Front side, b) Back side.

11.3 Bridge deck

The LBD solutions were found to be the best option as discussed in Section 8.3. Figure 70 a) illustrates the cross-section design. Detailed drawings can be found in Appendix A2. Because of transportation size restriction, panels are divided into three lengths up to 15 m in length. The width of the panels is 3 meters so that they can lay flat on a truck floor under transportation. The panels layout installed on the bridge is illustrated in Figure 70 b). The end profile has a 6 cm long extruded edge, as indicated by the orange arrow in Figure 70 a). This edge is designed to keep the asphalt in place. The bridge deck profiles are joined by bolts, to the underlying I-beams. The FSW bridge deck shows great potential, but there is still some detailing remaining. The joints between the FSW panels in both longitudinal and transverse direction is not addressed in this study. Also, detailed calculation and design concerning the connection to the I-beams must be done.

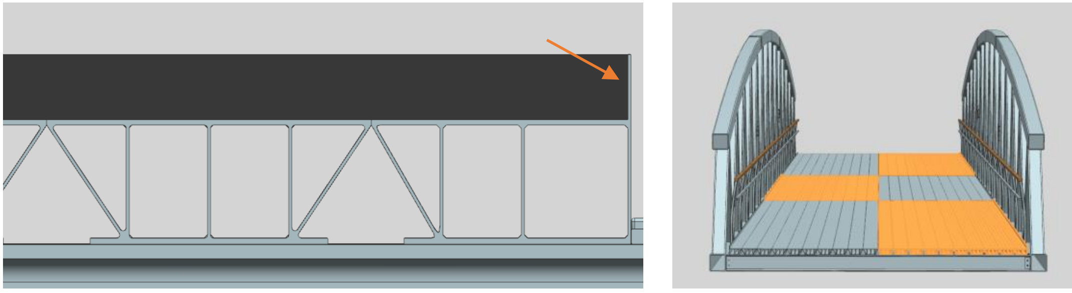

(a) (b)

Figure 70: Bridge deck profile: a) FSW bridge deck with end profile. b) FSW panel lay out.

11.4 Railing

The handrails are designed to explore and demonstrate some of the possibilities within an aluminum design. The railing is illustrated in Figure 71 a). The railing consists of wooden top rail at the height of 1.4 m and stainless-steel wires to ensure adequate safety. Due to ergonomic findings [27] the railing also has an extra rail in the height of 90 cm. The railing is bolted onto the lower chord top flange and utilizes the multifunction extrusion of the lower chord. The bridge has a very efficient and compact design. By having the rails bent inward, the needed clearance to the trusses is obtained. The inwards angle on the handrails also prevents people from from climbing on the rails [27]. Easy connection between the aluminum and wood is obtained by a Christmas tree design [16] on the top handrail seen in Figure 71 b). The connection strength is not analyzed for the Christmas tree design, but could also be combined with gluing or bolting. Another aluminum specific design is the design of the clips [16] shown in Figure 71 c) on the lower handrail. No structural calculation has been performed on the railing system, and further detailing needs to be done. These solutions show the great potential of aluminum. A fast and easy assembly will be obtained with these methods.

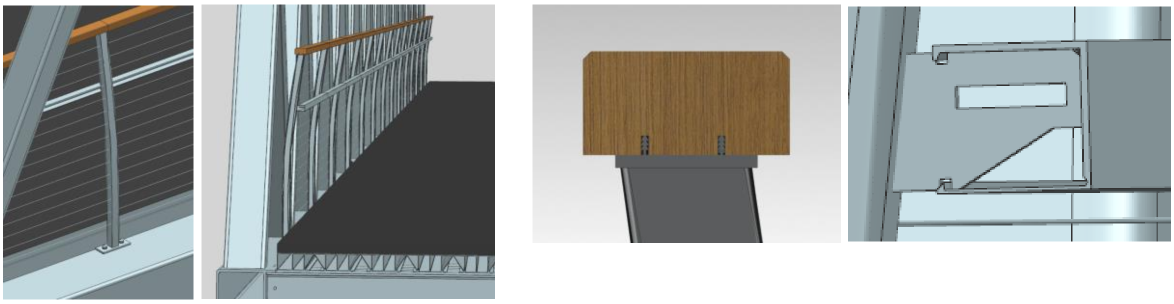

(a) (b) (c)

Figure 71: Handrailing: (a) Railing connection to lower chord and perspective view (c) Top handrail connection (d) Lower handrail connection.

11.5 Discussion

The pedestrian bridge concepts show the favorable result with a low self-weight. Smart and creative use of FSW and extruded profiles gives the pedestrian bridge concepts unique solutions. There is still some work that needs to be done until a fully functioning and safe bridge solution is ready. The relative vertical deflection over the transverse bridge span is not fulfilling the criteria for deflection. Anyhow this pedestrian bridge concept demonstrates the potential of utilizing aluminum as a bridge construction material in the lightweight pedestrian bridge segment.

12 Comparison Between Aluminum Concept and Baseline Solution from NPRA

In this section, the developed aluminum concept bridge, see Figure 72, is compared with the chosen baseline solution from NPRA, shown in Figure 73. Fabrication cost, weight, and structural integrity is the comparison basis. Aspects like assembly, transportation, and installation are hard to compare due to lack of information. The NPRA cost estimate is calculated for an alternative bridge solution for the Forus bridge in Stavanger [68]. The cost estimate of the FRP truss bridge is for a bridge with a length of 40 m and 6.6 m width, the estimate includes also a special pedestrian bridge railing. Very few composite bridges and structures exist in Norway. The price is therefore mostly based upon composite value from international estimates. This method is presumably a good way to estimate the prices in Norway as well since the bridge can be produced and shipped from anywhere in the world [68]. The cost estimate is not directly related to the Paradis bridge in Bergen, but dimensions and surrounding conditions are very similar to the Forus bridge. It will, therefore, give a good cost estimate of the Paradis bridge. The cost estimate from MA is primarily based upon fabrication cost in NOK/kg of the bridge structure. MA uses the same estimate for their regular gangways and is presumably a good estimate for this conceptual pedestrian bridge as well [69]. The additional cost is added for railings in NOK/m. This estimate is based upon one of MA railing systems. The values for weight and cost comparison are tabulated in Table 30.

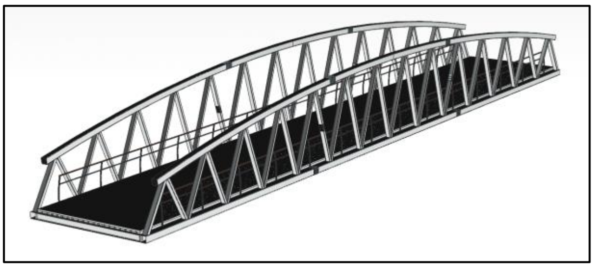

Figure 72: Aluminum pedestrian bridge concept.

Figure 73: Baseline solution from NPRA.

Table 30: Comparison between aluminum concept and Paradis bridge.

	Aluminum Concept Bridge	GFRP Paradis Bridge
Weight of bridge: [tons]	23	42
*Total weight: [tons]	63	87
Estimated fabrication cost: [NOK]	6 650 000	6 350 000
*The total weight includes the steel inserts in the GFRP joints and the asphalt layer.		

As tabulated in Table 30, the aluminum bridge is found to be a much lighter bridge construction than the GFRP bridge solution. Even with more detailed analysis and worst-case scenarios of the aluminum concept which can increase the bridge load. The aluminum concept can experience a 45% weight increase before it reaches GFRP solution weight. There are also other arguments for the aluminum solution to be lighter than the GFRP bridge. For instant aluminum comes better out of the specific strength – specific stiffness ratio comparison shown in Section 2.4. The GFRP Paradis bridge also has challenges with joint design, where steel inserts are used as mention in Section 3.2. Degradation and aging due to low thermal resistance and UV radiation, GFRP must be designed accordingly to these phenomena. These aspects may add some extra weight to the GFRP solution which is not added in the aluminum design.

The fabrication cost of the bridges is found almost identical. The values are tabulated in Table 30. As discussed earlier in this section, there is related some uncertainty to the estimates. Regardless the cost comparison gives a good indication on how the two bridges are compared to each other. Aluminum has proven to be competitive on initial cost on some specific pedestrian bridge projects. In general, due to higher initial cost compared to conventional bridge materials both GFRP and aluminum benefit from the increased use of LCCA. Compared to GFRP, aluminum has two distinct advantages as construction material. Aluminum is field proven with excellent results in very harsh environments both on shore and off shore. Norway's climate varies with extreme cold, humid environment, and salty roads. With aluminum's unique corrosion properties and toughness at low temperature, it will make a design which fit for all environments more easily. The consequences of long-term degradation of GFRP is still in need of research. The second advantage is aluminum's recyclability after ended lifetime, whereas GFRP ends up as scrap. This advantage makes aluminum more environmental friendly solution. To summarize, the aluminum is found highly competitive as a lightweight bridge material. Compared to the baseline solution from NPRA, the aluminum concept bridge shows a promising result.

13 Summary and Recommendations for Further Work

13.1 Summary and Conclusions

The primary objective of this thesis is to evaluate the potential of aluminum solutions within pedestrian bridges. This seen in competition with common steel and concrete solutions as well as new materials such as FRP. In the theory chapter, a comparison of aluminum to other construction materials is made. Many existing and successful aluminum pedestrian bridges demonstrates aluminum's potential in this sector. As a construction material, aluminum contains several advantages. High specific strength, high corrosion resistance, no need of periodic maintenance and low residual stresses caused by constrained thermal deformation. The material is also field proven since 1933 as a bridge material. Concerning manufacturability of aluminum, smart and creative use of manufacturing methods gives the material an advantage. A pedestrian bridge can be designed with unique solutions by utilizing the possibilities of FSW and extrusion of profiles. Some downsides concerning aluminum as a construction material are susceptibility for fatigue, low stiffness compared to steel, low fire resistance, prone to local buckling and strength reduction in HAZ. The consequences of these aspects can very often be minimized with good design. The limited use of aluminum as bridge material is mostly based on the lack of knowledge and historical lack of standards and guidelines. The building sector's reliance on acquisition cost and warranty condition for their investments and not LCCA have also put a limitation for aluminum pedestrian bridge projects.

The manufacturing capabilities of MA is only mentioned in relevant chapters concerning the development of the pedestrian bridge concept. The feasibility of introducing aluminum of the two bridges from NPRA is covered in Chapter 3. The GFRP bridge at Paradis in Bergen was found to be the most suitable case. This finding is due to aluminum and FRP competition as materials in the lightweight pedestrian bridge segment. Both materials hold many of the same qualities with different disadvantages.

The development of the aluminum pedestrian bridge concept is based on the structural requirements of the Paradis bridge. These requirements gave a useful foundation for the comparison. The initial evaluation of the bridge concept provides a 23-ton bridge structure with a fabrication cost of 6.65 MNOK. Compared to the baseline solution from NPRA the aluminum bridge only has 45% of the weight in aluminum as GRFP in the baseline solution. The initial cost estimate of Paradis bridge is 6.35 MNOK with a weight of 42 tons in GFRP. The estimated fabrication cost ended up almost equal for the two concepts, and only the significant deviation in weight is differentiating them. As discussed in Chapter 12 aluminum has two distinct advantages as construction material compared to GFRP. Aluminum is field proven with outstanding results both onshore and offshore. With several environmental independent and resistant material properties, aluminum is suitable for the large climate variations in Norway. The second advantage is aluminum recyclability after ended lifetime, which is a significant environmentally gain.

Aluminum has a bright future if increased knowledge among builders and engineers, better standards and guidelines, and increased focus on LCCA becomes a reality. The development of the aluminum pedestrian bridge in this thesis, demonstrates aluminum capabilities applicable for pedestrian bridges in Norway.

13.2 Further Work

The further work short-term recommendations for this particular study would be:

- Further evaluation of a TBD concept with double sided FSW panels.
- The nonlinear inelastic analysis should be adopted in the future development the bridge.
- Thermal analysis.
- Further detailing and Structural analysis of railing system.
- The joint between the FSW panels in both longitudinal and transverse direction is not addressed in this study and between the FSW panels and bridge deck I-beams.
- More detailed studies of the structural behavior of joints and splices.
- In-depth analysis of eigenfrequencies and eigenmodes.
- Bridge specific details like fugues, bridge bearings, and expansion joints.
- General weight optimization and further detailing of the bridge concept.
- Fatigue analysis of bridge structure.

For medium and long-term work that needs to be done to further promote and prove aluminum as the future for pedestrian bridge material is:

- Raise awareness of aluminum's advantages as construction material among students, builders, and engineers.
- Further development of pedestrian bridge design guidelines for aluminum.

14 References

1. Siwowski, T., *Aluminium bridges–Past, present and future.* Structural engineering international, 2006. **16**(4): p. 286-293.
2. Ole Øystein Knudsen, D.N., Rune Gaarder, Tor Arne Hammer, *New materials in tunnels and bridges*, in *NPRA reports*. 2016, Norwegian Public Roads Administration. p. 26.
3. page], A.I.a.B.W. *Aluminium; Infrastructure and Bridges*. 2017 [cited 2017 24.05.2017]; Available from: https://aluminium.ca/en/aluminium/infrastructure-and-bridges.
4. Joux, S. *Aluminium Bridges*. in *Key Engineering Materials*. 2016. Trans Tech Publ.
5. Administration, P.R., *Bruprosjektering Prosjektering av bruer, ferjekaier og andre bærende konstruksjoner*, in *Håndbok N400*. 2015, Public Road Administration.
6. Kosteas, D. *Sustainability, Durability and Structural Advantages as Leverage in Promoting Aluminium Structures*. in *Key Engineering Materials*. 2016. Trans Tech Publ.
7. Mazzolani, F.M., *Competing issues for aluminium alloys in structural engineering.* Progress in Structural Engineering and Materials, 2004. **6**(4): p. 185-196.
8. MatWeb. *Aluminum Alloy Heat Treatment Temper Designations*. 2017 [cited 2017 28.03]; Available from: http://www.matweb.com/reference/aluminumtemper.aspx.
9. SIELSKI, R.A., *Review of structural design of aluminum ships and craft.* Transactions-Society of Naval Architects and Marine Engineers, 2007. **115**: p. 1-30.
10. R.J. Bucci, G.N., E.A. Starke, Jr, *Selecting Aluminum Alloys to Resist Failure by Fracture Mechanisms*.* ASM Handbook, 1996. **19**: p. 771-812.
11. *Eurokode 9: Prosjektering av aluminiumskonstruksjoner = Eurocode 9: Design of aluminium structures. Part 1-1: General structural rules : Del 1-1 : Allmenne regler*. Eurocode 9: Design of aluminium structures. Part 1-1: General structural rules. Vol. NS-EN 1999-1-1:2007+A1:2009+NA:2009. 2009, Lysaker: Standard Norge.
12. Vigh, L.G., et al., *Conceptual Design of an Aluminium Bridge in Alma, QC.* Key Engineering Materials, 2016. **710**.
13. Kosteas, D., *Aluminium Footbridges.* The 24th Annual Bridges Conference, 2016.
14. Valberg, H.S., *Extrusion*. 2010, Cambridge: Cambridge: Cambridge University Press. 320-346.
15. page], A.E.W. *Aluminum Extrution*. (n.d.) [cited 2017 27.06.2017]; Available from: http://www.abralco.com/index.php/about-aluminium/aluminum-extrusion.
16. [Håndbok], K., *Konstruktørhåndbok; suksess med aluminiumsprofiler*. 2015: SAPA. 200.
17. Mishra, R.S. and Z.Y. Ma, *Friction stir welding and processing.* Materials Science and Engineering: R: Reports, 2005. **50**(1–2): p. 1-78.
18. SAPA, *Friction Stir Welding*. 2011, SAPA.
19. Gharavi, F., et al., *Corrosion behavior of Al6061 alloy weldment produced by friction stir welding process.* Journal of Materials Research and Technology, 2015. **4**(3): p. 314-322.
20. HyBond. *HyBond a bonding revolution*. 2015 [cited 2017 24.05.2017]; Available from: http://www.hybond.no/.
21. Mathers, G., *The welding of aluminium and its alloys*. 2002: Woodhead publishing.
22. Dieter, G.E. and D. Bacon, *Mechanical metallurgy*. SI metric ed. ed. McGraw-Hill series in materials science and engineering. 1988, London: McGraw-Hill.
23. Pedram, M. and M.R. Khedmati, *The effect of welding on the strength of aluminium stiffened plates subject to combined uniaxial compression and lateral pressure.*

International Journal of Naval Architecture and Ocean Engineering, 2014. **6**(1): p. 39-59.
24. note], M.a.P.S.C.L. *2 Material and Prcess Selection Charts* 2010 [cited 2017 19.06.2017]; Available from: http://www.grantadesign.com/download/pdf/teaching_resource_books/2-Materials-Charts-2010.pdf.
25. Potyrała, P.B., *Use of Fibre Reinforced Polymer Composites in Bridge Construction. State of the Art in Hybrid and All-Composite Structures*, in *Enginyeria de la Construcció* 2011, Univeritat Poletècnica de Catalunya.
26. [pdf], A.B.D. *Aluminium Bridge Design*. [Presentation] 2015 26.11.2015 [cited 2017 21.06.2017]; Available from: https://www.eiseverywhere.com/file_uploads/b6dea4980e1919e820459b0c9c8e0bee_16.00PML20151107BridgeConferenceMelbourne.pdf.
27. Keil, A. and C. McKenna, *Pedestrian Bridges : Ramps, Walkways, Structures*. DETAIL Practice. 2013, Berlin: DETAIL.
28. Bendik Manum, S.D., *Konsept bru i Aluminum, møte*, C.A.R. Brekke, Editor. 2017.
29. Krenk, S. and J. Høgsberg, *Statics and mechanics of structures*. 2013: Springer Science & Business Media.
30. Kumar, S.R.S.K.A.R.S., *Design of Steel Structures*. 2006, Indian Institute of Technology Madras.
31. Makes, L. *Cable Tie Truss Bridges*. [cited 2017 21.06.2017]; Available from: http://www.instructables.com/id/Teach-Engineering-Truss-Bridges/.
32. Larsen, P.K., *Dimensjonering av stålkonstruksjoner*. 2. utg. ed. 2010, Trondheim: Tapir akademisk forl.
33. page], T.-a.b.W. *Tied-arch bridges*. (n.d.). [cited 2017 24.05.2017]; Available from: http://www.steelconstruction.info/Tied-arch_bridges.
34. URS Corporation, I., *Deck Alternative Screening Report; Final*, in *Bascule Bridge Lightweight Solid Deck*. 2012, Florida Department of Transportation. p. 112.
35. URS Corporation, I., *Research Program Notes; Draft*, in *Bascule Bridge Lightweight Solid Deck Retrofit Research Project*. 2015, Florida Department of Transportation. p. 42.
36. paper], A.p.o.b.d.E.P., *Asphalt pavements on bridge decks*. 2013, European Asphalt Pavement Association p. 12.
37. Fordal, S.K., *Meeting at Prøven Transport AS*, C.A.R. Brekke, Editor. 2017.
38. vegvesen, S., *Veg- og gateutforming*, in *Håndbok N100: Veg- og gateutforming*. 2014, Staten vegvesen: www.vegvesen.no. p. 177.
39. page], A.-B.ü.d.A.W. *Alu-Brücke über die A5*. 2015 [cited 2017 21.06.2017]; Available from: http://www.ingenieurbau-trends.de/alu-bruecke-ueber-die-a5/
40. as, J.H., *Fv 44 Gausel st. - Hans & Gretestien* in *Forprosjekt*. 2014, Statens vegvesen Region Vest.
41. Stian Persson, K.v.I., *FRP pedestrain bridge Norway*, P.R. Administraion, Editor. 2016: Brukonferansen 2016.
42. Reiso, M., *Masteroppgave*, C.A.R. Brekke, Editor. 2017.
43. Hildre, H.P., *Intro and phase 1*, in *IPM model*. 2001, NTNU: it's learning - NTNU.
44. Ulrich, K.T. and S.D. Eppinger, *Product design and development*. 5th ed. ed. 2012, New York: McGraw-Hill.
45. Skjelstad, *Design for X, den praktiske estetikk*. 2003, SINTEF.
46. handout], D.f.M.-G.L., *Design for Manufacturing - Guidelines*. 2002, University of New Mexico.

47. Administration, P.R., *Universell utforming av veger og gater*, in *V 129*. 2014, Public Road Administration.
48. Norge, S., *NS-EN 1991-2: 2003+ NA: 2010: Eurokode 1: Laster på konstruksjoner, Del 2: Trafikklast på bruer*. 2003, Brussel: CEN.
49. *Eurokode 1: : Laster på konstruksjoner. Del 1-3. Allmenne laster. Snølaster = Eurocode 1: Actions on structures : Part 1-3: General actions, Snow loads*. Eurocode 1: Actions on structures : Part 1-3: General actions, Snow loads. Vol. NS-EN 1991-1-3:2003+NA:2008. 2008, Oslo: Standard Norge.
50. Norge, S., *NS-EN 1991-1-4: 2005+ NA: 2009: Eurokode 1: Laster på konstruksjoner, Del 1-4: Allmenne laster, Vindlaster*. 2009, Brussel: CEN.
51. Administration, P.R., *APPROVAL IN PRINCIPLE Bridge Paradis*. 2016, Public Road Administration.
52. Norge, S., *NS-EN 1991-1-5: 2003+ NA: 2008: Eurokode 1: Laster på konstruksjoner, Del 1-5: Allmenne laster, Termisk påvirkning*. 2008, Brussel: CEN.
53. Administration, P.R., *Rekkverk og vegens sideområder*, in *Håndbok N101*. 2014, Public Road Administration.
54. Jakobsen, M.M., *Produktutvikling : verktøykasse for utvikling av konkurransedyktige produkter*. 1997, Oslo: Fortuna forl.
55. Johannessen, J., *Tekniske tabeller*. Utg. nr 2. ed. 2002, Oslo: Cappelen.
56. Lundberg, S., *Structural test of helideck top-profile HMA5360; test report and results*. 2009, Marine Aluminium.
57. Blingnault C, K.S.W., Thomas W M, Rusell M J, *Friction stir weld integrity and its importance to the rolling stock industry*. 2008, The Welding Institute: Southern African Institute of Welding (SAIW) conference, Integrity of Welded Structures in the Energy, Processing and Transport Industries in Southern Africa, Gold Reef City, 28-29 May 2008.
58. Aspnes, M.A., *Asfaltering av bro-dekke*, C.A.R. Brekke, Editor. 2017. p. 1.
59. page], N.v.a.v.m.s.w. *Natural vibration analysis versus mesh size*. (n.d.) [cited 2017 16.06.2017]; Available from: http://help.SCiA.net/16.0/en/rb/calculation/natural_vibration_analysis.htm.
60. page], M.s.w. *Mesh setup*. (n.d.) [cited 2017 16.06.2017]; Available from: http://help.SCiA.net/15.0/en/rb/basics/mesh_setup.htm.
61. analysis, C.m.f.d. *Calculations model for dynamic analysis*. (n.d) [cited 2017 15.06.2017]; Available from: http://help.SCiA.net/16.0/en/rb/calculation/calculation_model_for_dynamic_analysis.htm.
62. Wen, Q. and Y. Qi, *Rearch on design of aluminum truss bridge*. 2011. p. 1776-1779.
63. Waløen, Å.Ø., *Kompendiet - Dimensjonering ved elementmetoden*. 1995, NTH: NTNU.
64. page], T.B.a.D.o.W.C.b.R.H.S.U.P.S.L.W. *The Behaviour and Design of Welded Connections between Rectangular Hollow Sections Under Predominantly Static Loading*. (n.d.) [cited 2017 19.06.2017]; Available from: http://fgg-web.fgg.uni-lj.si/~/pmoze/esdep/master/wg13/l0300.htm.
65. Packer, J.A. *HSS Splices*. 2016 21.12,2016 01.06.2017]; Available from: https://steeltubeinstitute.org/hss/2016/06/30/hss-splices/.
66. Hansen, K. *Expansion Bolts for HSS: An analysis of a new, viable option for HSS connections*. 2014 [cited 2017 01.06.2017]; Available from: http://www.atlastube.com/atlas-observer/hollow-structural-section/expansion-bolts-for-hss-a-new-viable-option-for-hss-connections.
67. connections, E. *Expressed connections*. (n.d) [cited 2017 01.06.2017]; Available from: http://www.steelconstruction.info/Expressed_connections.

68. Persson, S., *Masteroppgave NTNU - Kostnadsoverslag*, C.A.R. Brekke, Editor. 2017.
69. Lundberg, S., *Masteroppgave - NAPIC - Kostandsoverslag*, C.A.R. Brekke, Editor. 2017.

Appendix A:

A1: Method 1 Two Heights

Loads and supports illustrated in Figure A1.1. Hinged and sliding supports on both short sides. The point load is a “free force” of 100 kN and is placed using coordinates at the center of the plate.

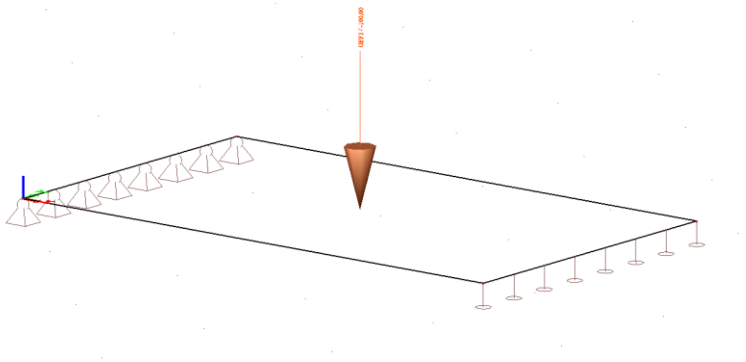

Figure: A1.1

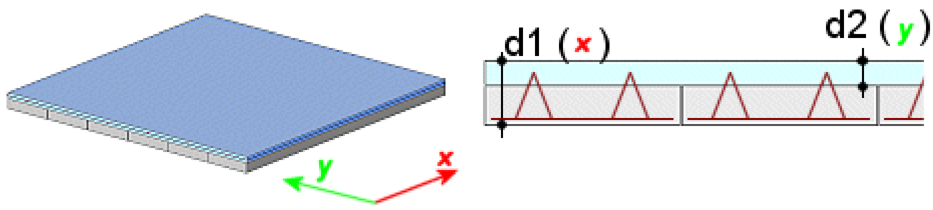

Figure: A1.2

In SCIA help the method is described as *“This type of orthotropy is suitable for slabs that feature "different height" in two parallel directions.”*. *“The panels and the topping are "linked" together through reinforcement protruding from the panels and entering the topping.”* http://help.SCiA.net/15.0/en/rb/modelling/orthotropy_manager.htm And is clearly developed for orthotropic concrete slabs with a casted in situ top layer as illustrated in Figure A1.2. With the assumption that the height could be take out from the section modulus formula for a massive, square cross-section. The height was found by using the moment of inertia of the HMA5360 helideck profile.

$$W_x = \frac{I_x}{y} = 1.5{\times}10^5\ \mathrm{mm}^2$$

By utilizing the point load distribution, 80% of the section modulus of seven panels was added to the equation.

$$0{,}8 \times 7 \times W_x = \frac{1}{6} b h^2 \rightarrow h = \sqrt{\frac{6 \times 0.8 \times 7 \times W_x}{b}} = 49.7\ mm^2$$

Flexural rigidity = Bending stiffness. Membrane theory describes the mechanical properties of shells when twisting and bending moments are small enough to be negligible. The flexure and membrane height is set to equal values. With these assumptions, the total displacement was way too high by applying a height of 50 mm as illustrated in Figure A1 and Table A1. The stiffness in x- direction had little influence on the total displacement. To test $d_1 = 75$mm was used and $d_2 = 20mm$. Theses measures gave the right displacement, but with two unknown factors, this method could not be used in this case. SCIA support was contacted without replay. The method has potential since the distribution of loads in both directions seems to be distributed nicely.

$F\ (kN)$	$d_1\ (mm)$	$d_2\ (mm)$	$u_z\ (mm)$	$u_y\ (mm)$
100	50	40	-60	0
100	75	20	-23	0

Table A1.1

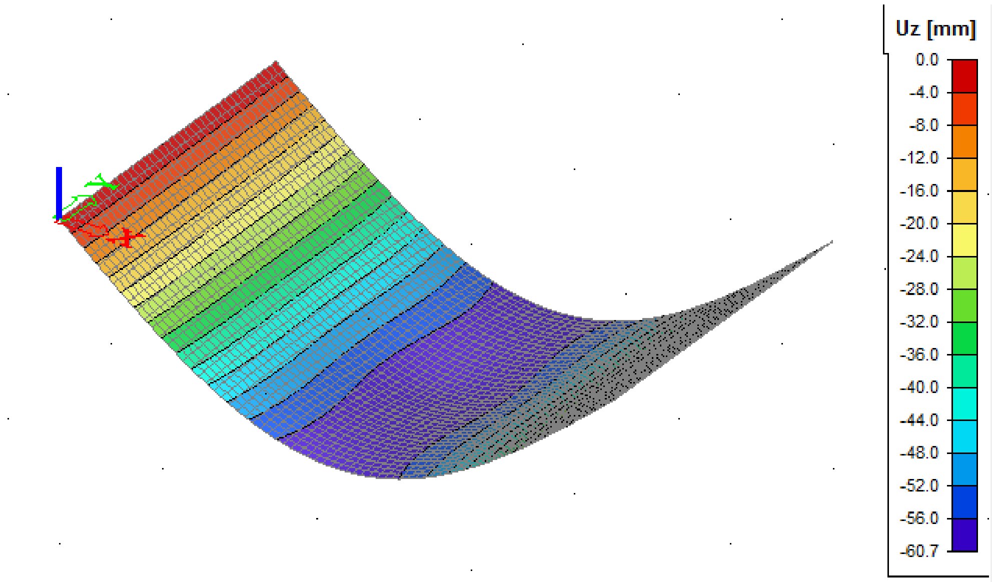

Figure A1.3

A2: Cost Estimate Underlaying

Nr:	Name	Description	Quantity	m/profile
1	LC1	Lower chord 1	4	84.5
2	LC2	Lower chord 2	2	
3	TC1	Top chord 1	4	80.7
4	TC2	Top chord 2	2	
5	I-beam_t	I-beam transverse	15	182.8
6	I-beam_d	I-beam diagonal	14	
7	Truss diagonals	Truss diagonals	4	207.6
8	Truss diagonals 2	Truss diagonals 2	2	
9	Flange	Flange	58	12.8
10	Splice	Splice	4(8)	-
11	Tension splice	Tension splice	16	-
12	Bridge deck profile	Bridge deck profile	54	756
13	Bridge deck end profile	Bridge deck end profile	6	84
14	T1 assembly	Truss 1 assembly	4	-
15	T2 assembly	Truss 2 assembly	2	-
16	FSW 1 assembly	FSW 1 assembly	4(6)	-
17	Railing assembly	Railing assembly	28	84
18	Bridge	Bridge total assembly	1	-

Table A2.1

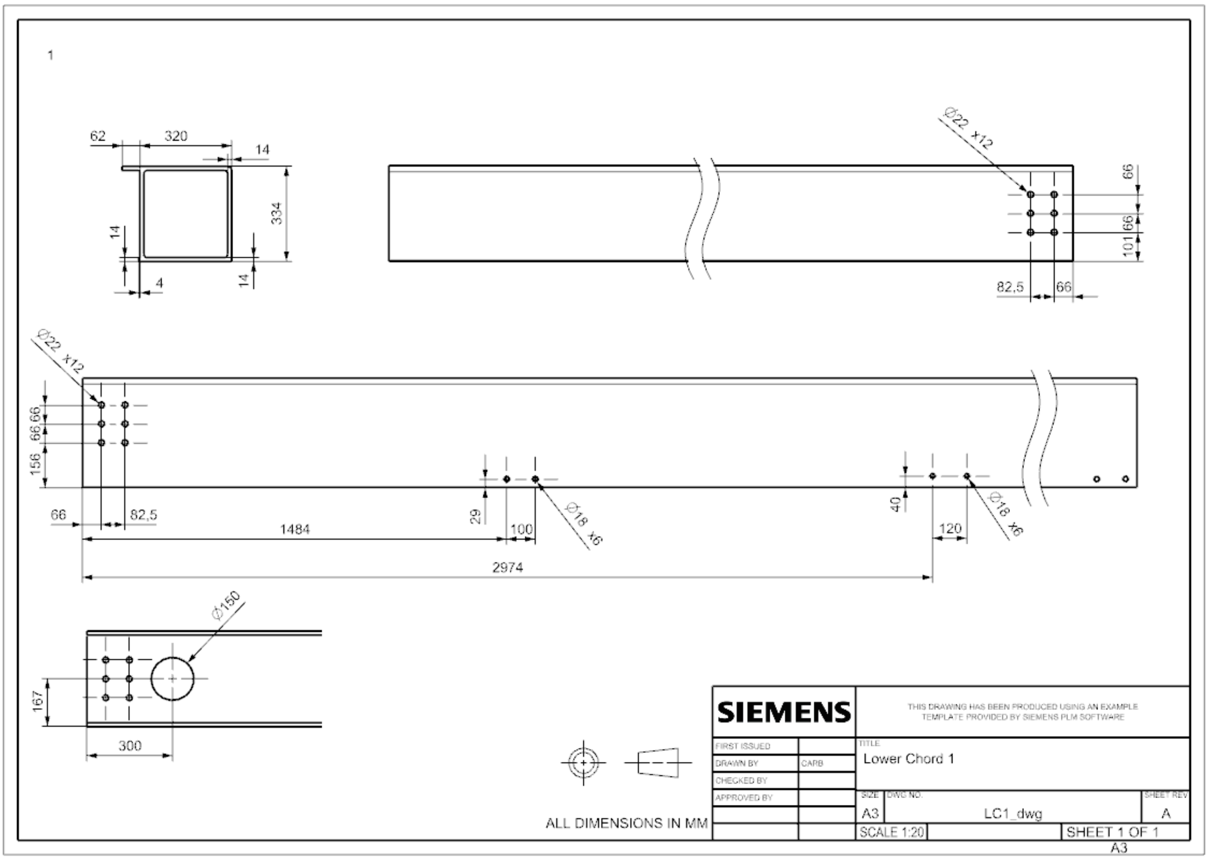
1
SIEMENS
THIS DRAWING HAS BEEN PRODUCED USING AN EXAMPLE TEMPLATE PROVIDED BY SIEMENS PLM SOFTWARE
Lower Chord 1
A3
LC1_dwg
A
SCALE 1:20
SHEET 1 OF 1
ALL DIMENSIONS IN MM

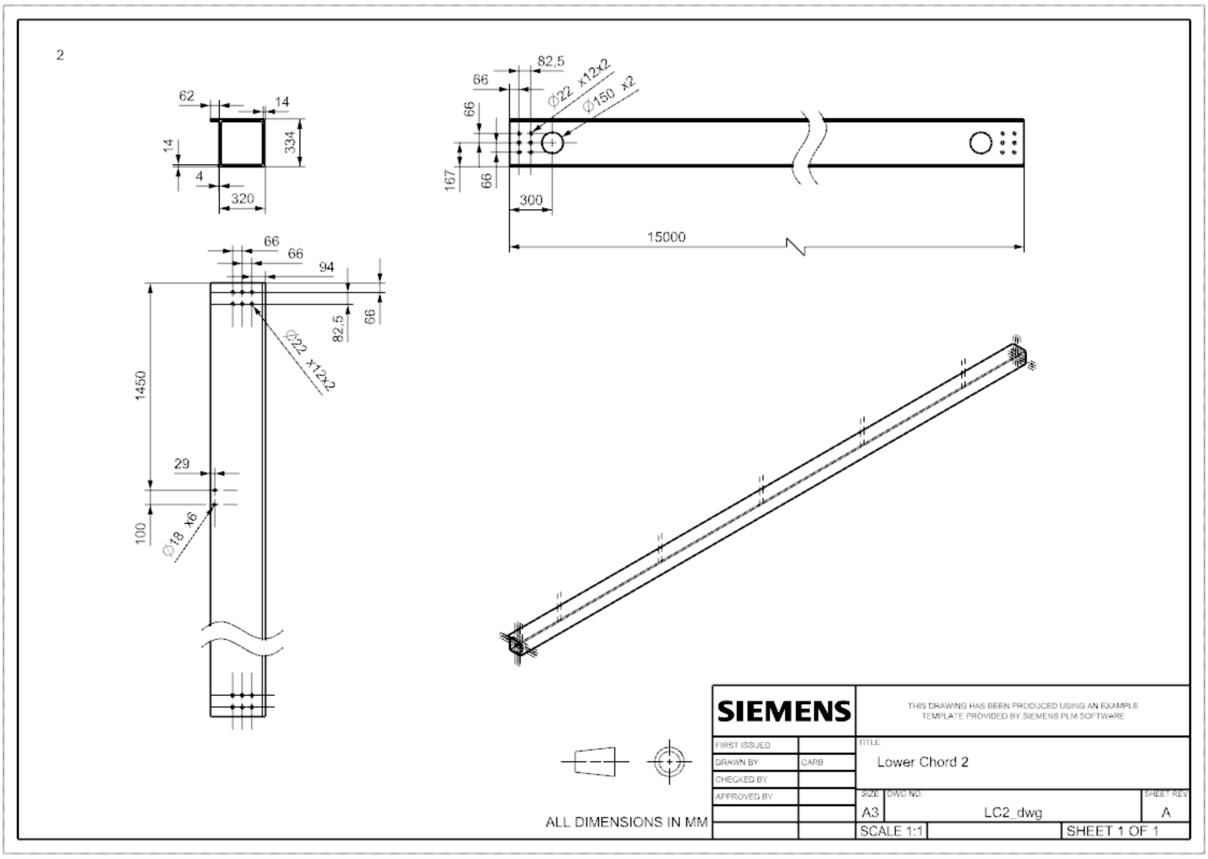
2
SIEMENS
THIS DRAWING HAS BEEN PRODUCED USING AN EXAMPLE TEMPLATE PROVIDED BY SIEMENS PLM SOFTWARE
Lower Chord 2
A3
LC2_dwg
A
SCALE 1:1
SHEET 1 OF 1
ALL DIMENSIONS IN MM

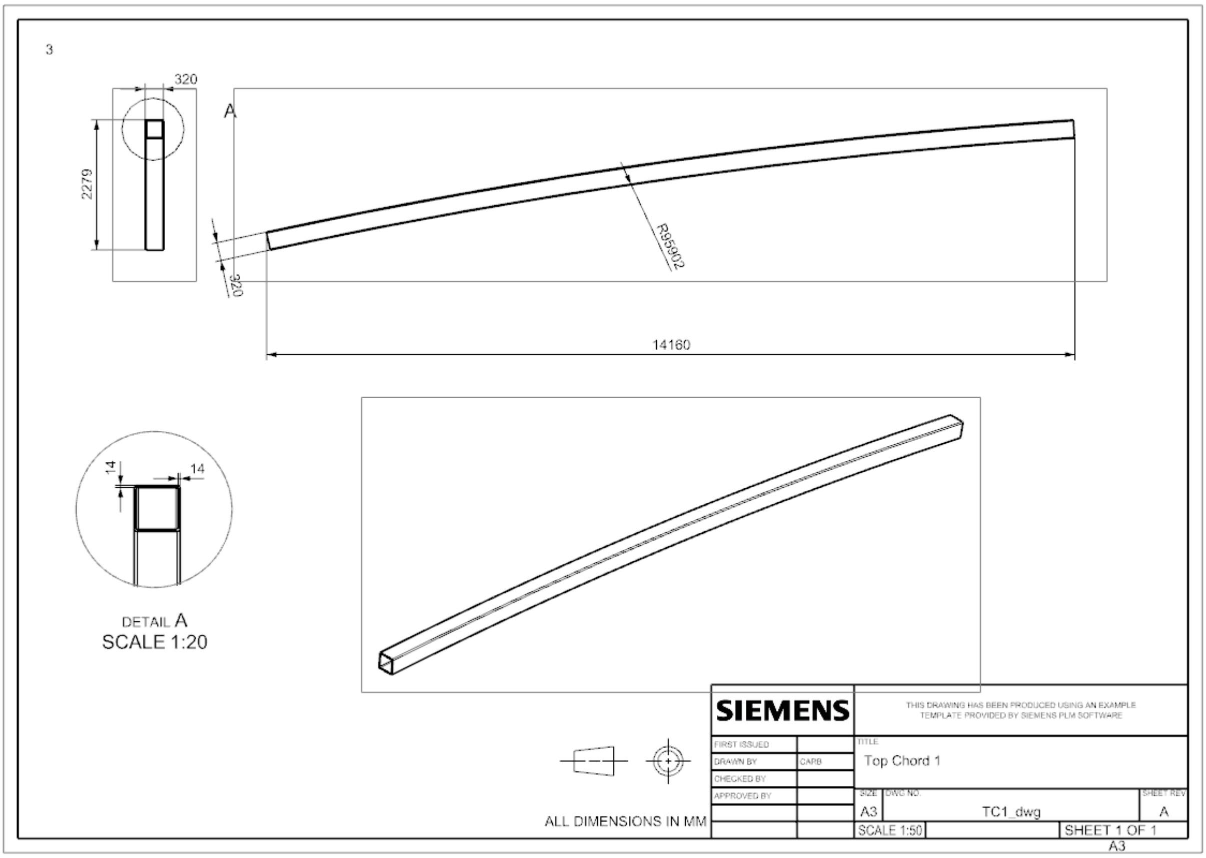
3
320
2279
A
R95902
320
14160
14
14
DETAIL A
SCALE 1:20
SIEMENS
THIS DRAWING HAS BEEN PRODUCED USING AN EXAMPLE TEMPLATE PROVIDED BY SIEMENS PLM SOFTWARE
FIRST ISSUED
DRAWN BY
CARB
CHECKED BY
APPROVED BY
TITLE
Top Chord 1
SIZE
DWG NO.
SHEET REV
A3
TC1_dwg
A
ALL DIMENSIONS IN MM
SCALE 1:50
SHEET 1 OF 1
A3

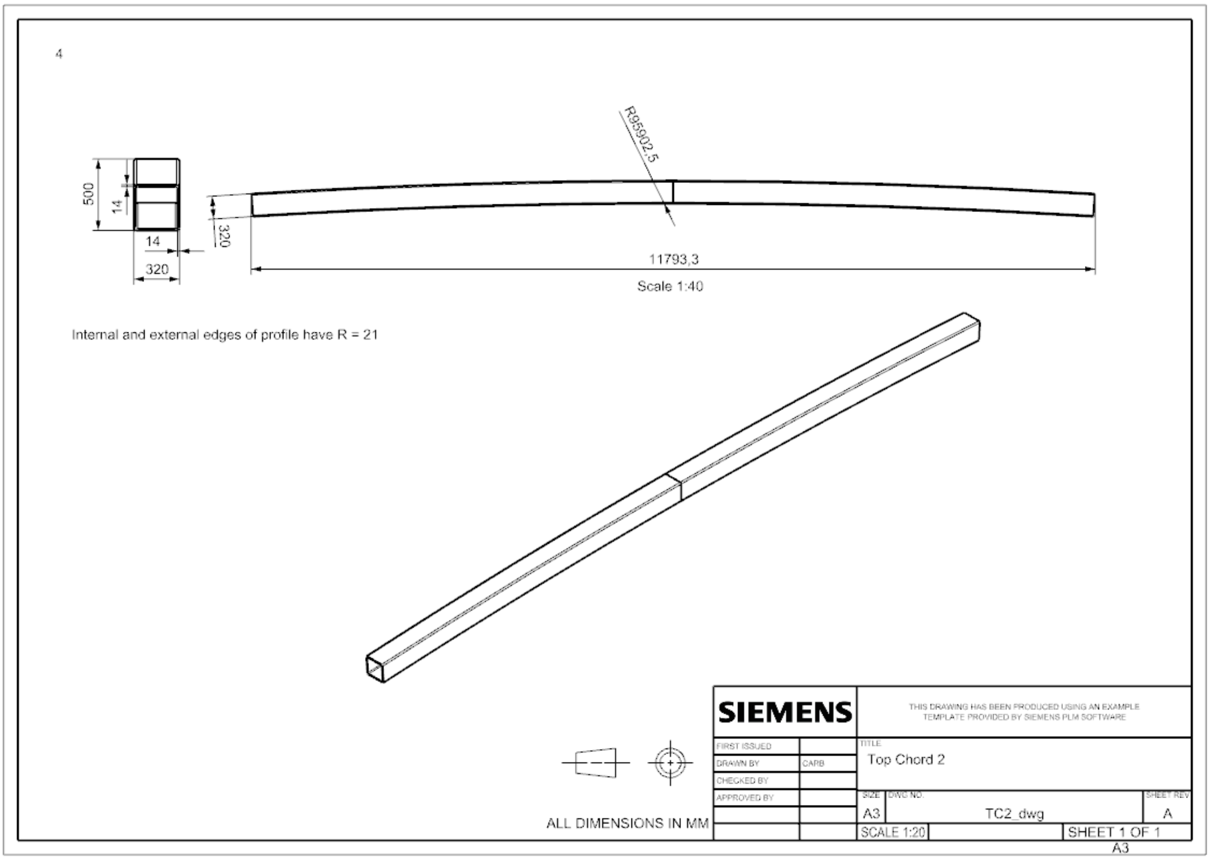
4
R95902,5
500
14
320
14
320
11793,3
Scale 1:40
Internal and external edges of profile have R = 21
SIEMENS
THIS DRAWING HAS BEEN PRODUCED USING AN EXAMPLE TEMPLATE PROVIDED BY SIEMENS PLM SOFTWARE
FIRST ISSUED
DRAWN BY
CARB
CHECKED BY
APPROVED BY
TITLE
Top Chord 2
SIZE
DWG NO.
SHEET REV
A3
TC2_dwg
A
ALL DIMENSIONS IN MM
SCALE 1:20
SHEET 1 OF 1
A3

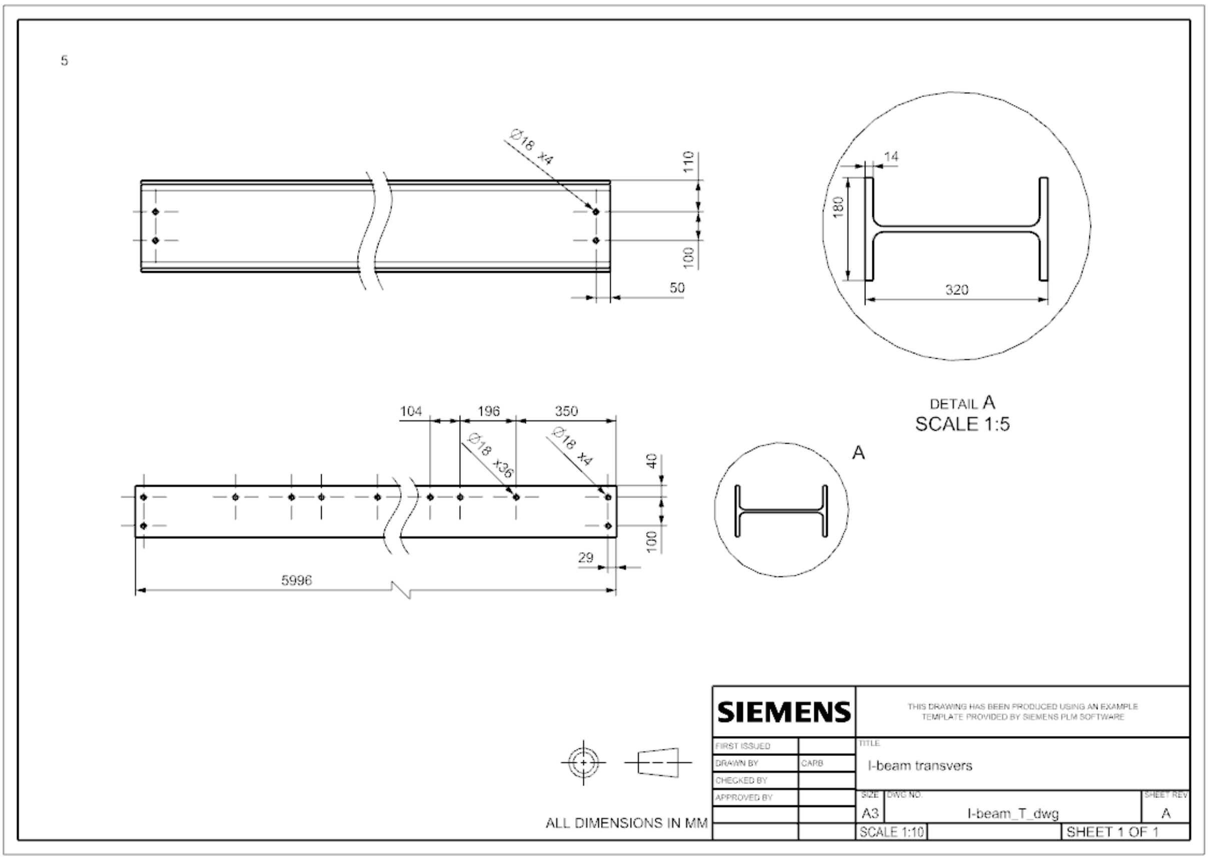
5
Ø18 x4
110
100
50
14
180
320
DETAIL A
SCALE 1:5
104
196
350
Ø18 x36
Ø18 x4
40
100
29
5996
A
SIEMENS
THIS DRAWING HAS BEEN PRODUCED USING AN EXAMPLE TEMPLATE PROVIDED BY SIEMENS PLM SOFTWARE
FIRST ISSUED
DRAWN BY CAPB
CHECKED BY
APPROVED BY
TITLE
I-beam transvers
SIZE A3
DWG NO. I-beam_T_dwg
SHEET REV A
SCALE 1:10
SHEET 1 OF 1
ALL DIMENSIONS IN MM

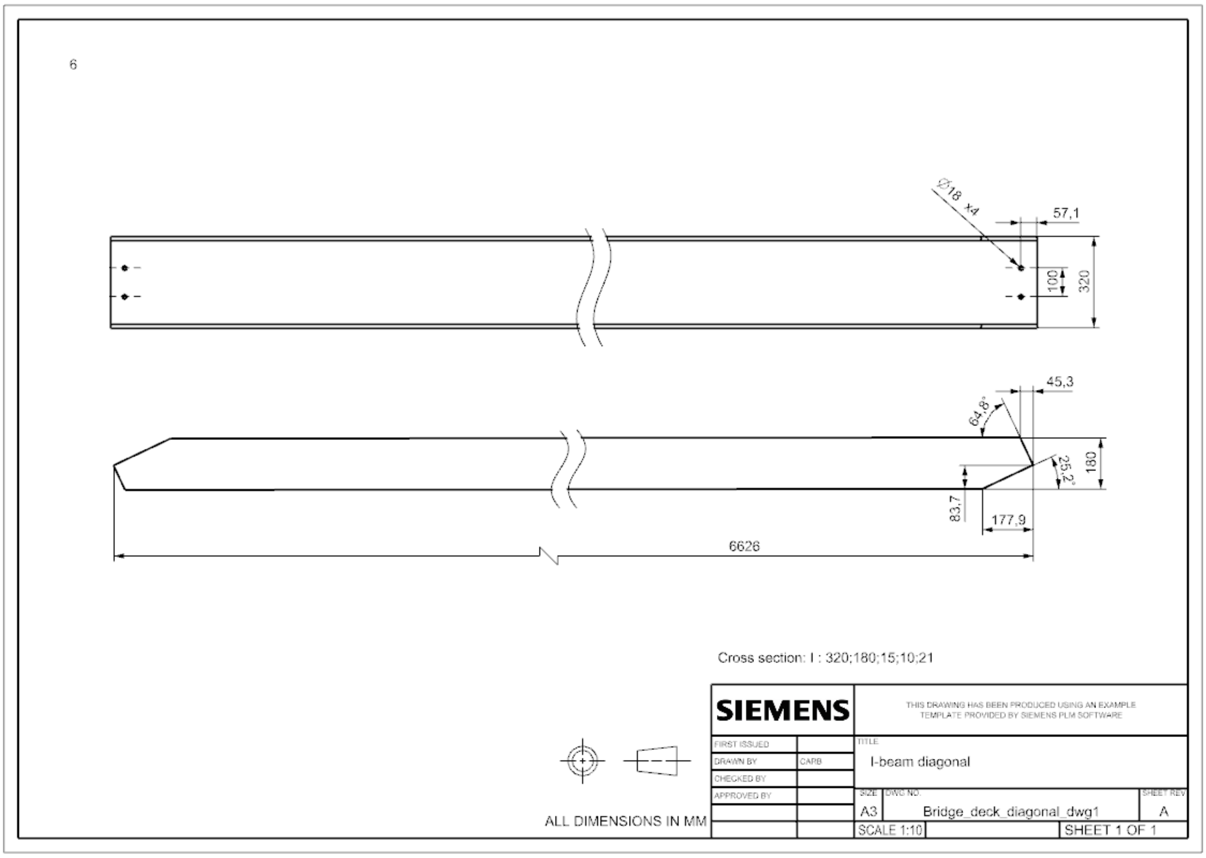
6
Ø18 x4
57,1
100
320
45,3
64,8°
25,2°
180
83,7
177,9
6626
Cross section: I : 320;180;15;10;21
SIEMENS
THIS DRAWING HAS BEEN PRODUCED USING AN EXAMPLE TEMPLATE PROVIDED BY SIEMENS PLM SOFTWARE
FIRST ISSUED
DRAWN BY CAPB
CHECKED BY
APPROVED BY
TITLE
I-beam diagonal
SIZE A3
DWG NO. Bridge_deck_diagonal_dwg1
SHEET REV A
SCALE 1:10
SHEET 1 OF 1
ALL DIMENSIONS IN MM

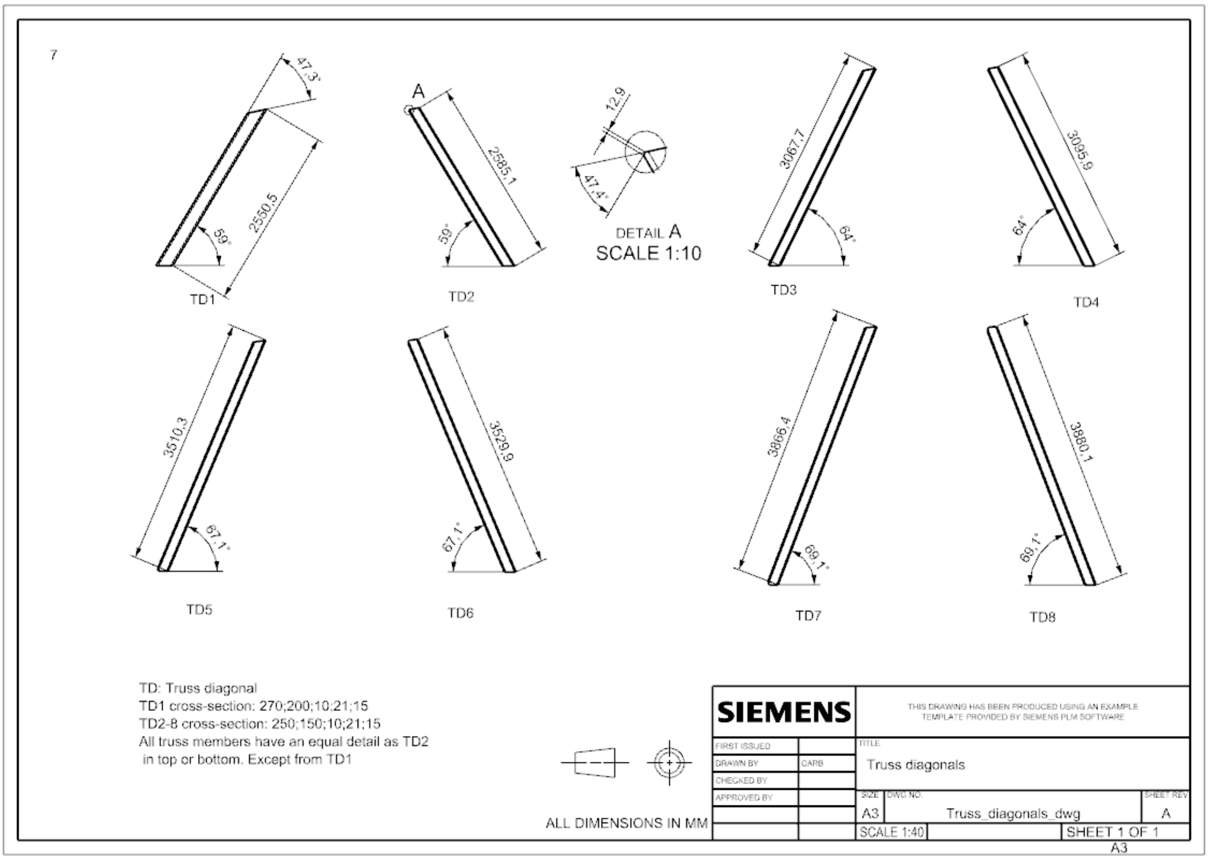
7
47.3°
2550.5
59°
TD1
A
2585.1
59°
TD2
12.9
47.4°
DETAIL A
SCALE 1:10
3067.7
64°
TD3
3095.9
64°
TD4
3510.3
67.1°
TD5
3529.9
67.1°
TD6
3866.4
69.1°
TD7
3880.1
69.1°
TD8
TD: Truss diagonal
TD1 cross-section: 270;200;10;21;15
TD2-8 cross-section: 250;150;10;21;15
All truss members have an equal detail as TD2
in top or bottom. Except from TD1
SIEMENS
THIS DRAWING HAS BEEN PRODUCED USING AN EXAMPLE
TEMPLATE PROVIDED BY SIEMENS PLM SOFTWARE
FIRST ISSUED
DRAWN BY
CARB
CHECKED BY
APPROVED BY
TITLE
Truss diagonals
SIZE
DWG NO.
SHEET REV
A3
Truss_diagonals_dwg
A
ALL DIMENSIONS IN MM
SCALE 1:40
SHEET 1 OF 1
A3

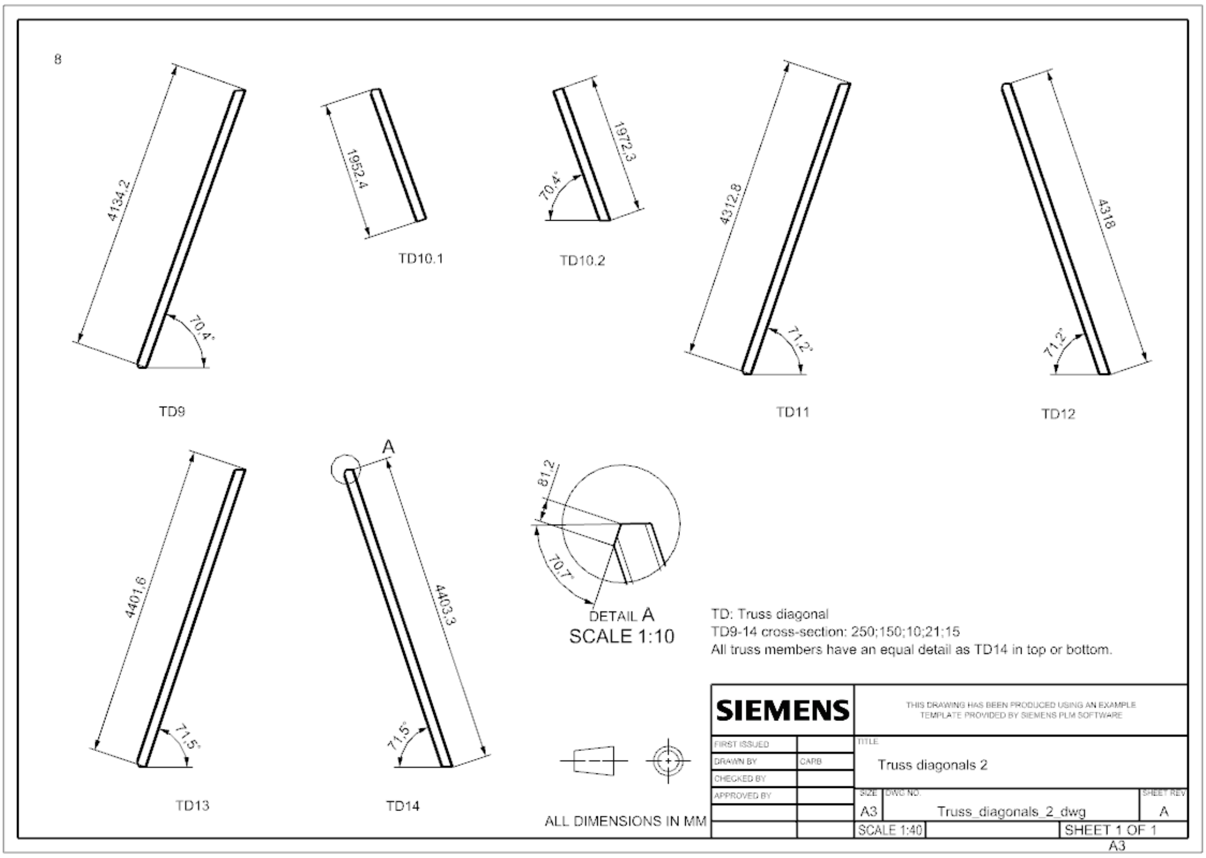
8
4134.2
70.4°
TD9
1952.4
TD10.1
1972.3
70.4°
TD10.2
4312.8
71.2°
TD11
4318
71.2°
TD12
4401.6
71.5°
TD13
A
4403.3
71.5°
TD14
81.2
70.7°
DETAIL A
SCALE 1:10
TD: Truss diagonal
TD9-14 cross-section: 250;150;10;21;15
All truss members have an equal detail as TD14 in top or bottom.
SIEMENS
THIS DRAWING HAS BEEN PRODUCED USING AN EXAMPLE
TEMPLATE PROVIDED BY SIEMENS PLM SOFTWARE
FIRST ISSUED
DRAWN BY
CARB
CHECKED BY
APPROVED BY
TITLE
Truss diagonals 2
SIZE
DWG NO.
SHEET REV
A3
Truss_diagonals_2_dwg
A
ALL DIMENSIONS IN MM
SCALE 1:40
SHEET 1 OF 1
A3

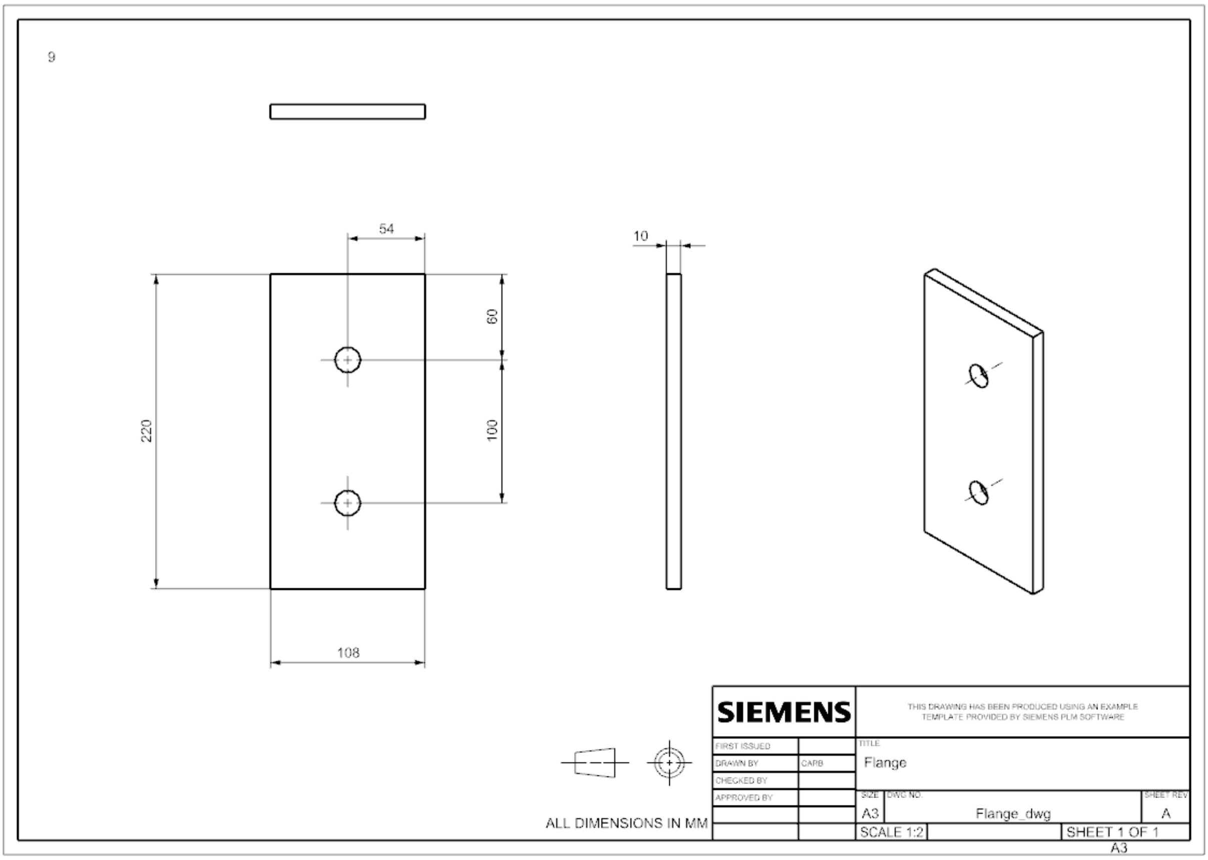
9
54
10
60
100
220
108
SIEMENS
THIS DRAWING HAS BEEN PRODUCED USING AN EXAMPLE TEMPLATE PROVIDED BY SIEMENS PLM SOFTWARE
FIRST ISSUED
DRAWN BY
CARB
CHECKED BY
APPROVED BY
TITLE
Flange
SIZE
DWG NO.
SHEET REV
A3
Flange_dwg
A
ALL DIMENSIONS IN MM
SCALE 1:2
SHEET 1 OF 1
A3

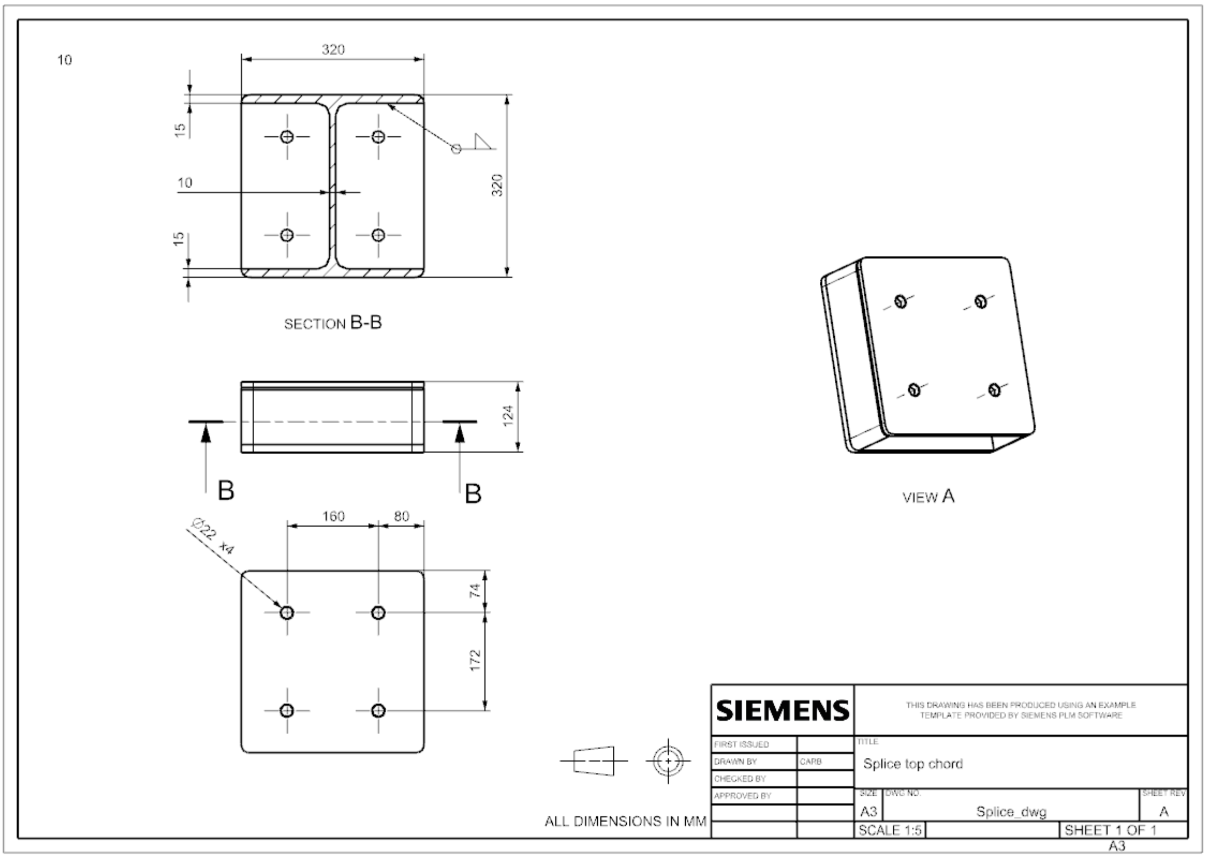
10
320
15
10
15
320
SECTION B-B
124
B
B
Ø22 x4
160
80
74
172
VIEW A
SIEMENS
THIS DRAWING HAS BEEN PRODUCED USING AN EXAMPLE TEMPLATE PROVIDED BY SIEMENS PLM SOFTWARE
FIRST ISSUED
DRAWN BY
CARB
CHECKED BY
APPROVED BY
TITLE
Splice top chord
SIZE
DWG NO.
SHEET REV
A3
Splice_dwg
A
ALL DIMENSIONS IN MM
SCALE 1:5
SHEET 1 OF 1
A3

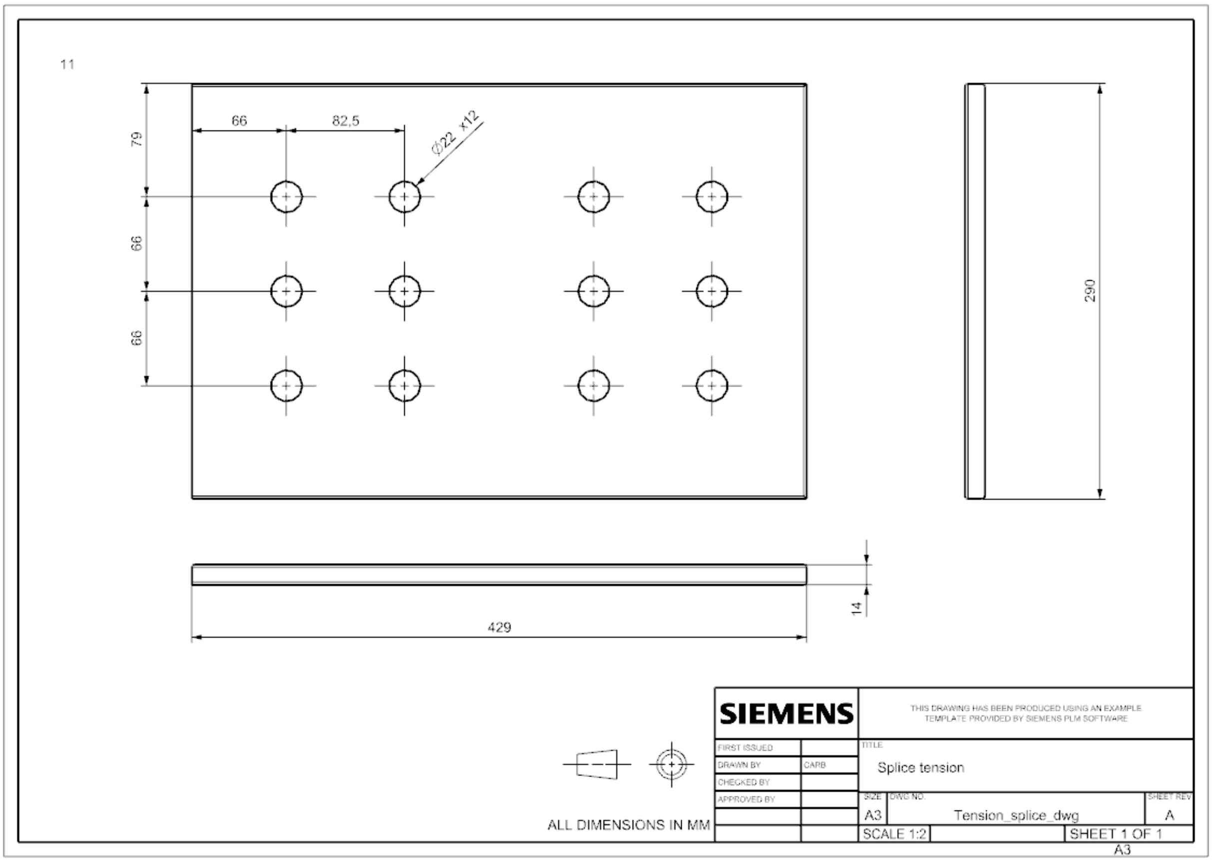
11
66
82,5
Ø22 x12
79
66
66
290
14
429
SIEMENS
THIS DRAWING HAS BEEN PRODUCED USING AN EXAMPLE TEMPLATE PROVIDED BY SIEMENS PLM SOFTWARE
FIRST ISSUED
DRAWN BY
CARB
CHECKED BY
APPROVED BY
TITLE
Splice tension
SIZE
DWG NO.
SHEET REV
A3
Tension_splice_dwg
A
ALL DIMENSIONS IN MM
SCALE 1:2
SHEET 1 OF 1
A3

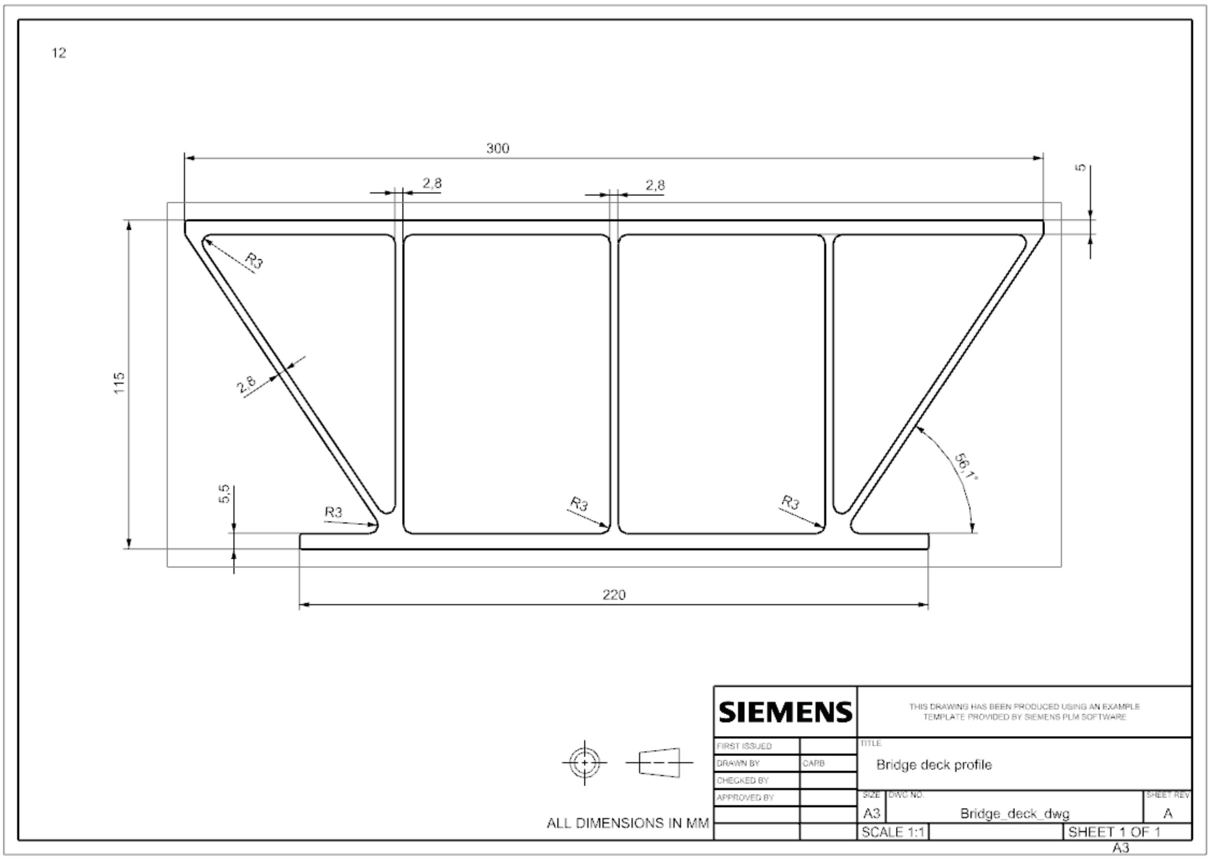
12
300
2,8
2,8
5
R3
115
2,8
56,1°
5,5
R3
R3
R3
220
SIEMENS
THIS DRAWING HAS BEEN PRODUCED USING AN EXAMPLE TEMPLATE PROVIDED BY SIEMENS PLM SOFTWARE
FIRST ISSUED
DRAWN BY
CARB
CHECKED BY
APPROVED BY
TITLE
Bridge deck profile
SIZE
DWG NO.
SHEET REV
A3
Bridge_deck_dwg
A
ALL DIMENSIONS IN MM
SCALE 1:1
SHEET 1 OF 1
A3

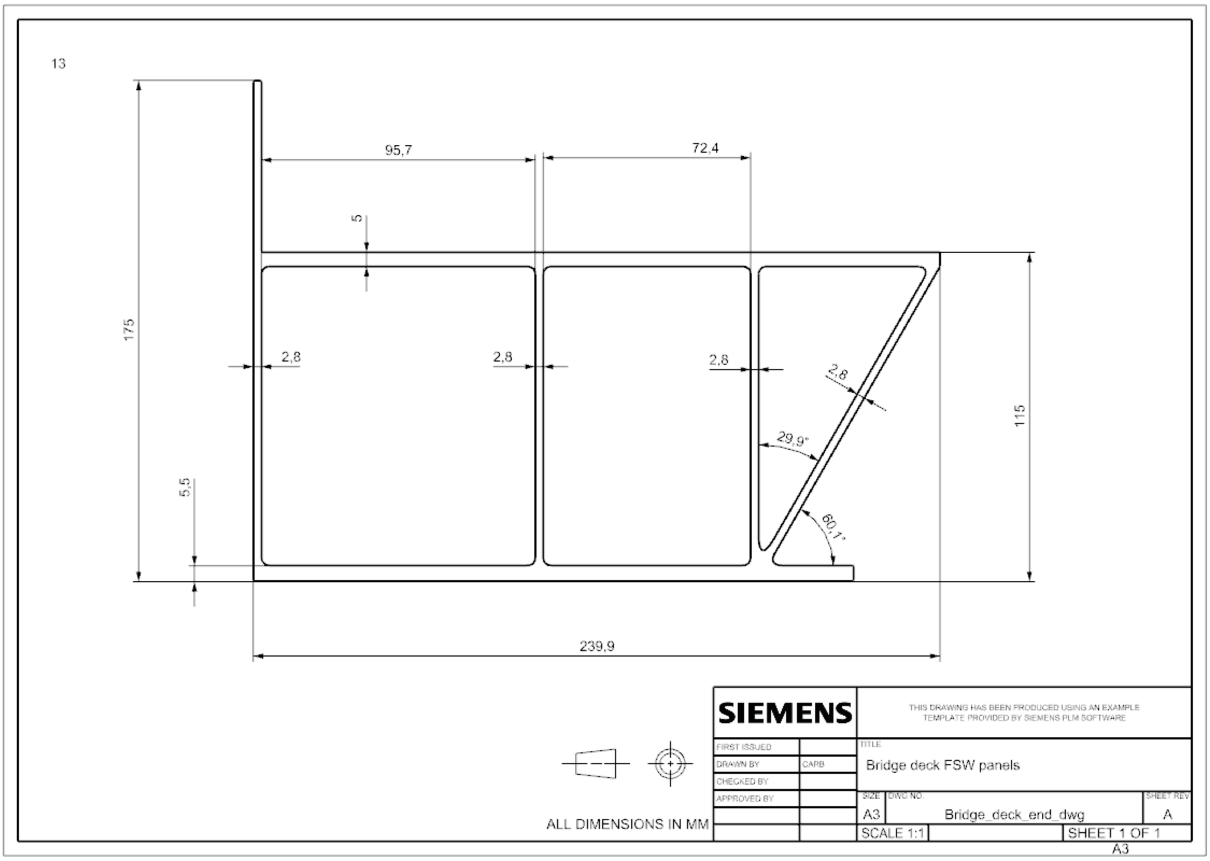
13
95,7
72,4
5
175
2,8
2,8
2,8
2,8
29,9°
115
5,5
60,1°
239,9
SIEMENS
THIS DRAWING HAS BEEN PRODUCED USING AN EXAMPLE TEMPLATE PROVIDED BY SIEMENS PLM SOFTWARE
FIRST ISSUED
DRAWN BY CARB
CHECKED BY
APPROVED BY
TITLE
Bridge deck FSW panels
SIZE DWG NO. SHEET REV
A3 Bridge_deck_end_dwg A
SCALE 1:1 SHEET 1 OF 1
A3
ALL DIMENSIONS IN MM

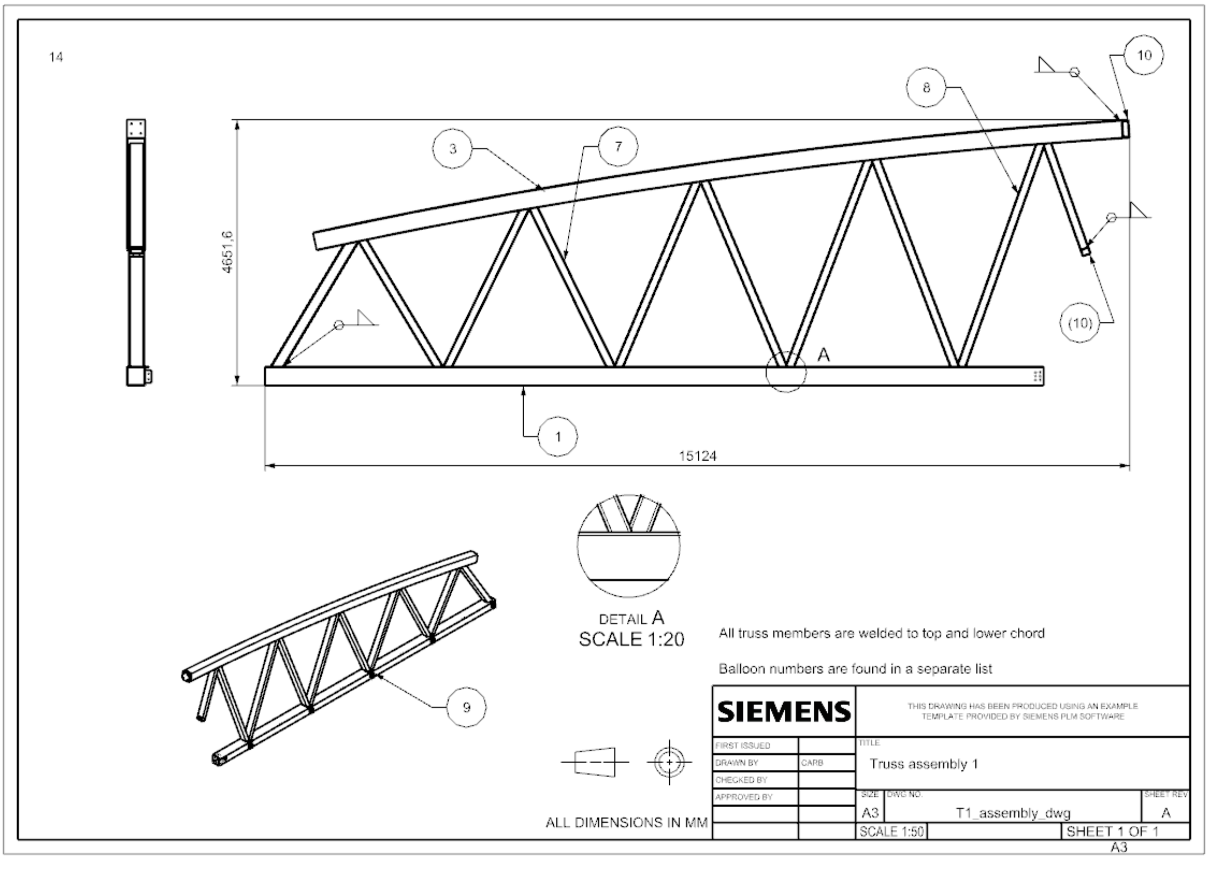
14
10
8
3
7
4651,6
A
(10)
1
15124
DETAIL A
SCALE 1:20
All truss members are welded to top and lower chord
Balloon numbers are found in a separate list
9
SIEMENS
THIS DRAWING HAS BEEN PRODUCED USING AN EXAMPLE TEMPLATE PROVIDED BY SIEMENS PLM SOFTWARE
FIRST ISSUED
DRAWN BY CARB
CHECKED BY
APPROVED BY
TITLE
Truss assembly 1
SIZE DWG NO. SHEET REV
A3 T1_assembly_dwg A
SCALE 1:50 SHEET 1 OF 1
A3
ALL DIMENSIONS IN MM

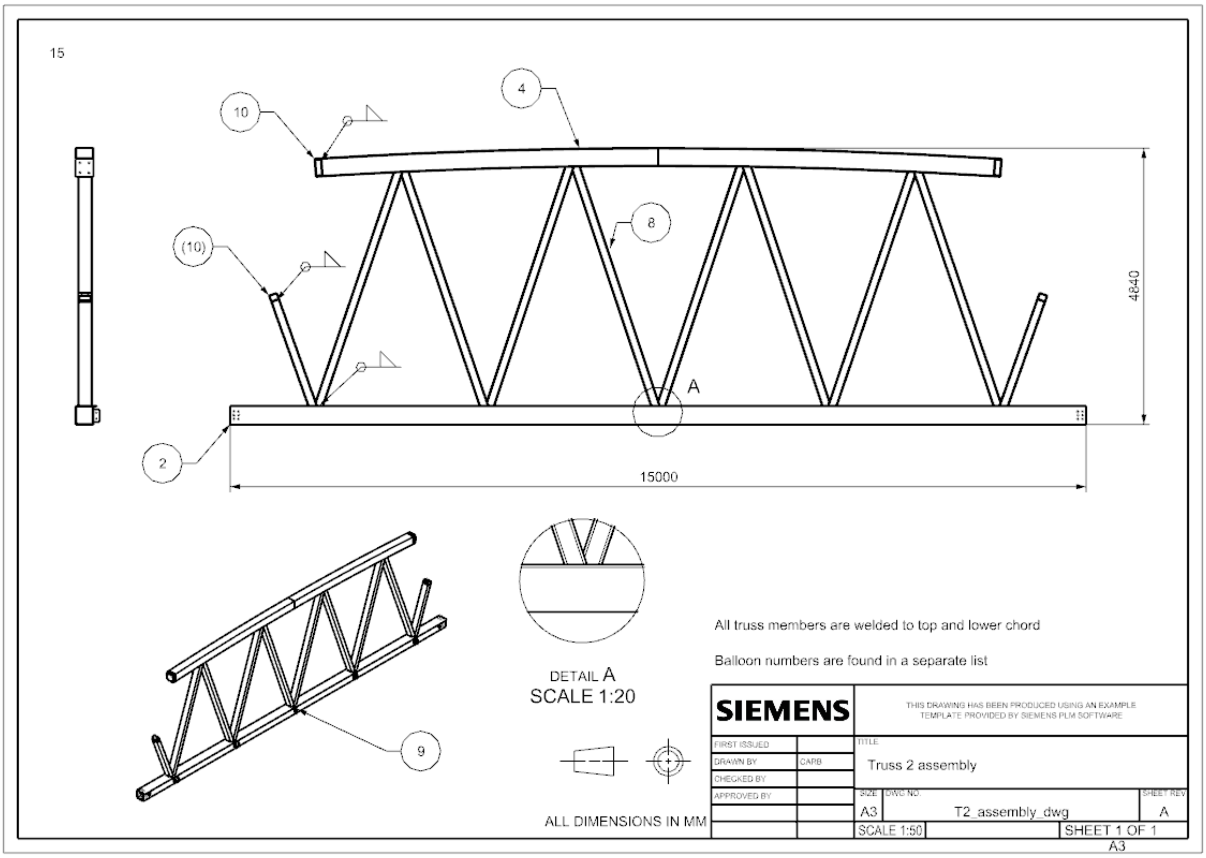
15
4
10
(10)
8
A
4840
2
15000
9
DETAIL A
SCALE 1:20
All truss members are welded to top and lower chord
Balloon numbers are found in a separate list
SIEMENS
THIS DRAWING HAS BEEN PRODUCED USING AN EXAMPLE TEMPLATE PROVIDED BY SIEMENS PLM SOFTWARE
FIRST ISSUED
DRAWN BY
CARB
CHECKED BY
APPROVED BY
TITLE
Truss 2 assembly
SIZE
DWG NO.
SHEET REV
A3
T2_assembly_dwg
A
SCALE 1:50
SHEET 1 OF 1
A3
ALL DIMENSIONS IN MM

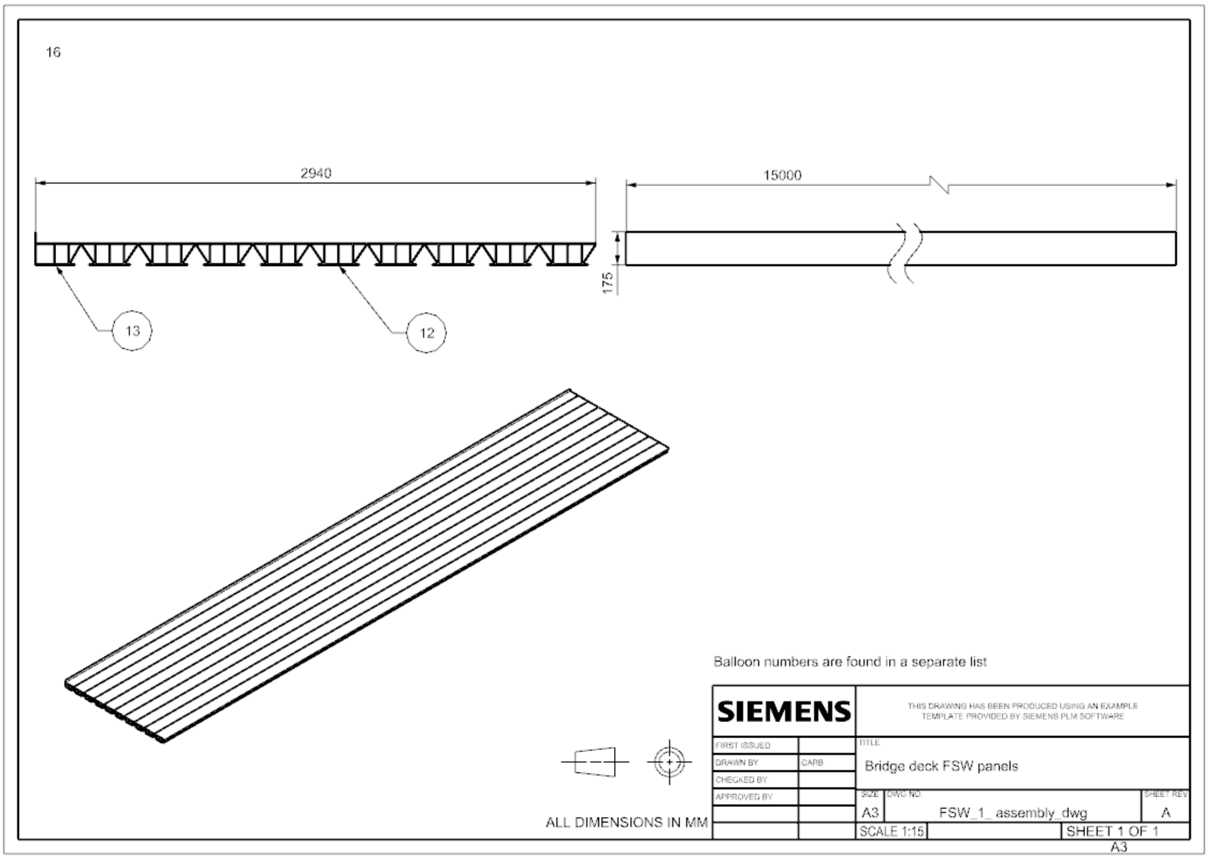
16
2940
15000
175
13
12
Balloon numbers are found in a separate list
SIEMENS
THIS DRAWING HAS BEEN PRODUCED USING AN EXAMPLE TEMPLATE PROVIDED BY SIEMENS PLM SOFTWARE
FIRST ISSUED
DRAWN BY
CARB
CHECKED BY
APPROVED BY
TITLE
Bridge deck FSW panels
SIZE
DWG NO.
SHEET REV
A3
FSW_1_ assembly_dwg
A
SCALE 1:15
SHEET 1 OF 1
A3
ALL DIMENSIONS IN MM

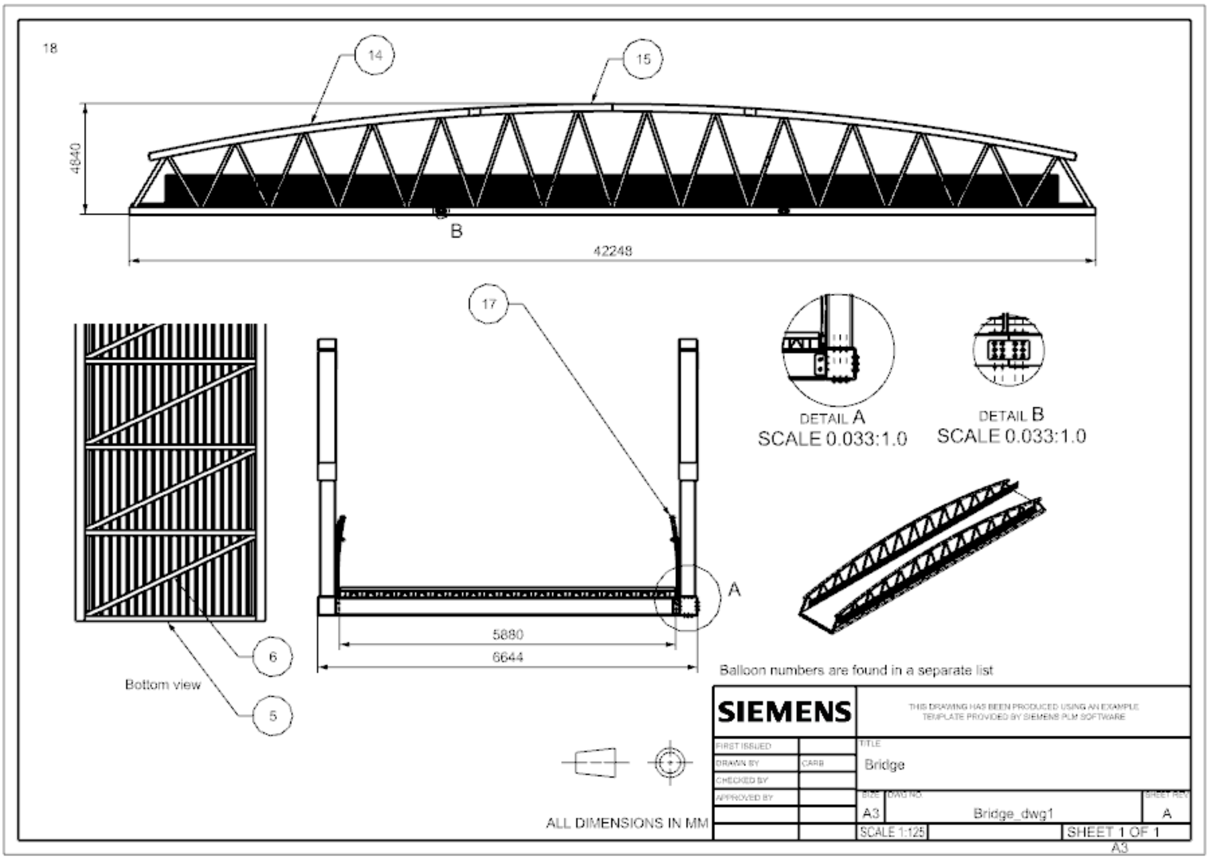
18
14
15
4840
B
42248
17
DETAIL A
SCALE 0.033:1.0
DETAIL B
SCALE 0.033:1.0
A
5880
6644
6
Bottom view
5
Balloon numbers are found in a separate list
SIEMENS
THIS DRAWING HAS BEEN PRODUCED USING AN EXAMPLE TEMPLATE PROVIDED BY SIEMENS PLM SOFTWARE
Bridge
A3
Bridge_dwg1
A
ALL DIMENSIONS IN MM
SCALE 1:125
SHEET 1 OF 1
A3

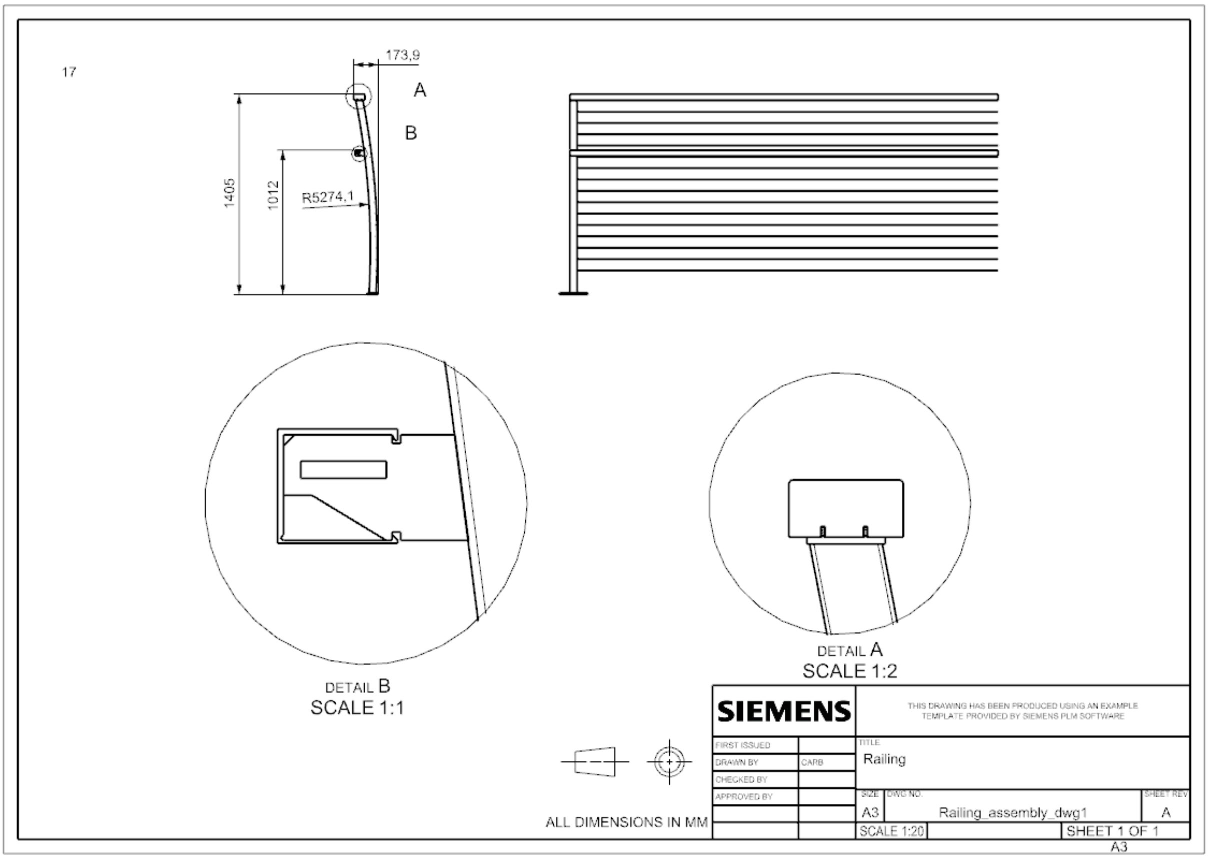
17
173,9
A
B
1405
1012
R5274,1
DETAIL A
SCALE 1:2
DETAIL B
SCALE 1:1
SIEMENS
THIS DRAWING HAS BEEN PRODUCED USING AN EXAMPLE TEMPLATE PROVIDED BY SIEMENS PLM SOFTWARE
Railing
A3
Railing_assembly_dwg1
A
ALL DIMENSIONS IN MM
SCALE 1:20
SHEET 1 OF 1
A3

A3: NS-EN 1999-1-1 Check with SCiA Engineering

Aluminium check

Linear calculation, Extreme : Member
Selection : All
Combinations : LC1

Beam Case	Css Material	dx [m]	Unity check [-]	Stability Check [-]	Section check [-]
B2 LC1/1	CS10 - RHS EN-AW 6082 (EP/O,EP/H,ET) T6 (5-15)	0,000	0,90	0,90	**0,50**
B3 LC1/1	CS10 - RHS EN-AW 6082 (EP/O,EP/H,ET) T6 (5-15)	0,000	0,91	0,91	**0,50**
B4 LC1/1	CS9 - RHS EN-AW 6082 (EP/O,EP/H,ET) T6 (5-15)	13,594	15,87	15,87	**0,32**
B5 LC1/1	CS3 - CFRHS250X150X10 EN-AW 6082 (EP/O,EP/H,ET) T6 (5-15)	0,000	0,24	0,00	**0,24**
B6 LC1/1	CS3 - CFRHS250X150X10 EN-AW 6082 (EP/O,EP/H,ET) T6 (5-15)	0,000	0,87	0,87	**0,26**
B7 LC1/1	CS3 - CFRHS250X150X10 EN-AW 6082 (EP/O,EP/H,ET) T6 (5-15)	3,428	0,27	0,00	**0,27**
B8 LC1/1	CS3 - CFRHS250X150X10 EN-AW 6082 (EP/O,EP/H,ET) T6 (5-15)	0,000	0,71	0,71	**0,16**
B9 LC1/1	CS3 - CFRHS250X150X10 EN-AW 6082 (EP/O,EP/H,ET) T6 (5-15)	3,864	0,16	0,00	**0,16**
B10 LC1/1	CS3 - CFRHS250X150X10 EN-AW 6082 (EP/O,EP/H,ET) T6 (5-15)	0,000	0,53	0,53	**0,10**
B11 LC1/1	CS3 - CFRHS250X150X10 EN-AW 6082 (EP/O,EP/H,ET) T6 (5-15)	0,000	0,11	0,00	**0,11**
B12 LC1/1	CS3 - CFRHS250X150X10 EN-AW 6082 (EP/O,EP/H,ET) T6 (5-15)	0,000	0,38	0,38	**0,06**
B13 LC1/1	CS3 - CFRHS250X150X10 EN-AW 6082 (EP/O,EP/H,ET) T6 (5-15)	2,239	0,06	0,00	**0,06**
B14 LC1/1	CS3 - CFRHS250X150X10 EN-AW 6082 (EP/O,EP/H,ET) T6 (5-15)	0,000	0,21	0,21	**0,03**
B15 LC1/1	CS3 - CFRHS250X150X10 EN-AW 6082 (EP/O,EP/H,ET) T6 (5-15)	0,000	0,04	0,00	**0,04**
B16 LC1/1	CS3 - CFRHS250X150X10 EN-AW 6082 (EP/O,EP/H,ET) T6 (5-15)	0,000	0,01	0,00	**0,01**
B17 LC1/1	CS3 - CFRHS250X150X10 EN-AW 6082 (EP/O,EP/H,ET) T6 (5-15)	4,735	0,02	0,00	**0,02**
B18 LC1/1	CS3 - CFRHS250X150X10 EN-AW 6082 (EP/O,EP/H,ET) T6 (5-15)	0,000	0,35	0,00	**0,35**
B19 LC1/1	CS3 - CFRHS250X150X10 EN-AW 6082 (EP/O,EP/H,ET) T6 (5-15)	0,000	0,87	0,87	**0,26**
B20 LC1/1	CS3 - CFRHS250X150X10 EN-AW 6082 (EP/O,EP/H,ET) T6 (5-15)	3,428	0,27	0,00	**0,27**
B21 LC1/1	CS3 - CFRHS250X150X10 EN-AW 6082 (EP/O,EP/H,ET) T6 (5-15)	0,000	0,71	0,71	**0,16**
B22 LC1/1	CS3 - CFRHS250X150X10 EN-AW 6082 (EP/O,EP/H,ET) T6 (5-15)	3,864	0,16	0,00	**0,16**
B23 LC1/1	CS3 - CFRHS250X150X10 EN-AW 6082 (EP/O,EP/H,ET) T6 (5-15)	0,000	0,53	0,53	**0,10**
B24 LC1/1	CS3 - CFRHS250X150X10 EN-AW 6082 (EP/O,EP/H,ET) T6 (5-15)	0,000	0,11	0,00	**0,11**
B25 LC1/1	CS3 - CFRHS250X150X10 EN-AW 6082 (EP/O,EP/H,ET) T6 (5-15)	0,000	0,38	0,38	**0,06**
B26 LC1/1	CS3 - CFRHS250X150X10 EN-AW 6082 (EP/O,EP/H,ET) T6 (5-15)	2,239	0,06	0,00	**0,06**
B27 LC1/1	CS3 - CFRHS250X150X10 EN-AW 6082 (EP/O,EP/H,ET) T6 (5-15)	0,000	0,20	0,20	**0,03**
B28 LC1/1	CS3 - CFRHS250X150X10 EN-AW 6082 (EP/O,EP/H,ET) T6 (5-15)	0,000	0,04	0,00	**0,04**
B29 LC1/1	CS3 - CFRHS250X150X10 EN-AW 6082 (EP/O,EP/H,ET) T6 (5-15)	4,729	0,01	0,00	**0,01**
B30 LC1/1	CS3 - CFRHS250X150X10 EN-AW 6082 (EP/O,EP/H,ET) T6 (5-15)	4,735	0,02	0,00	**0,02**
B32 LC1/1	CS10 - RHS EN-AW 6082 (EP/O,EP/H,ET) T6 (5-15)	0,000	0,87	0,87	**0,47**
B33 LC1/1	CS10 - RHS EN-AW 6082 (EP/O,EP/H,ET) T6 (5-15)	0,000	0,87	0,87	**0,47**
B34	CS9 - RHS	13,594	16,55	16,55	**0,34**

Beam Case	Css Material	dx [m]	Unity check [-]	Stability Check [-]	Section check [-]
LC1/1	EN-AW 6082 (EP/O,EP/H,ET) T6 (5-15)				
B35 LC1/1	CS3 - CFRHS250X150X10 EN-AW 6082 (EP/O,EP/H,ET) T6 (5-15)	0,000	0,35	0,00	**0,35**
B36 LC1/1	CS3 - CFRHS250X150X10 EN-AW 6082 (EP/O,EP/H,ET) T6 (5-15)	0,000	0,91	0,91	**0,28**
B37 LC1/1	CS3 - CFRHS250X150X10 EN-AW 6082 (EP/O,EP/H,ET) T6 (5-15)	3,428	0,28	0,00	**0,28**
B38 LC1/1	CS3 - CFRHS250X150X10 EN-AW 6082 (EP/O,EP/H,ET) T6 (5-15)	0,000	0,75	0,75	**0,17**
B39 LC1/1	CS3 - CFRHS250X150X10 EN-AW 6082 (EP/O,EP/H,ET) T6 (5-15)	3,864	0,18	0,00	**0,18**
B40 LC1/1	CS3 - CFRHS250X150X10 EN-AW 6082 (EP/O,EP/H,ET) T6 (5-15)	0,000	0,58	0,58	**0,11**
B41 LC1/1	CS3 - CFRHS250X150X10 EN-AW 6082 (EP/O,EP/H,ET) T6 (5-15)	0,000	0,12	0,00	**0,12**
B42 LC1/1	CS3 - CFRHS250X150X10 EN-AW 6082 (EP/O,EP/H,ET) T6 (5-15)	0,000	0,42	0,42	**0,07**
B43 LC1/1	CS3 - CFRHS250X150X10 EN-AW 6082 (EP/O,EP/H,ET) T6 (5-15)	0,000	0,08	0,00	**0,08**
B44 LC1/1	CS3 - CFRHS250X150X10 EN-AW 6082 (EP/O,EP/H,ET) T6 (5-15)	0,000	0,27	0,27	**0,04**
B45 LC1/1	CS3 - CFRHS250X150X10 EN-AW 6082 (EP/O,EP/H,ET) T6 (5-15)	0,000	0,05	0,00	**0,05**
B46 LC1/1	CS3 - CFRHS250X150X10 EN-AW 6082 (EP/O,EP/H,ET) T6 (5-15)	0,000	0,09	0,09	**0,02**
B47 LC1/1	CS3 - CFRHS250X150X10 EN-AW 6082 (EP/O,EP/H,ET) T6 (5-15)	0,000	0,03	0,00	**0,03**
B48 LC1/1	CS3 - CFRHS250X150X10 EN-AW 6082 (EP/O,EP/H,ET) T6 (5-15)	0,000	0,35	0,00	**0,35**
B49 LC1/1	CS3 - CFRHS250X150X10 EN-AW 6082 (EP/O,EP/H,ET) T6 (5-15)	0,000	0,91	0,91	**0,28**
B50 LC1/1	CS3 - CFRHS250X150X10 EN-AW 6082 (EP/O,EP/H,ET) T6 (5-15)	3,428	0,28	0,00	**0,28**
B51 LC1/1	CS3 - CFRHS250X150X10 EN-AW 6082 (EP/O,EP/H,ET) T6 (5-15)	0,000	0,75	0,75	**0,17**
B52 LC1/1	CS3 - CFRHS250X150X10 EN-AW 6082 (EP/O,EP/H,ET) T6 (5-15)	3,864	0,18	0,00	**0,18**
B53 LC1/1	CS3 - CFRHS250X150X10 EN-AW 6082 (EP/O,EP/H,ET) T6 (5-15)	0,000	0,58	0,58	**0,11**
B54 LC1/1	CS3 - CFRHS250X150X10 EN-AW 6082 (EP/O,EP/H,ET) T6 (5-15)	0,000	0,12	0,00	**0,12**
B55 LC1/1	CS3 - CFRHS250X150X10 EN-AW 6082 (EP/O,EP/H,ET) T6 (5-15)	0,000	0,42	0,42	**0,07**
B56 LC1/1	CS3 - CFRHS250X150X10 EN-AW 6082 (EP/O,EP/H,ET) T6 (5-15)	0,000	0,08	0,00	**0,08**
B57 LC1/1	CS3 - CFRHS250X150X10 EN-AW 6082 (EP/O,EP/H,ET) T6 (5-15)	0,000	0,27	0,27	**0,04**
B58 LC1/1	CS3 - CFRHS250X150X10 EN-AW 6082 (EP/O,EP/H,ET) T6 (5-15)	0,000	0,05	0,00	**0,05**
B59 LC1/1	CS3 - CFRHS250X150X10 EN-AW 6082 (EP/O,EP/H,ET) T6 (5-15)	0,000	0,09	0,09	**0,02**
B60 LC1/1	CS3 - CFRHS250X150X10 EN-AW 6082 (EP/O,EP/H,ET) T6 (5-15)	0,000	0,03	0,00	**0,03**
B348 LC1/1	CS9 - RHS EN-AW 6082 (EP/O,EP/H,ET) T6 (5-15)	3,000	0,10	0,00	**0,10**
B349 LC1/1	CS9 - RHS EN-AW 6082 (EP/O,EP/H,ET) T6 (5-15)	39,000	0,12	0,00	**0,12**
B350 LC1/1	CS11 - I EN-AW 6082 (EP/O,EP/H,ET) T6 (5-15)	0,000	1,10	1,10	**0,41**
B351 LC1/1	CS11 - I EN-AW 6082 (EP/O,EP/H,ET) T6 (5-15)	6,000	0,53	0,00	**0,53**
B352 LC1/1	CS11 - I EN-AW 6082 (EP/O,EP/H,ET) T6 (5-15)	0,000	0,57	0,57	**0,38**
B353 LC1/1	CS11 - I EN-AW 6082 (EP/O,EP/H,ET) T6 (5-15)	6,000	0,26	0,00	**0,26**
B354 LC1/1	CS11 - I EN-AW 6082 (EP/O,EP/H,ET) T6 (5-15)	2,700	0,33	0,33	**0,24**
B355 LC1/1	CS11 - I EN-AW 6082 (EP/O,EP/H,ET) T6 (5-15)	3,000	0,82	0,82	**0,25**

Beam Case	Css Material	dx [m]	Unity check [-]	Stability Check [-]	Section check [-]
B356 LC1/1	CS11 - I EN-AW 6082 (EP/O,EP/H,ET) T6 (5-15)	3,000	0,27	0,27	**0,22**
B357 LC1/1	CS11 - I EN-AW 6082 (EP/O,EP/H,ET) T6 (5-15)	2,700	0,22	0,22	**0,22**
B358 LC1/1	CS11 - I EN-AW 6082 (EP/O,EP/H,ET) T6 (5-15)	3,000	0,21	0,00	**0,21**
B359 LC1/1	CS11 - I EN-AW 6082 (EP/O,EP/H,ET) T6 (5-15)	3,000	0,70	0,70	**0,23**
B360 LC1/1	CS11 - I EN-AW 6082 (EP/O,EP/H,ET) T6 (5-15)	6,000	0,24	0,00	**0,24**
B361 LC1/1	CS11 - I EN-AW 6082 (EP/O,EP/H,ET) T6 (5-15)	6,000	0,38	0,00	**0,38**
B362 LC1/1	CS11 - I EN-AW 6082 (EP/O,EP/H,ET) T6 (5-15)	6,000	0,55	0,00	**0,55**
B363 LC1/1	CS11 - I EN-AW 6082 (EP/O,EP/H,ET) T6 (5-15)	6,000	0,80	0,00	**0,80**
B364 LC1/1	CS11 - I EN-AW 6082 (EP/O,EP/H,ET) T6 (5-15)	6,000	0,57	0,00	**0,57**
B365 LC1/1	CS11 - I EN-AW 6082 (EP/O,EP/H,ET) T6 (5-15)	0,000	0,51	0,00	**0,51**
B366 LC1/1	CS11 - I EN-AW 6082 (EP/O,EP/H,ET) T6 (5-15)	0,000	0,42	0,00	**0,42**
B367 LC1/1	CS11 - I EN-AW 6082 (EP/O,EP/H,ET) T6 (5-15)	0,000	0,32	0,00	**0,32**
B368 LC1/1	CS11 - I EN-AW 6082 (EP/O,EP/H,ET) T6 (5-15)	0,000	0,23	0,00	**0,23**
B369 LC1/1	CS11 - I EN-AW 6082 (EP/O,EP/H,ET) T6 (5-15)	3,019	0,20	0,00	**0,20**
B370 LC1/1	CS11 - I EN-AW 6082 (EP/O,EP/H,ET) T6 (5-15)	3,019	0,18	0,00	**0,18**
B371 LC1/1	CS11 - I EN-AW 6082 (EP/O,EP/H,ET) T6 (5-15)	3,354	0,18	0,00	**0,18**
B372 LC1/1	CS11 - I EN-AW 6082 (EP/O,EP/H,ET) T6 (5-15)	6,708	0,81	0,81	**0,65**
B373 LC1/1	CS11 - I EN-AW 6082 (EP/O,EP/H,ET) T6 (5-15)	0,000	0,50	0,00	**0,50**
B374 LC1/1	CS11 - I EN-AW 6082 (EP/O,EP/H,ET) T6 (5-15)	0,000	0,39	0,00	**0,39**
B375 LC1/1	CS11 - I EN-AW 6082 (EP/O,EP/H,ET) T6 (5-15)	0,000	0,28	0,00	**0,28**
B376 LC1/1	CS11 - I EN-AW 6082 (EP/O,EP/H,ET) T6 (5-15)	0,000	0,19	0,00	**0,19**
B377 LC1/1	CS11 - I EN-AW 6082 (EP/O,EP/H,ET) T6 (5-15)	3,354	0,19	0,19	**0,17**
B378 LC1/1	CS11 - I EN-AW 6082 (EP/O,EP/H,ET) T6 (5-15)	3,354	0,19	0,19	**0,17**